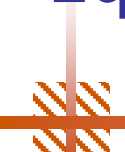


# High-Fidelity, Computational Modeling of Non-Equilibrium Discharges for Combustion Applications



**Laxminarayan L. Raja**

Contributions:

**Douglas Breden, Rochan Upadhyay, Shankar Mahadevan**

Dept. of Aerospace Engr. and Engr. Mech,  
The University of Texas at Austin  
Austin, Texas 78712

AFOSR Plasma-Assisted Combustion  
Multi-University Research Initiative Review (MURI) Review  
Arlington, VA, USA  
(22<sup>nd</sup> – 24<sup>th</sup> October 2013)

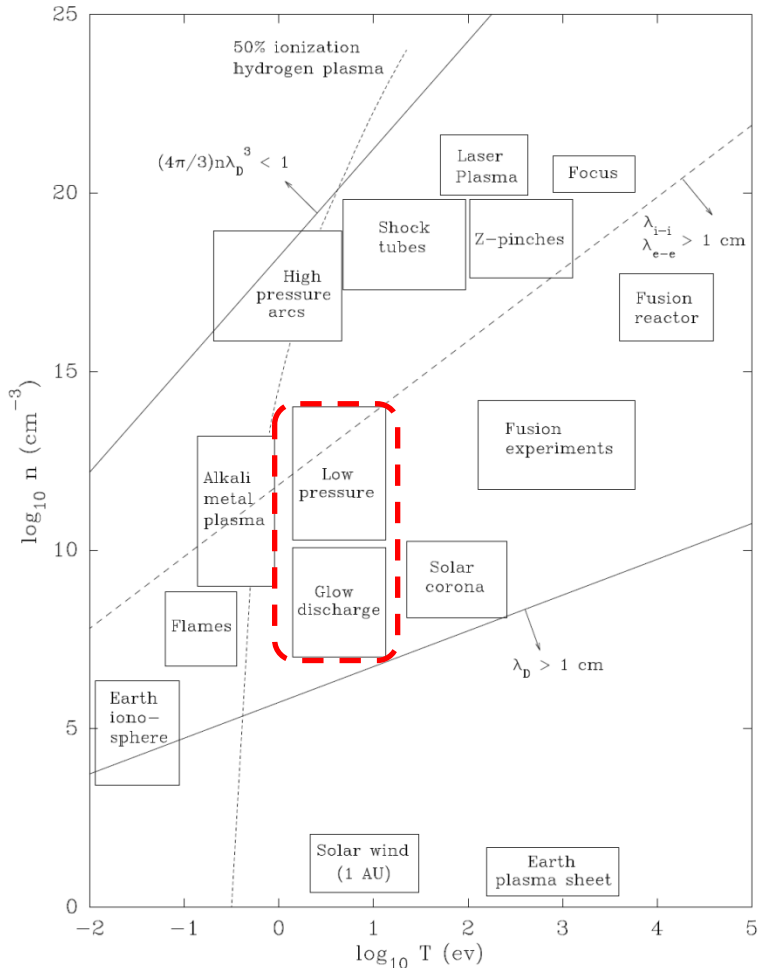
<b>Report Documentation Page</b>			Form Approved OMB No. 0704-0188	
<p>Public reporting burden for the collection of information is estimated to average 1 hour per response, including the time for reviewing instructions, searching existing data sources, gathering and maintaining the data needed, and completing and reviewing the collection of information. Send comments regarding this burden estimate or any other aspect of this collection of information, including suggestions for reducing this burden, to Washington Headquarters Services, Directorate for Information Operations and Reports, 1215 Jefferson Davis Highway, Suite 1204, Arlington VA 22202-4302. Respondents should be aware that notwithstanding any other provision of law, no person shall be subject to a penalty for failing to comply with a collection of information if it does not display a currently valid OMB control number.</p>				
1. REPORT DATE <b>OCT 2013</b>	2. REPORT TYPE	3. DATES COVERED <b>00-00-2013 to 00-00-2013</b>		
4. TITLE AND SUBTITLE <b>High-Fidelity, Computational Modeling of Non-Equilibrium Discharges for Combustion Applications</b>			5a. CONTRACT NUMBER	
			5b. GRANT NUMBER	
			5c. PROGRAM ELEMENT NUMBER	
6. AUTHOR(S)			5d. PROJECT NUMBER	
			5e. TASK NUMBER	
			5f. WORK UNIT NUMBER	
7. PERFORMING ORGANIZATION NAME(S) AND ADDRESS(ES) <b>University of Texas at Austin, Department of Aerospace Engr. and Engr. Mech, Austin, TX, 78712</b>			8. PERFORMING ORGANIZATION REPORT NUMBER	
9. SPONSORING/MONITORING AGENCY NAME(S) AND ADDRESS(ES)			10. SPONSOR/MONITOR'S ACRONYM(S)	
			11. SPONSOR/MONITOR'S REPORT NUMBER(S)	
12. DISTRIBUTION/AVAILABILITY STATEMENT <b>Approved for public release; distribution unlimited</b>				
13. SUPPLEMENTARY NOTES				
14. ABSTRACT				
15. SUBJECT TERMS				
16. SECURITY CLASSIFICATION OF:			17. LIMITATION OF ABSTRACT <b>Same as Report (SAR)</b>	18. NUMBER OF PAGES <b>86</b>
a. REPORT <b>unclassified</b>	b. ABSTRACT <b>unclassified</b>	c. THIS PAGE <b>unclassified</b>	19a. NAME OF RESPONSIBLE PERSON	

# Motivation

- There is significant evidence to show cold (non-equilibrium) plasma discharges have distinct advantages as combustion ignition / stabilization sources
- At high pressures relevant to applications, cold plasmas generated by nanosecond pulsing that result in streamer like constricted discharges
- Significant experimental difficulty in probing the structure and properties of streamers (small length scales, short time scales)
- High-fidelity computational modeling can play an important role in describing physics and chemistry in these discharges

# Cold (non-equilibrium) plasma discharge in plasma parameter space

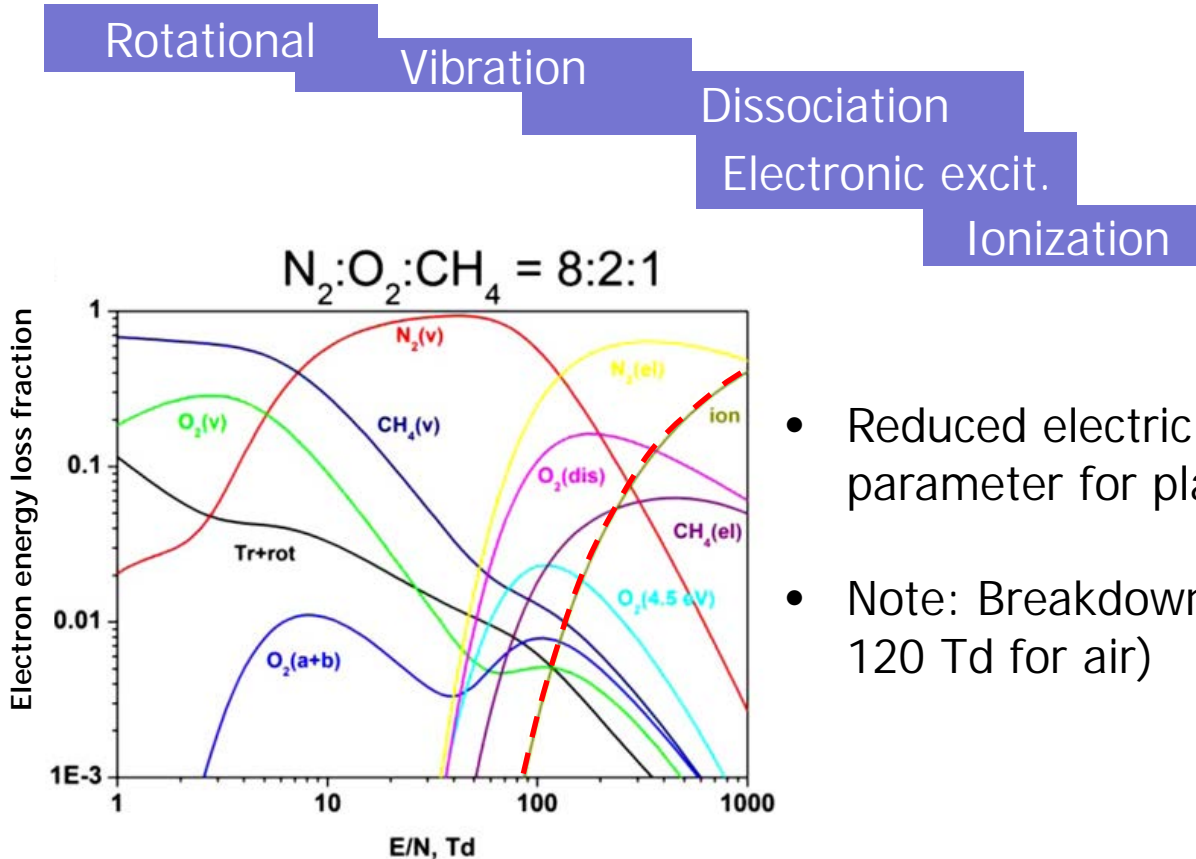
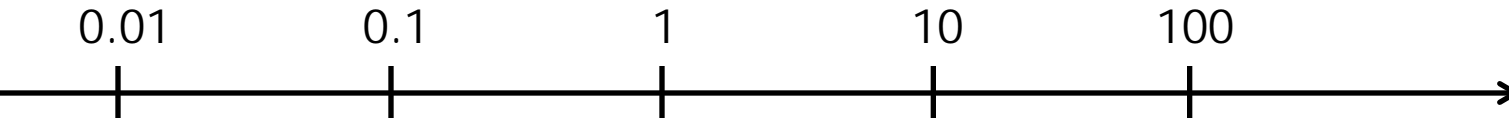
- Thermal plasmas (“Hot”)
  - Most electrical energy goes into gas heating (~10,000 K)
  - All species can be characterized by the same temperature (in thermal equilibrium)
  
- Non-thermal plasmas (“Cold”)
  - Electrical power is absorbed by electrons which in turn produce radicals and ions.
  - Electrons have high temperature (~10,000 K and more)
  - Ions and Neutrals remain at lower temperature (~300-1000 K)
  - Not in thermal equilibrium (non-equilibrium plasma)



From : NRL plasma formulary  
<http://wwwppd.nrl.navy.mil/nrlformulary/>

# Characteristic molecular energies and electron energy loss pathways

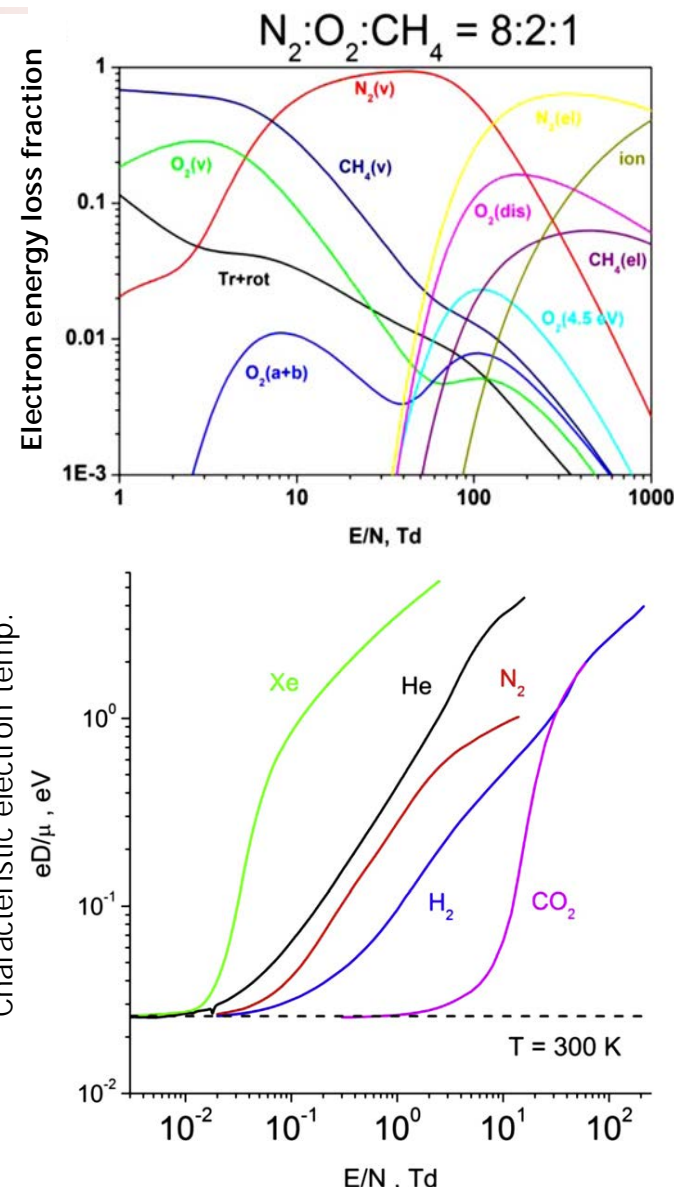
Characteristic energy (eV)



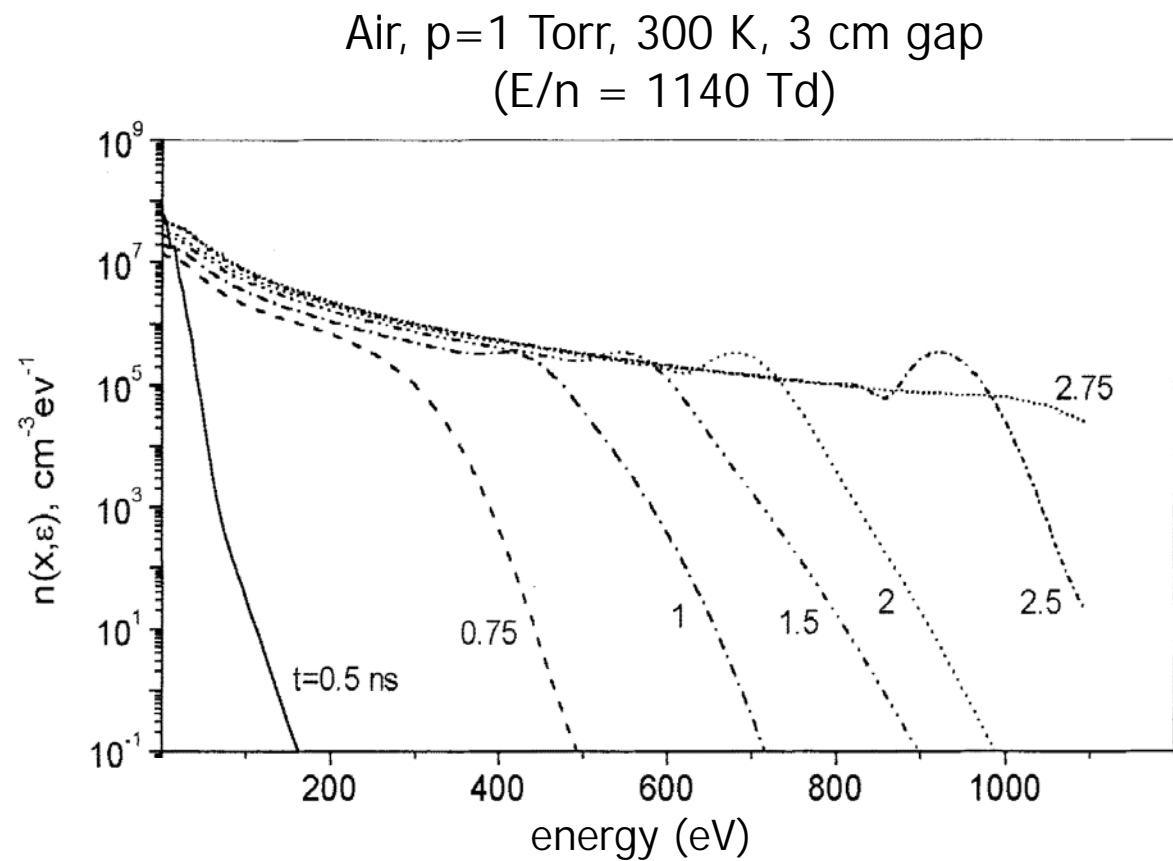
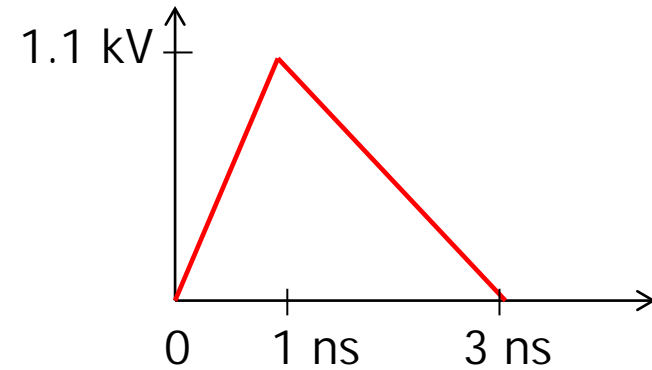
- Reduced electric field  $E/N$  is an important parameter for plasmas ( $1 \text{ Td} = 10^{-17} \text{ V cm}^2$ )
- Note: Breakdown threshold  $\sim 100 \text{ Td}$  (e.g. 120 Td for air)

# Approach to sustain non-equilibrium at high pressures (automotive and aerospace appl.)

- In principle can maintain non-equilibrium by high discharge voltages (i.e. high E/n)
  - (Rate of energy gain by electrons) > (Rate of energy loss to gas heating)
- However at high pressures non-equilibrium discharges are susceptible to Glow-to-Arc Transitions (GAT)
  - Discharge instabilities cause gas temperature to rise rapidly
- GAT has time-scale of ~100's ns
- Can sustain non-equilibrium, by repeated pulsing on nanosecond time scales
  - First demonstration in early 2000 [Kruger et al. 2002]



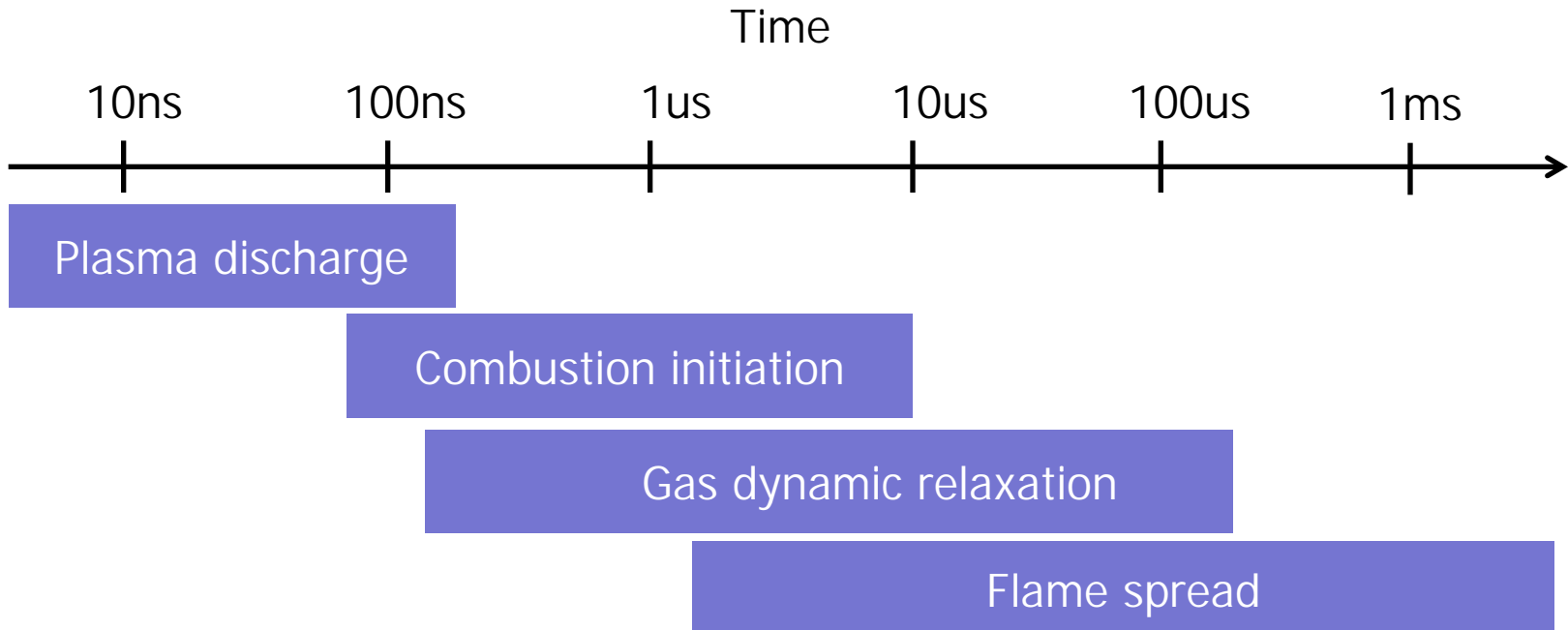
# Nanosecond pulsing produces enhanced tail in the electron Energy Dist. Func. (EEDF)



- Power budget for nanosecond pulsed discharge is much lower than a DC discharge

# Computational challenges for plasma ignition and flame spread prediction

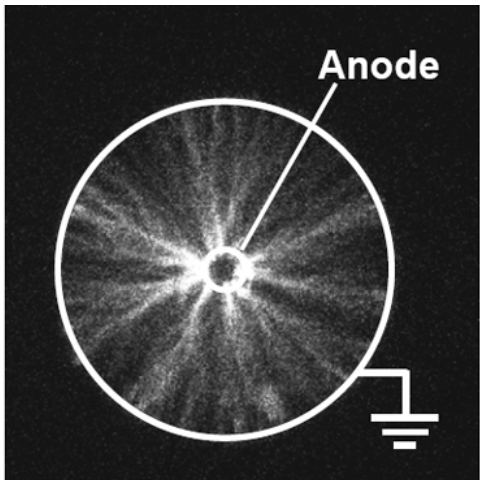
11



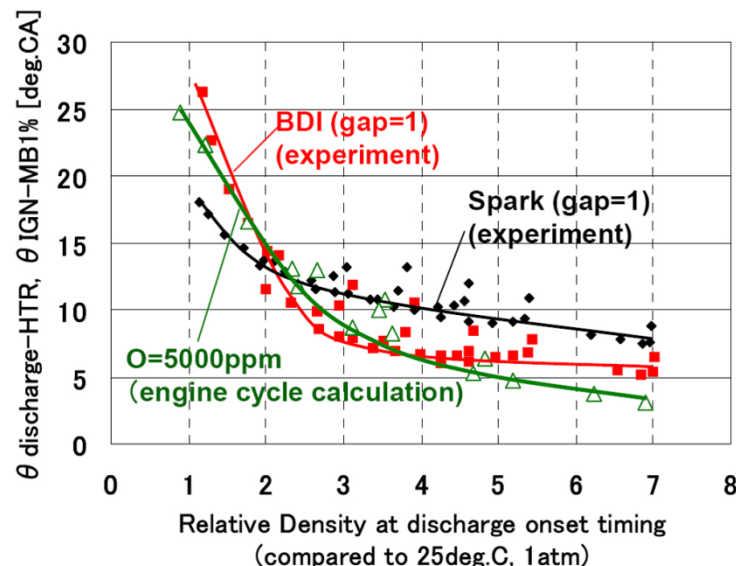
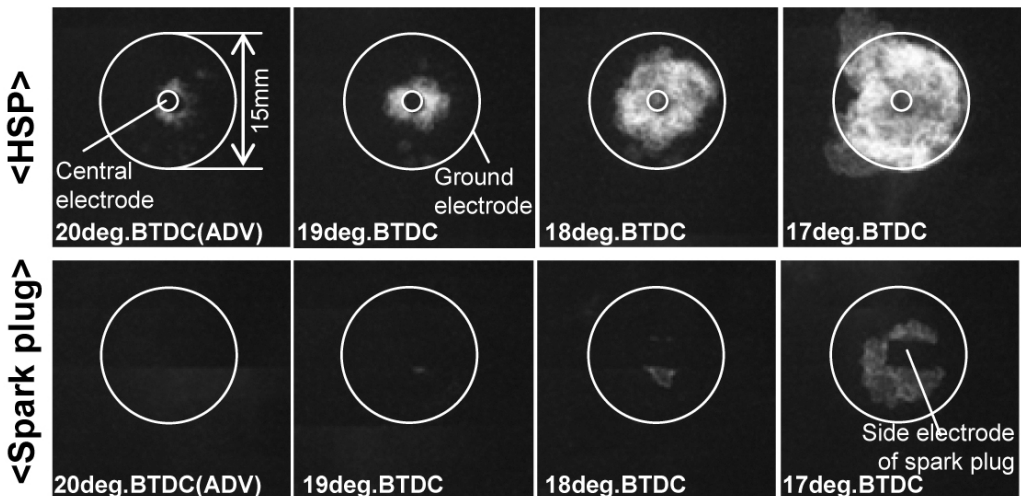
- Multiple physical and chemical processes with vast disparity in time scales
- Complex chemistries with high degree of uncertainty

# Coaxial electrode cold plasma igniter for automotive combustion applications

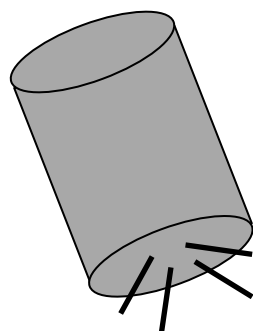
Coaxial electrode igniter



1200 rpm, A/F=15.1( $\Phi=1.0$ ), ADV: 20 deg.BTDC, iso-octane



# Single electrode (Corona) excitation for automotive ignition applications



RF : Freq. ~10 MHz  
Voltage ~100kV

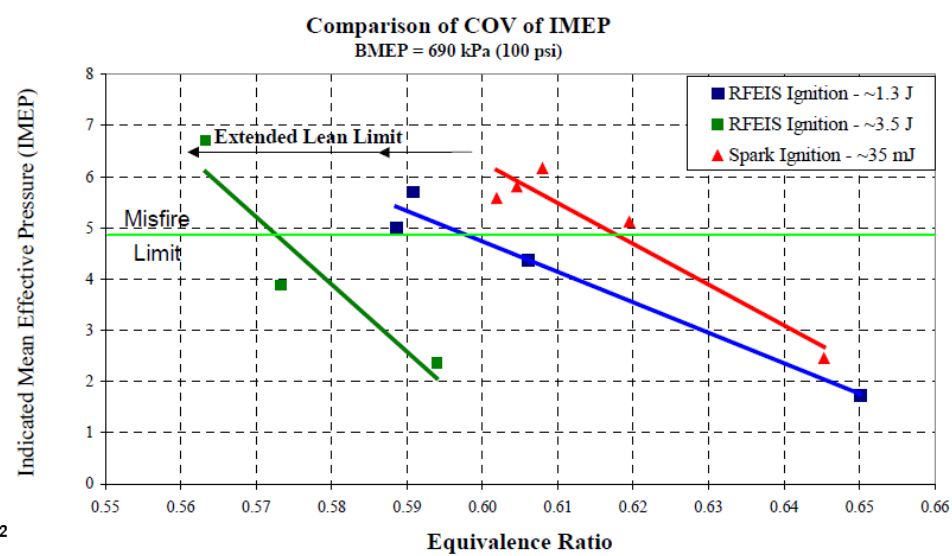
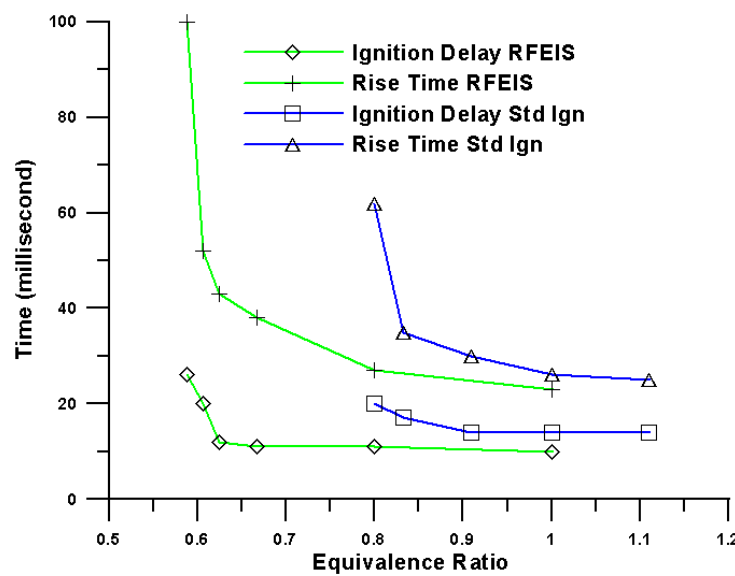
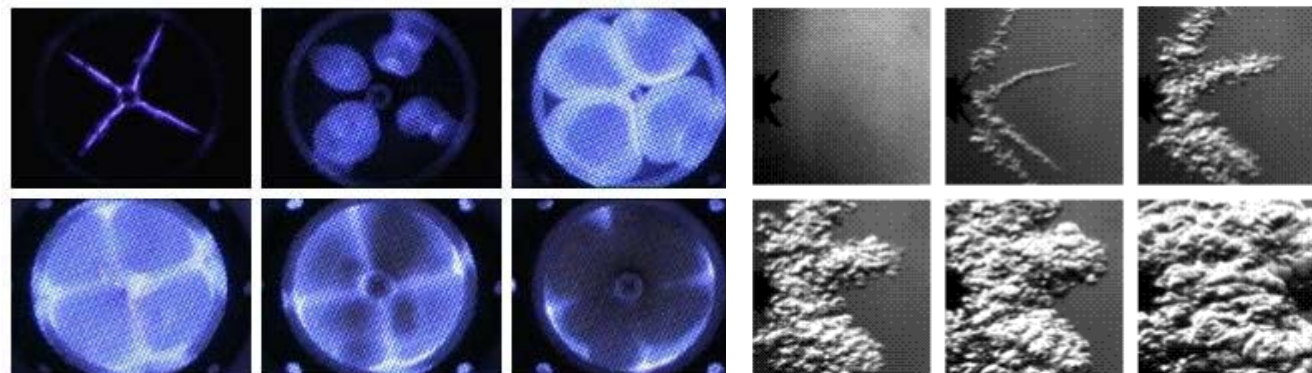
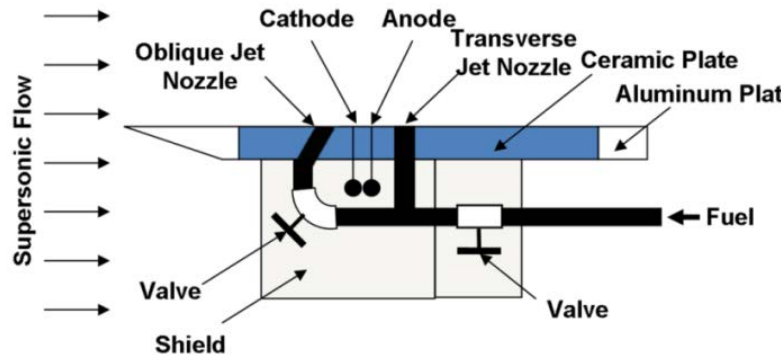
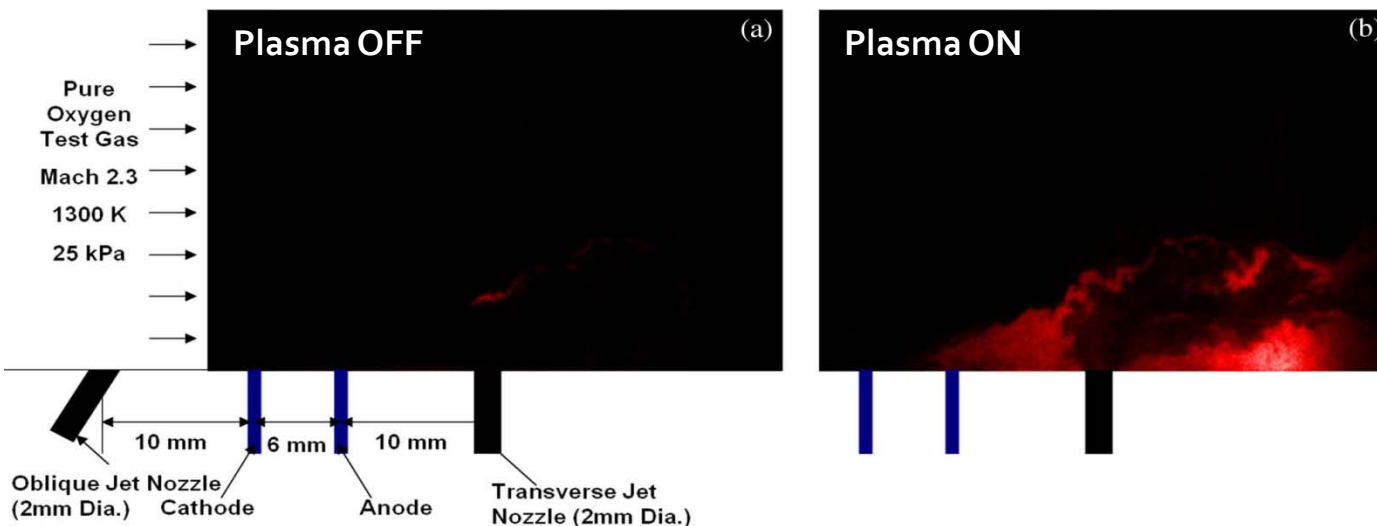


Figure 18. Lean Misfire Limit Comparison at 690 kPa BMEP

# Nanosecond pulsed ignition of supersonic combustion



- 7 kV unipolar pulses
- 20 ns pulse width
- 50 kHz pulse freq.



OH PLIF

# Approach

- High fidelity multi-dimensional computational simulations of the plasma processes relevant to plasma assisted combustion
  - Self-consistent plasma
  - Multi-species
  - Multi-temperature
  - Gas-phase kinetics
  - Surface kinetics
- Plasma model + Gas dynamic model
  - Two-way gas dynamic / plasma coupling

# Plasma model

- Species continuity

$$\frac{\partial n_k}{\partial t} + \vec{\nabla} \cdot \vec{f}_k = \dot{G}_k \quad k = 1, \dots, K_g (k \neq k_b)$$

- Ideal Gas Law

$$p = \sum_k n_k k_B T_k$$

- Drift-Diffusion approximation with bulk convection

$$\vec{f}_k \equiv n_k \vec{u}_k = -\mu_k n_k \vec{\nabla} \phi - D_k \vec{\nabla} n_k + n_k \vec{V}$$

- Poisson's equation

$$\nabla^2 \phi = -\frac{e}{\epsilon_0} \sum_k Z_k n_k$$

- Electron Energy Equation

$$\frac{\partial e_e}{\partial t} + \vec{\nabla} \cdot ((\frac{5}{3} \mu_e \vec{E} + \vec{V}) e_e - \kappa_e \vec{\nabla} e_e) = (+e \vec{f}_e \cdot \vec{\nabla} \phi) - \frac{3}{2} k_B n_e \frac{2m_e}{m_{k_b}} (T_e - T_g) \bar{v}_{k,k_b} - e \sum_i \Delta E_i^e r_i$$

# Plasma model

- Gas Energy Equation
  - Ions and Neutrals have temperature  $T_g$
  - $T_g$  assumed constant, or obtained by solving Gas Energy

$$\frac{\partial \sum_{k \in H} n_k h_k}{\partial t} + \vec{\nabla} \cdot (\sum_{k \in H} \vec{f}_k h_k - \sum_{k \in H} \kappa_k \vec{\nabla} T_g) = \eta_{\text{Th}} (-e \sum_{k \in H} \vec{f}_k \cdot \vec{\nabla} \phi) + \frac{3}{2} k_B n_e \frac{2m_e}{m_{k_b}} (T_e - T_g) \bar{v}_{k,k_b} - e \sum_i \Delta E_i^g r_i$$

$$S_{T_g}$$

- If plasma model is solved with flow model,  $T_g$  is obtained from Navier-Stokes solver and only source terms are calculated by Gas Energy module

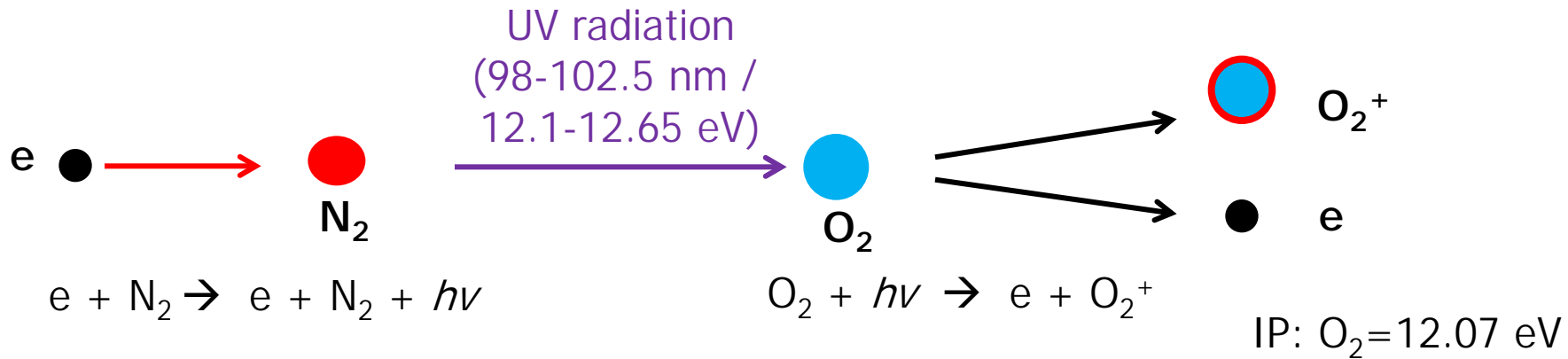
# Flow model (Compressible Navier-Stokes)

$$\iiint_V \frac{\partial \mathbf{U}}{\partial t} dV + \iint_{\partial V} \vec{\mathbf{F}}_{\text{inviscid}} \cdot \hat{n} dS = \iint_{\partial V} \vec{\mathbf{F}}_{\text{viscous}} \cdot \hat{n} dS + \iiint_V \mathbf{S} dV$$

$$\mathbf{U} = \begin{bmatrix} \rho \\ \rho u \\ \rho v \\ \rho e_t \end{bmatrix} \quad \mathbf{F}_{\text{inviscid}} = \begin{bmatrix} \rho u \\ \rho u^2 + p \\ \rho uv \\ (\rho e_t + p)u \end{bmatrix} \hat{i} + \begin{bmatrix} \rho v \\ \rho vu \\ \rho v^2 + p \\ (\rho e_t + p)v \end{bmatrix} \hat{j}$$

$$\mathbf{F}_{\text{viscous}} = \begin{bmatrix} 0 \\ \tau_{xx} \\ \tau_{xy} \\ u \tau_{xx} + v \tau_{xy} - \dot{q}_x \end{bmatrix} \hat{i} + \begin{bmatrix} 0 \\ \tau_{yx} \\ \tau_{yy} \\ u \tau_{yx} + v \tau_{yy} - \dot{q}_y \end{bmatrix} \hat{j} \quad \mathbf{S} = \begin{bmatrix} 0 \\ f_x \\ f_y \\ S + \vec{\mathbf{f}}_{\text{ES}} \cdot \vec{\mathbf{V}} \end{bmatrix}$$

# Photoionization (3-term Helmholtz equation model)



Integral Model (Zheleznyak et al 1982):

$$S_{ph}(\vec{r}) = \iiint \frac{I(\vec{r}') g(R)}{4\pi R^2} dV$$

Emission function:

$$I(\vec{r}) = \frac{P_q}{P + P_q} \xi S_i(\vec{r})$$

Absorption function:

$$\frac{g(R)}{P_{O2}} = \frac{\exp^{-\chi_{min} P_{O2} R} - \exp^{-\chi_{max} P_{O2} R}}{P_{O2} R \ln(\chi_{max}/\chi_{min})}$$

3-term expansion approach :

$$\nabla^2 S_{ph}^j - (\lambda_j P_{O2})^2 S_{ph}^j = -A_j P_{O2}^2 I(\vec{r}) \quad (j = 1, 2, 3)$$

$$S_{ph}(\vec{r}) = S_{ph}^1 + S_{ph}^2 + S_{ph}^3$$

	$A_j \text{ (cm}^{-1} \text{ Torr}^{-1}\text{)}$	$\lambda_j \text{ (cm}^{-1} \text{ Torr}^{-1}\text{)}$
$S_{ph}^1$	0.0067	0.0447
$S_{ph}^2$	0.0346	0.1121
$S_{ph}^3$	0.3059	0.5994

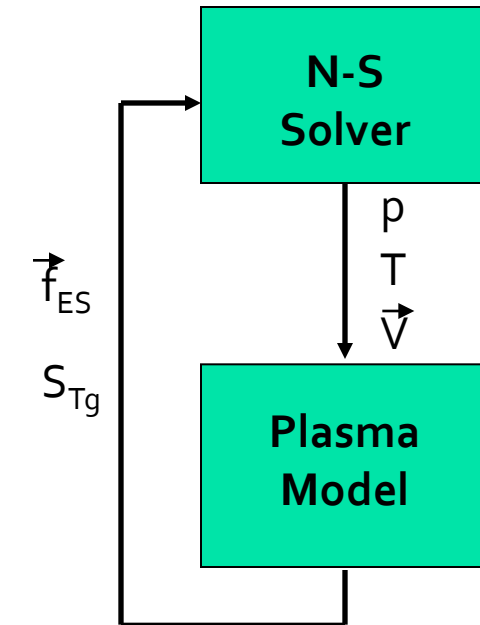
\* Luque A, Ebert U, Montijn C and Hundsorfer W 2007 Appl. Phys. Lett. 90 08150

+ Bourdon A, Pasko NP, Liu NY, Celestin S, Segue P and Maroude E 2007 Plasma Sources Sci. Technol. 16 656

# Mathematical approach to coupling plasma and flow physics

Electrostatic Force Term (No Magnetic field):

$$\vec{f}_{ES} = e \sum_k Z_k n_k \vec{E}$$



Gas Energy Source Term

$$S_{T_g} = \eta_{Th} (-e \sum_{k \in H} \vec{f}_k \cdot \vec{\nabla} \phi) + \frac{3}{2} k_B n_e \frac{2m_e}{m_{k_b}} (T_e - T_g) \bar{v}_{k,k_b} - e \sum_i \Delta E_i^g r_i$$

# Numerical approach

- 1D, 2D, 3D
- Fully unstructured, hybrid mesh
- Finite-volume spatial discretization, backward Euler time discretization (formally 1<sup>st</sup> order in space and time)
- Flow model:
  - AUSM family of spatial discretization  
(2<sup>nd</sup> order accuracy through gradient reconstruction)
  - 4<sup>th</sup> order RK time integration
- Domain decomposition parallel enabled

# Plasma chemistry mechanism

- Methane-air plasma chemistry mechanism
  - Species and pathways relevant to plasma time scale ( $\sim 10$ 's ns)

■ 26 Species :  
 $E$ ,  $O$ ,  $N_2$ ,  $O_2$ ,  $H$ ,  $N_2^+$ ,  $O_2^+$ ,  $N_4^+$ ,  $O_4^+$ ,  $O_2^+N_2$ ,  $O_2^-$ ,  $O^-$ ,  $O_2(a1)$ ,  $O_2(b1)$ ,  $O_2^*$ ,  
 $N_2(A)$ ,  $N_2(B)$ ,  $N_2C$ ,  $N_2(a1)$ ,  $CH_4$ ,  $CH_3$ ,  $CH_2$ ,  $CH_4^+$ ,  $CH_3^+$ ,  $CH_2^-$ ,  $H^-$

■ 85 Reactions :  
1) electron impact, 2) ion-ion, 3) ion-neutral, 4) neutral-neutral

# Methane-air plasma mechanism

Rxn	Reaction	A	B	C	Activation energy (eV)	Ref.
$G_1$	$E + N_2 \rightarrow E + N_2$ (rotational)	BOLSIG+			0.02	(22)
$G_2$	$E + N_2 \rightarrow E + N_2$ (vibrational)				1.0	(22)
$G_3$	$E + N_2 \rightarrow E + N_2(A)$				6.17	(22)
$G_4$	$E + N_2 \rightarrow E + N_2(B)$				7.35	(22)
$G_5$	$E + N_2 \rightarrow E + N_2(B)$				7.36	(22)
$G_6$	$E + N_2 \rightarrow E + N_2(B)$				8.16	(22)
$G_7$	$E + N_2 \rightarrow E + N_2(a1)$				8.4	(22)
$G_8$	$E + N_2 \rightarrow E + N_2(a1)$				8.55	(22)
$G_9$	$E + N_2 \rightarrow E + N_2(a1)$				8.89	(22)
$G_{10}$	$E + N_2 \rightarrow E + N_2(C)$				11.03	(22)
$G_{11}$	$E + N_2 \rightarrow E + N_2$ (electronic)	BOLSIG+			11.88	(22)
$G_{12}$	$E + N_2 \rightarrow E + N_2$ (electronic)	BOLSIG+			12.25	(22)
$G_{13}$	$E + N_2 \rightarrow E + N_2$ (electronic)	BOLSIG+			13.0	(22)
$G_{14}$	$E + N_2 \rightarrow 2E + N_2^+$	BOLSIG+			15.6	(22)
$G_{15}$	$E + O_2 \rightarrow E + O_2$ (rotational)	BOLSIG+			0.02	(22)
$G_{16}$	$E + O_2 \rightarrow E + O_2$	BOLSIG+			0.0193	(22)
$G_{17}$	$E + O_2 \rightarrow E + O_2(a1)$	BOLSIG+			0.98	(22)
$G_{18}$	$E + O_2 \rightarrow E + O_2(b1)$	BOLSIG+			1.63	(22)
$G_{19}$	$E + O_2 \rightarrow E + O_2^*$	BOLSIG+			4.5	(22)
$G_{20}$	$E + O_2 \rightarrow E + O_2$ (electronic)	BOLSIG+			6.0	(22)
$G_{21}$	$E + O_2 \rightarrow E + O_2$ (electronic)	BOLSIG+			8.4	(22)
$G_{22}$	$E + O_2 \rightarrow E + O_2$ (electronic)	BOLSIG+			9.97	(22)
$G_{23}$	$E + O_2 \rightarrow E + 2O$	BOLSIG+			5.58	(22)
$G_{24}$	$E + O_2 \rightarrow E + 2O$ ( $O + O(^1D)$ )	BOLSIG+			8.4	(22)
$G_{25}$	$E + O_2 \rightarrow 2E + O_2^+$	BOLSIG+			12.07	(22)
$G_{26}$	$E + O \rightarrow E + O$	BOLSIG+			6.34	(22)
$G_{27}$	$E + CH_4 \rightarrow E + CH_4$ (vibrational)	BOLSIG+			0.36	(23)
$G_{28}$	$E + CH_4 \rightarrow E + CH_4$	BOLSIG+			0.162	(23)
$G_{29}$	$E + CH_4 \rightarrow 2E + CH_4^+$	BOLSIG+			12.6	(23)
$G_{30}$	$E + CH_4 \rightarrow 2E + CH_3^+ + H$	BOLSIG+			14.3	(23)
$G_{31}$	$E + CH_4 \rightarrow E + CH_3 + H$	BOLSIG+			9.0	(23)
$G_{32}$	$E + CH_4 \rightarrow E + CH_3 + H$	BOLSIG+			10.0	(23)
$G_{33}$	$E + CH_4 \rightarrow E + CH_3 + H$	BOLSIG+			11.0	(23)
$G_{34}$	$E + CH_4 \rightarrow E + CH_3 + H$	BOLSIG+			12.0	(23)
$G_{35}$	$E + O_2^+ \rightarrow O + O$	BOLSIG+			-0.691	(22)
$G_{36}$	$E + O_4^+ \rightarrow O_2 + O_2$	BOLSIG+			-12.07	(22)
$G_{37}$	$E + O_2 \rightarrow O^- + O$	BOLSIG+			4.66	(22)
$G_{38}$	$E + CH_4 \rightarrow H^- + CH_3$	BOLSIG+			9.0	(22)
$G_{39}$	$E + CH_4 \rightarrow CH_2^- + CH_2$	BOLSIG+			10.8	(22)
$G_{40}$	$E + O_2(a1) \rightarrow E + O_2(b1)$	BOLSIG+			0.65	(22)
$G_{41}$	$E + O_2(a1) \rightarrow E + 2O$	BOLSIG+			6.34	(22)
$G_{42}$	$E + O_2(a1) \rightarrow O^- + O$	BOLSIG+			3.9	(22)
$G_{43}$	$E + O_2(b1) \rightarrow O^- + O$	BOLSIG+			3.7	(22)

# Methane-air plasma mechanism

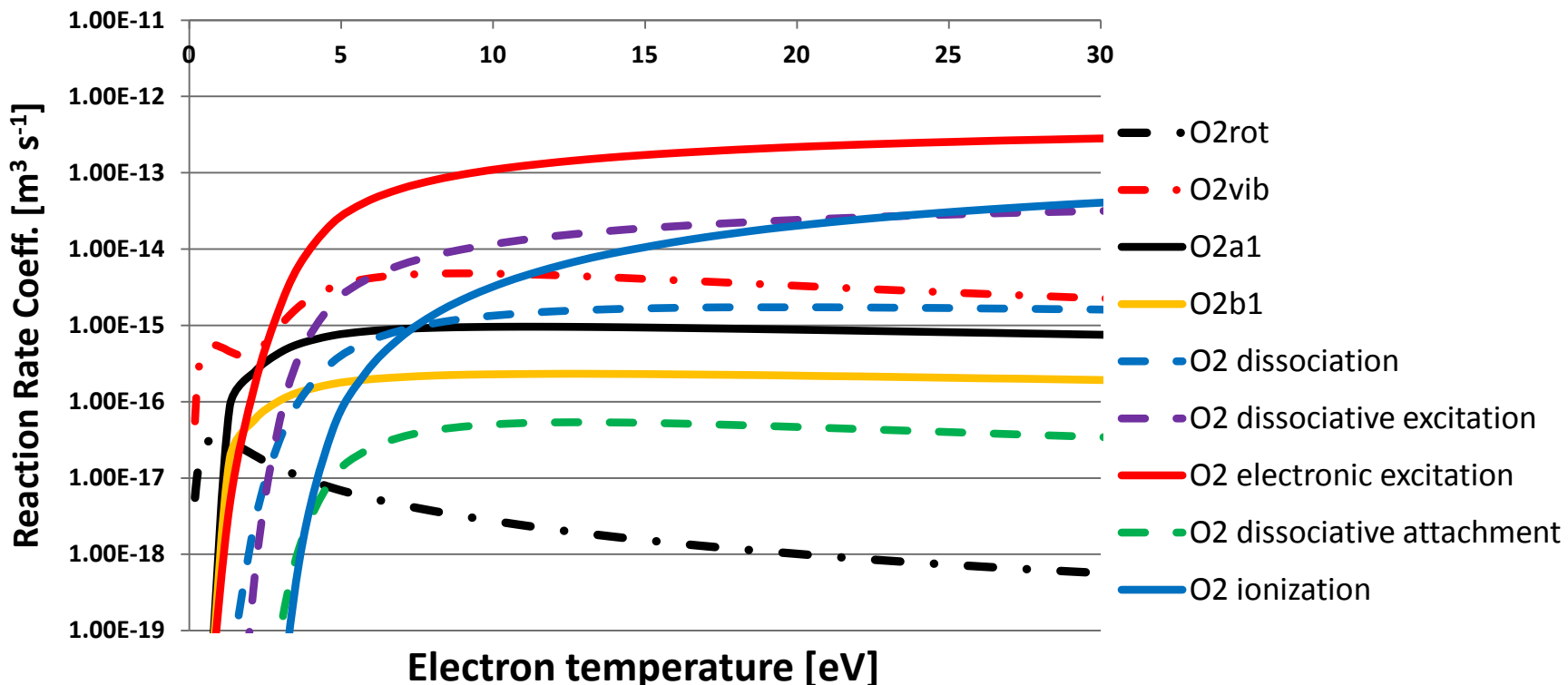
cluster ion formation  
 charge exchange  
 attachment  
 ion-ion recomb.  
 Neutral reactions  
 dissociative charge ex.  
 charge exchange  
 dissociative recomb.

Rxn	Reaction	A	B	C	Activation energy (eV)	Ref.
G <sub>44</sub>	N <sub>2</sub> <sup>+</sup> + N <sub>2</sub> + M → N <sub>4</sub> <sup>+</sup> + M	5.0e-41	0	0	1.0	(24)
G <sub>45</sub>	N <sub>4</sub> <sup>+</sup> + O <sub>2</sub> → O <sub>2</sub> <sup>+</sup> + 2N <sub>2</sub>	2.5e-16	0	0	-3.51	(24)
G <sub>46</sub>	N <sub>2</sub> <sup>+</sup> + O <sub>2</sub> → O <sub>2</sub> <sup>+</sup> + N <sub>2</sub>	1.04e-15	-0.5	0	-3.51	(24)
G <sub>47</sub>	O <sub>2</sub> <sup>+</sup> + 2N <sub>2</sub> → O <sub>2</sub> +N <sub>2</sub> + N <sub>2</sub>	8.1e-38	-2.0	0	-	(24)
G <sub>48</sub>	O <sub>2</sub> +N <sub>2</sub> + N <sub>2</sub> → O <sub>2</sub> <sup>+</sup> + 2N <sub>2</sub>	14.8	-5.3	2357	-	(24)
G <sub>49</sub>	O <sub>2</sub> +N <sub>2</sub> + O <sub>2</sub> → O <sub>4</sub> <sup>+</sup> + N <sub>2</sub>	1.0e-15	0	0	-	(24)
G <sub>50</sub>	O <sub>2</sub> <sup>+</sup> + O <sub>2</sub> + M → O <sub>4</sub> <sup>+</sup> + M	2.03e-34	-3.2	0	-	(24)
G <sub>51</sub>	E + 2O <sub>2</sub> → O <sub>2</sub> <sup>-</sup> + O <sub>2</sub>	6.0e-39	-1.0	0	-0.43	(24)
G <sub>52</sub>	O <sub>2</sub> <sup>-</sup> + O <sub>4</sub> <sup>+</sup> → 3O <sub>2</sub>	1.0e-13	0	0	-11.64	(24)
G <sub>53</sub>	O <sub>2</sub> <sup>-</sup> + O <sub>4</sub> <sup>+</sup> + M → 3O <sub>2</sub> + M	3.12e-31	-2.5	0	-11.64	(24)
G <sub>54</sub>	O <sub>2</sub> <sup>-</sup> + O <sub>2</sub> <sup>+</sup> + M → 2O <sub>2</sub> + M	3.12e-31	-2.5	0	-11.64	(24)
G <sub>55</sub>	O <sup>-</sup> + O <sub>2</sub> <sup>+</sup> → O + O <sub>2</sub>	3.464e-12	-0.5	0	-10.61	(24)
G <sub>56</sub>	N <sub>2</sub> A + O <sub>2</sub> → N <sub>2</sub> + 2O	1.7e-18	0	0	-1.05	(25)
G <sub>57</sub>	N <sub>2</sub> A + O <sub>2</sub> → N <sub>2</sub> + O <sub>2</sub> (b1)	7.5e-19	0	0	-4.54	(25)
G <sub>58</sub>	N <sub>2</sub> A + N <sub>2</sub> (A) → N <sub>2</sub> + N <sub>2</sub> (B)	7.7e-17	0	0	-4.99	(25)
G <sub>59</sub>	N <sub>2</sub> A + N <sub>2</sub> (A) → N <sub>2</sub> + N <sub>2</sub> (C)	1.6e-16	0	0	-1.31	(25)
G <sub>60</sub>	N <sub>2</sub> (A) + N <sub>2</sub> → N <sub>2</sub> + N <sub>2</sub> (B)	1.0e-16	0	1500	-0.32	(25)
G <sub>61</sub>	N <sub>2</sub> (A) + O → N <sub>2</sub> + O	3.0e-17	0	0	-6.17	(25)
G <sub>62</sub>	N <sub>2</sub> (B) + O <sub>2</sub> → N <sub>2</sub> + 2O	3.0e-16	0	0	-2.23	(25)
G <sub>63</sub>	N <sub>2</sub> (B) + N <sub>2</sub> → N <sub>2</sub> (A) + N <sub>2</sub>	1.0e-17	0	0	-1.18	(25)
G <sub>64</sub>	N <sub>2</sub> (a1) + O <sub>2</sub> → N <sub>2</sub> + 2O	2.8e-17	0	0	-3.28	(25)
G <sub>65</sub>	N <sub>2</sub> (a1) + N <sub>2</sub> → N <sub>2</sub> + N <sub>2</sub>	2.0e-19	0	0	-8.4	(25)
G <sub>66</sub>	N <sub>2</sub> (C) + O <sub>2</sub> → N <sub>2</sub> + 2O	3.0e-16	0	0	-5.91	(25)
G <sub>67</sub>	N <sub>2</sub> (C) + N <sub>2</sub> → N <sub>2</sub> (a1) + N <sub>2</sub>	1.0e-17	0	0	-2.63	(25)
G <sub>68</sub>	N <sub>2</sub> (C) → N <sub>2</sub> (B) + hν (photon)	3.0	0	0	-	(25)
G <sub>69</sub>	N <sub>2</sub> (A) + CH <sub>4</sub> → N <sub>2</sub> + CH <sub>4</sub>	3.0e-21	0	0	-6.17	(25)
G <sub>70</sub>	N <sub>2</sub> (B) + CH <sub>4</sub> → N <sub>2</sub> (A) + CH <sub>4</sub>	2.85e-16	0	0	-1.08	(25)
G <sub>71</sub>	N <sub>2</sub> (B) + CH <sub>4</sub> → N <sub>2</sub> + CH <sub>3</sub> + H	1.5e-17	0	0	3.15	(25)
G <sub>72</sub>	N <sub>2</sub> (a1) + CH <sub>4</sub> → N <sub>2</sub> + CH <sub>3</sub> + H	3.0e-16	0	0	2.1	(25)
G <sub>73</sub>	N <sub>2</sub> (C) + CH <sub>4</sub> → N <sub>2</sub> + CH <sub>3</sub> + H	3.0e-16	0	0	-0.8	(25)
G <sub>74</sub>	O <sub>2</sub> <sup>*</sup> + CH <sub>4</sub> → O <sub>2</sub> + CH <sub>3</sub> + H	3.0e-21	0	0	-	(25)
G <sub>75</sub>	O <sub>2</sub> <sup>*</sup> + O <sub>2</sub> → O <sub>2</sub> (a1) + O <sub>2</sub>	1.86e-19	0	0	-3.52	(25)
G <sub>76</sub>	O <sub>2</sub> <sup>*</sup> + O <sub>2</sub> → O <sub>2</sub> (b1) + O <sub>2</sub>	8.1e-20	0	0	-2.87	(25)
G <sub>77</sub>	O <sub>2</sub> <sup>*</sup> + O <sub>2</sub> → O <sub>2</sub> + O <sub>2</sub>	2.3e-20	0	0	-4.5	(25)
G <sub>78</sub>	O <sub>2</sub> <sup>*</sup> + O → O <sub>2</sub> + O	5.0e-18	0	0	-4.5	(25)
G <sub>79</sub>	O <sub>2</sub> <sup>*</sup> + O → O <sub>2</sub> (a1) + O	2.7e-18	0	0	-3.52	(25)
G <sub>80</sub>	O <sub>2</sub> <sup>*</sup> + O → O <sub>2</sub> (b1) + O	1.35e-18	0	0	-2.87	(25)
G <sub>81</sub>	N <sub>2</sub> <sup>+</sup> + CH <sub>4</sub> → N <sub>2</sub> + CH <sub>3</sub> <sup>+</sup> + H	1.3e-15	0	0	-	(25)
G <sub>82</sub>	CH <sub>4</sub> <sup>+</sup> + O <sub>2</sub> → CH <sub>4</sub> + O <sub>2</sub> <sup>+</sup>	5.0e-16	0	0	-	(25)
G <sub>83</sub>	E + CH <sub>4</sub> <sup>+</sup> → CH <sub>3</sub> + H	2.95e-12	-0.5	0	-	(25)
G <sub>84</sub>	E + CH <sub>4</sub> <sup>+</sup> → CH <sub>2</sub> + 2H	2.95e-12	-0.5	0	-	(25)
G <sub>85</sub>	E + CH <sub>3</sub> <sup>+</sup> → CH <sub>2</sub> + H	6.06e-12	-0.5	0	-	(25)

# Electron impact reaction rate coefficient computed using off-line Boltzmann solver

- Bolsig+ (Hagelaar and Pitchford, 2005)

$$\left. \begin{array}{l} k = k(E/N) \\ T_e = T_e(E/N) \end{array} \right\} \quad k = k(T_e) \quad (\text{Recovers non-local aspects of electron energy transport})$$

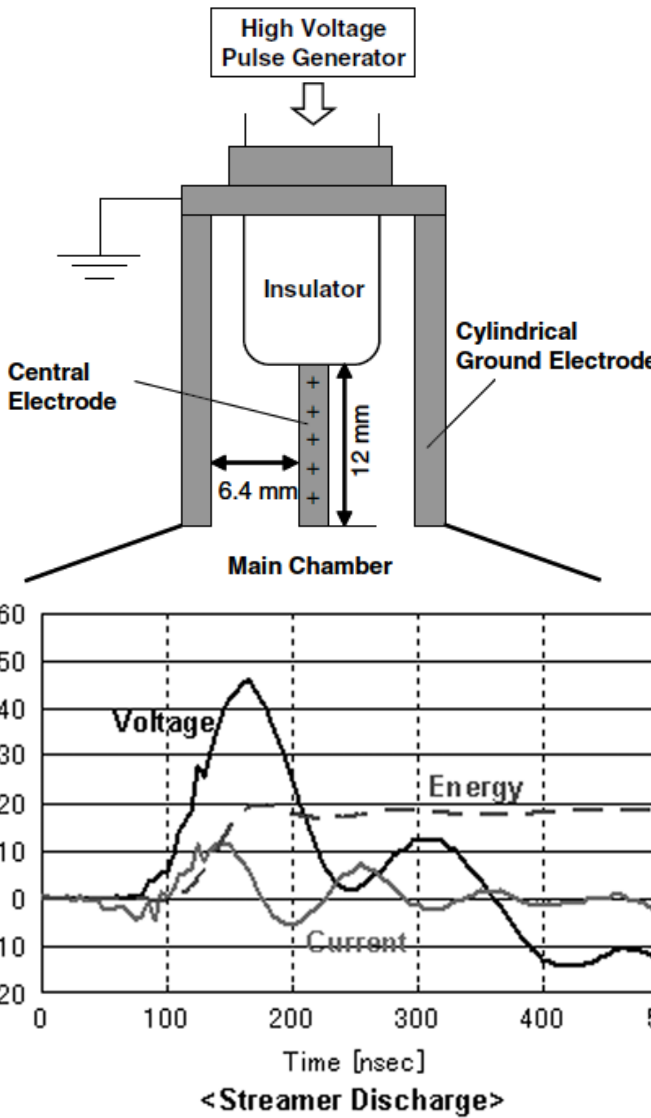


# Coaxial electrode Nanosecond Pulsed Plasma (NSP)

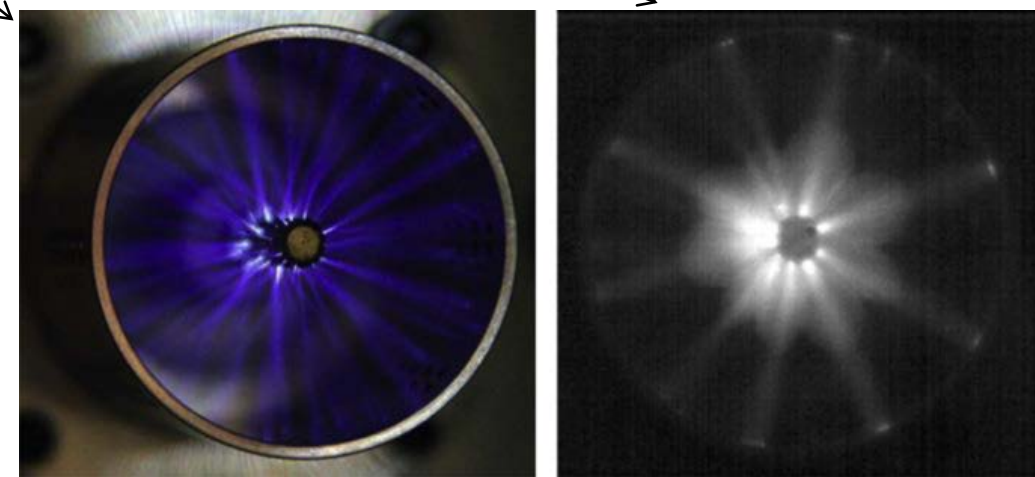
## Reference:

D. Breden, L. L. Raja, C. A. Idicheria, P. M. Najt, and S. Mahadevan, "A numerical study of high-pressure non-equilibrium streamers for combustion ignition application," *Journal of Applied Physics*, Vol. 114, 2013, pp. 083302-1-14.

# Coaxial electrode NSP discharge



- Describe initial plasma kernel formation stage
  - ~ 10's ns of physical time
- Experimental observations
  - Unbranched streamers propagate from inner high-voltage electrode to outer ground electrode
  - Streamer dia (sub-mm)
  - Brighter discharge near inner electrode
  - Flame spreads from inner electrode to outer ground electrode

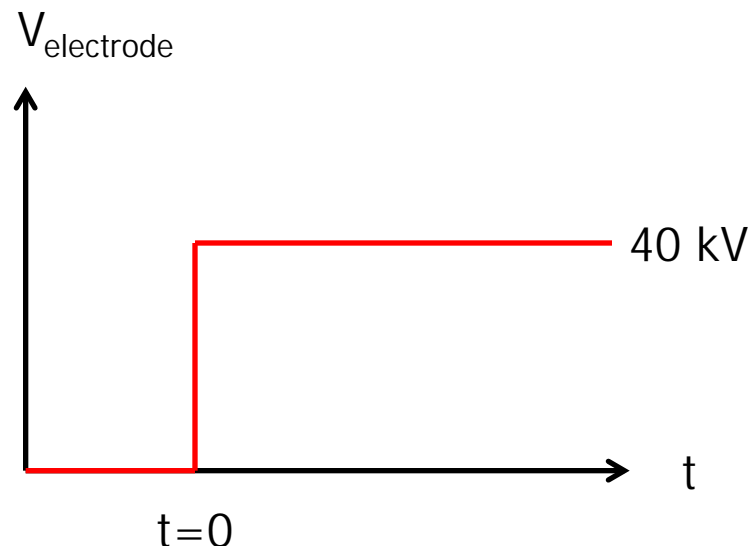


Ref: Shiraishi et al. J Phys. D: Appl. Phys., 42, (2009) 135208.

Ref: D. Singleton, S.J. Pendleton and M. Gundersen, J. Phys. D: Appl. Phys., 2011, Vol. 44, 022001.

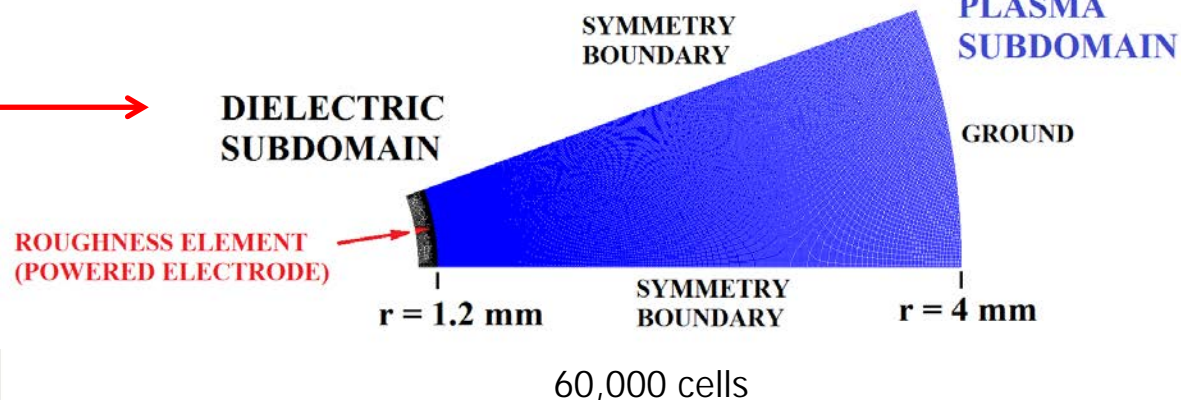
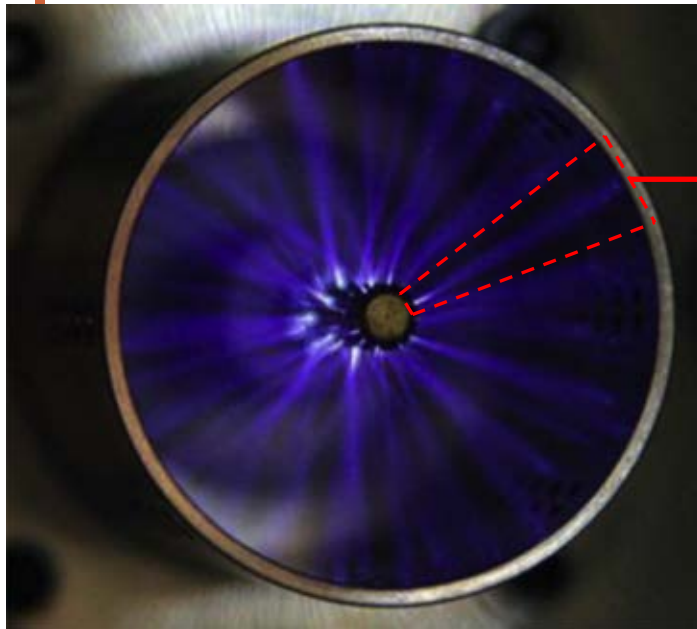
# Coaxial electrode NSP discharge simulation conditions

- Simulation conditions:
  - 10 atmospheres
  - 700 K fixed gas temperature
  - 40 kV applied voltage ( $E/n \sim 143$  Td)
  - lean A/F ratio (40:1 air/methane)

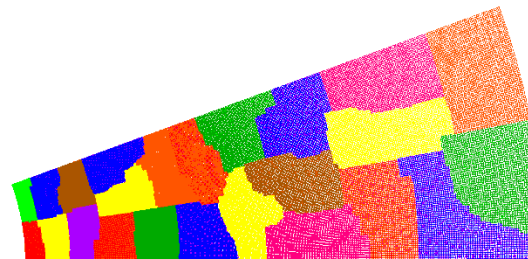


# Coaxial electrode NSP plasma simulation domain

30



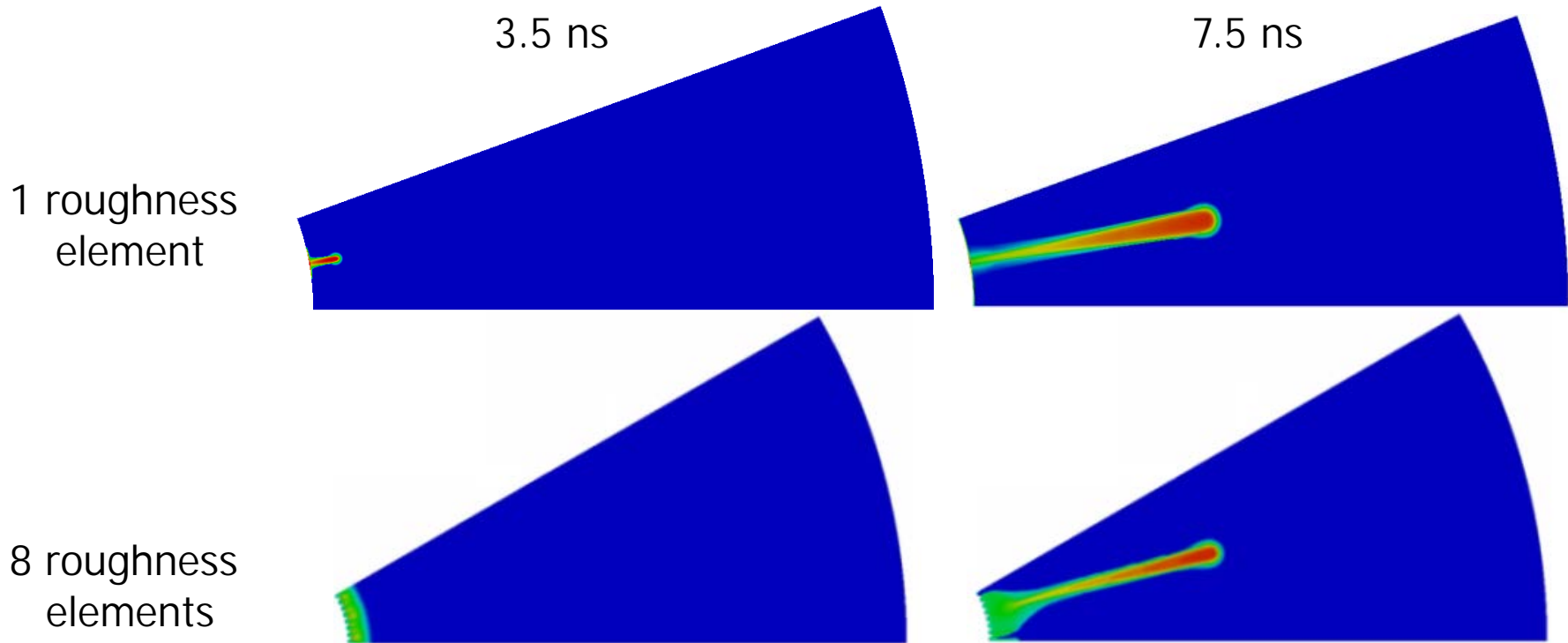
- Simulation domain : sector of circle
  - 20 deg. sector angle
  - Characteristic size for single streamer propagation
  - Roughness element on inner electrode to pin location of streamer



24 processor partition

# Sensitivity to roughness element configuration

Conditions:  $P=10 \text{ atm}$ ,  $T_{\text{gas}}=700 \text{ K}$ ,  $40 \text{ kV}$ ,  $40:1 \text{ A/F ratio (lean)}$

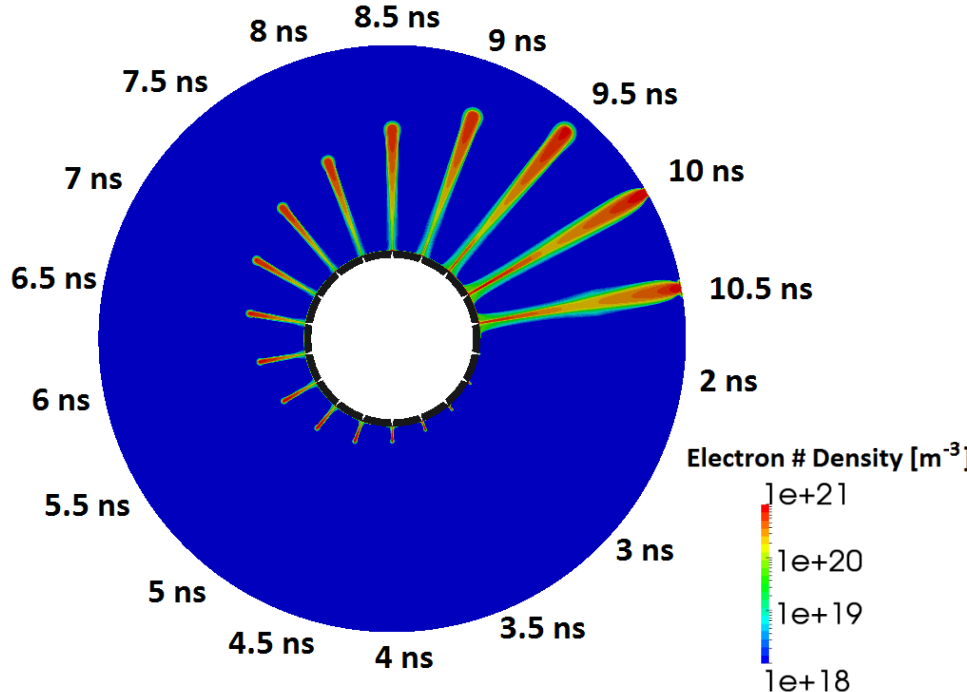


- Verified insensitivity to roughness element configuration
- Verified characteristic sector angle for single streamer

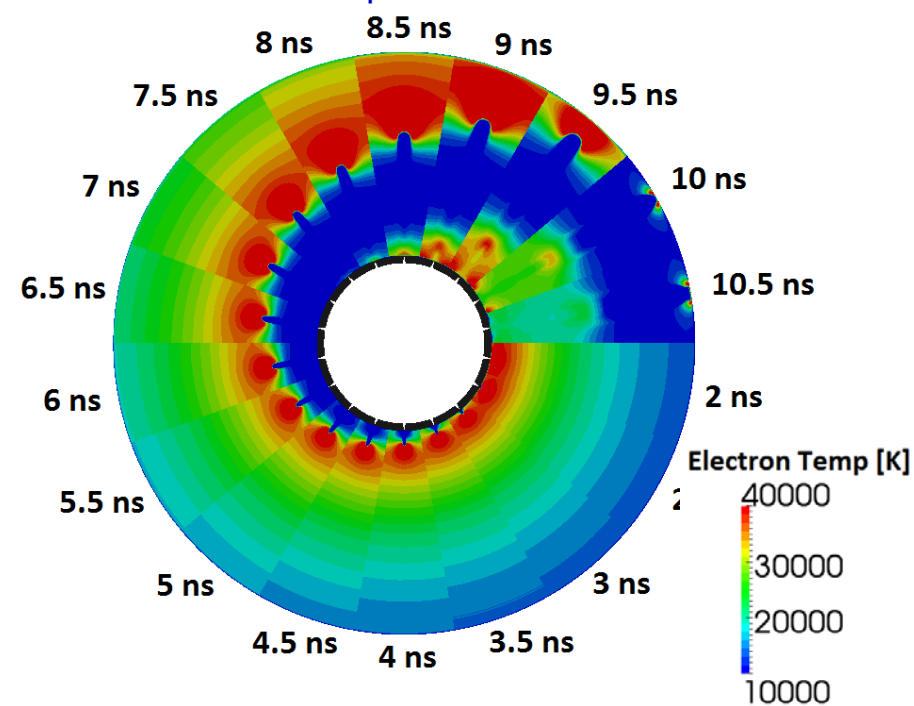
# Time evolution of electron density and temperature for coaxial electrode NSP

Conditions:  $P=10$  atm,  $T_{\text{gas}}=700$  K, 40 kV, 40:1 A/F ratio (lean)

Electron density transient



Electron temperature transient

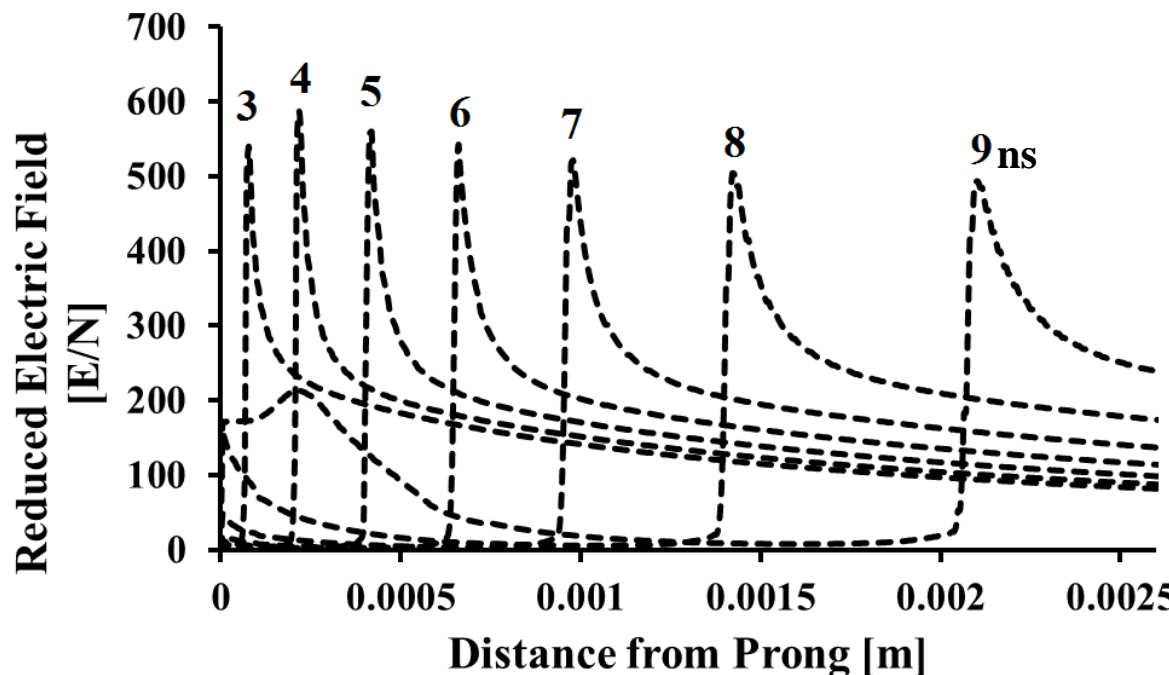


- 2 ns induction time (defined: time to reach threshold of  $10^{19} \text{ m}^{-3}$ )
- Streamers bridge electrode gap in about 10 ns
- $N_e(\text{peak}) \sim 10^{21} \text{ m}^{-3}$ ,  $T_e(\text{head}) \sim 4\text{eV}$ ,  $T_e(\text{body}) \sim 1\text{eV}$
- Secondary streamer (electron attachment luminosity? Self-sustaining?)

# Reduced electric field profiles along axis of coaxial electrode NSP

33

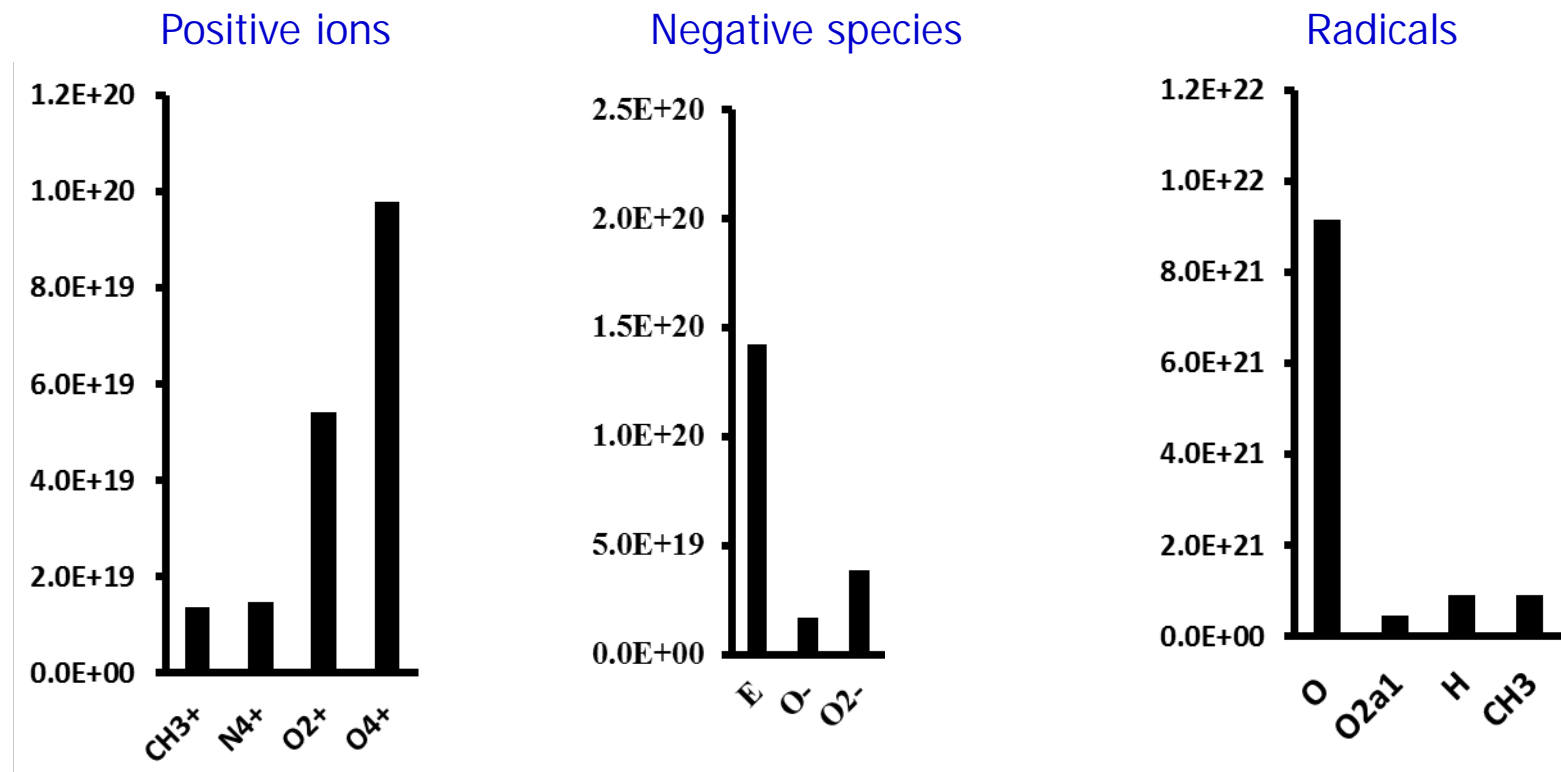
Conditions:  $P=10 \text{ atm}$ ,  $T_{\text{gas}}=700 \text{ K}$ , 40 kV, 40:1 A/F ratio (lean)



- Recall breakdown  $E/n$  about 120 Td (for air)
- Head of streamer has significant over-voltages ( $\sim 500 \text{ Td}$ )  $\rightarrow$  high  $T_e$
- Body of streamer has no sustaining E-field ( $E/n \sim 10 \text{ Td}$ )  $\rightarrow$  low  $T_e$
- Secondary streamer formation at end of pulse with  $E/n \sim 200 \text{ Td}$

# Species yields for coaxial electrode NSP (volume-averaged at 9.5 ns)

Conditions: P=10 atm, T<sub>gas</sub>=700 K, 40 kV, 40:1 A/F ratio (lean)

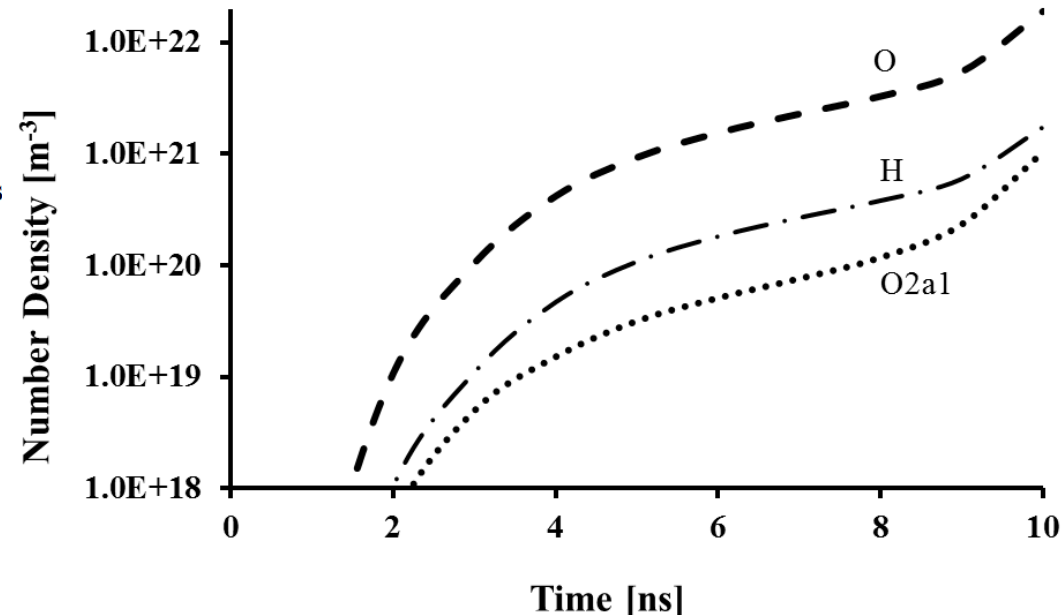
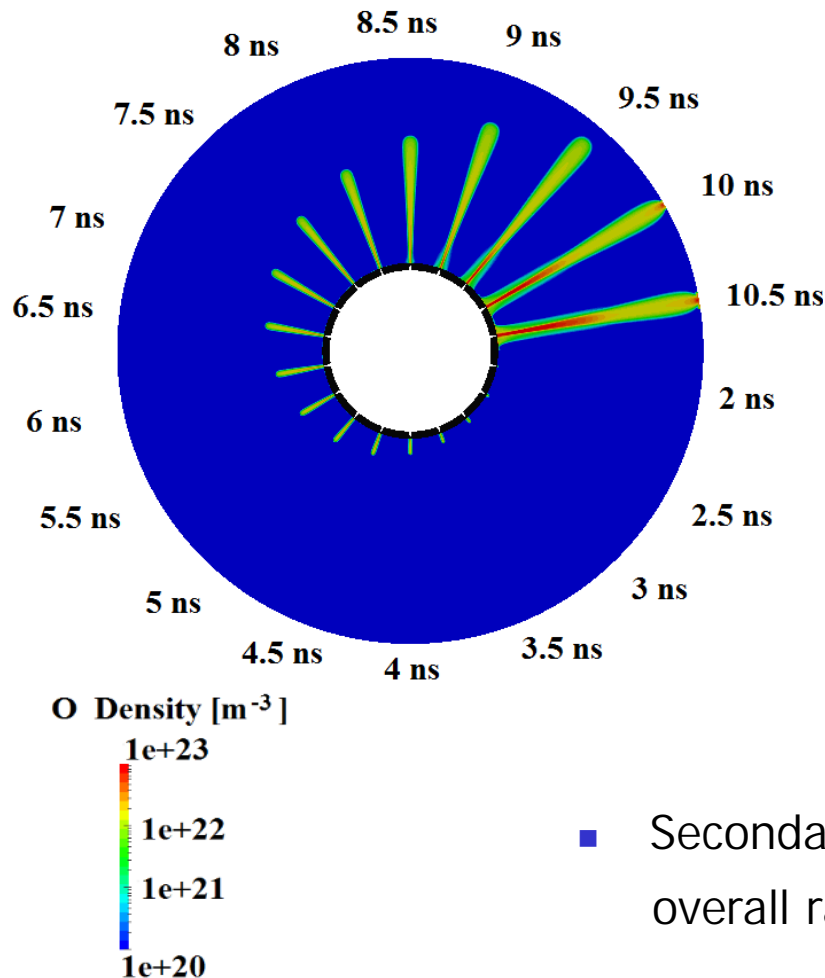


- Charged species ( $\sim 10^{20} \text{ m}^{-3}$ )
- Dominant radical O ( $\sim 10^{22} \text{ m}^{-3}$ )

# Time evolution of radical densities and for coaxial electrode NSP

Conditions:  $P=10$  atm,  $T_{\text{gas}}=700$  K, 40 kV, 40:1 A/F ratio (lean)

O radical density transient

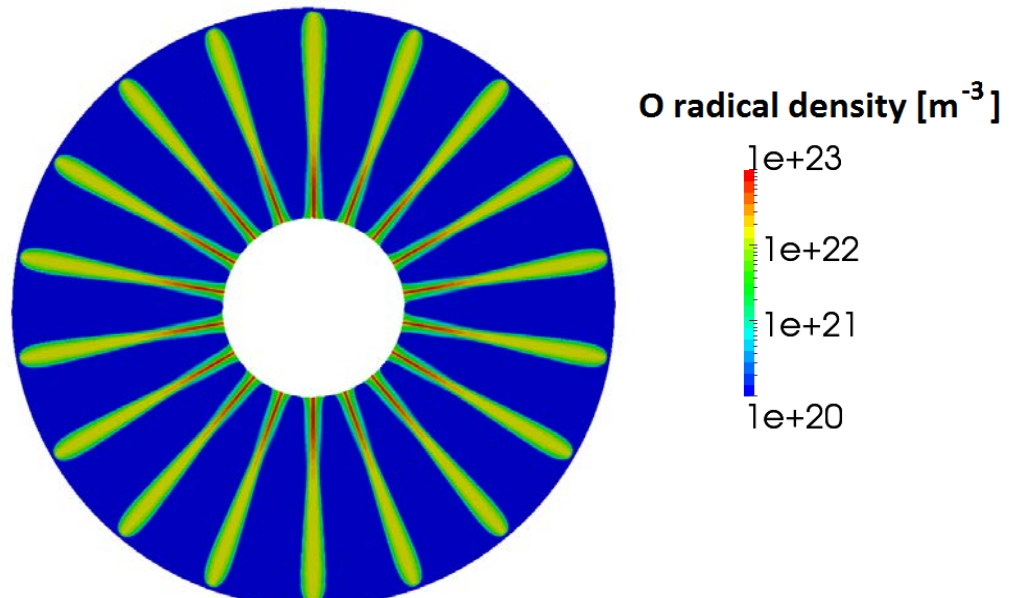


- Secondary streamer has significant impact on overall radical yield

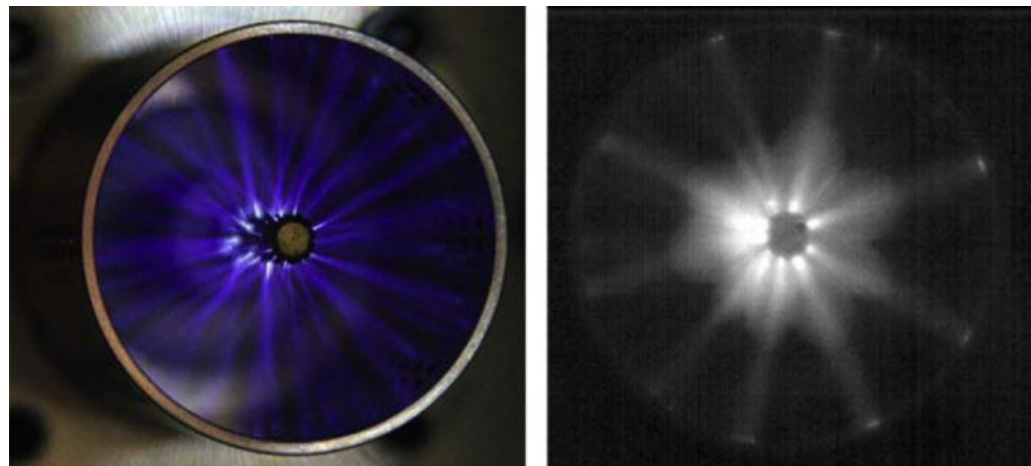
# O radical distribution in coaxial electrode NSP at end of transient

- Significant non-uniformity in O radical distribution

- $\sim 10^{23} \text{ m}^{-3}$  at inner electrode
  - Consequence of secondary streamer



- O radical concentration is evidence for experimentally observed flame spread profile ?

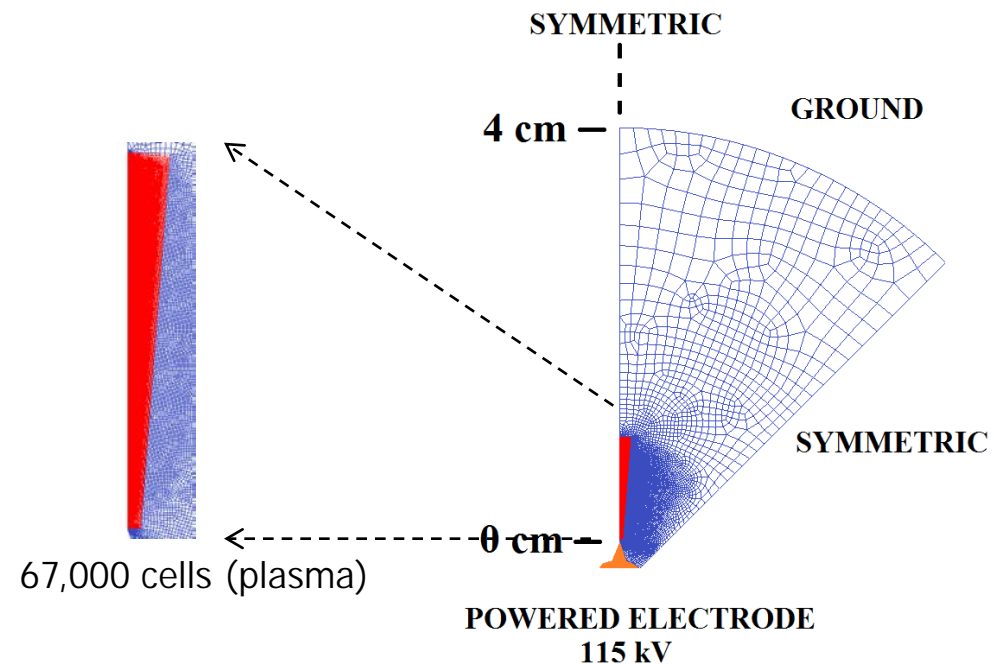
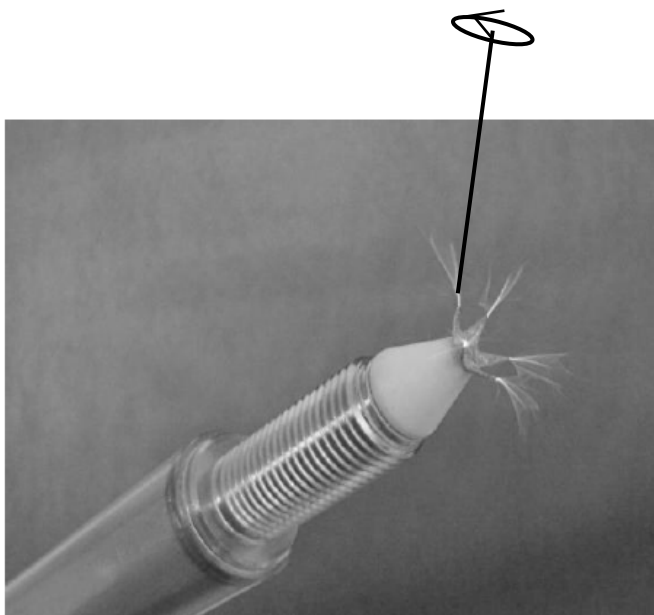


# Corona ignition – point to plane at infinity

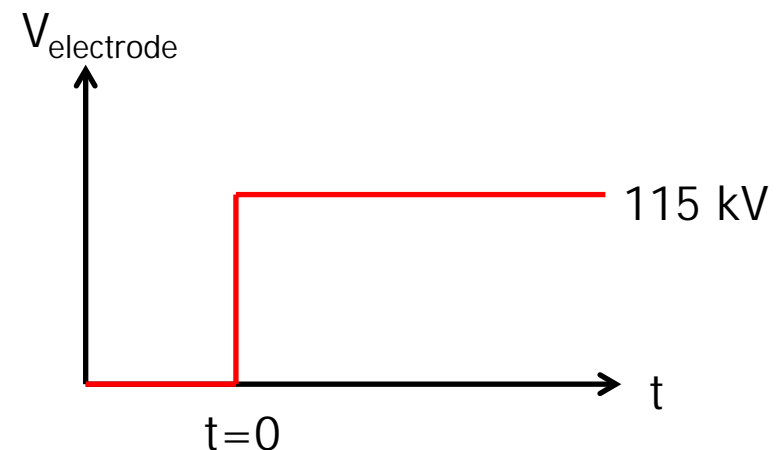
## Reference:

D. Breden, L. L. Raja, C. A. Idicheria, P. M. Najt, and S. Mahadevan, "A numerical study of high-pressure non-equilibrium streamers for combustion ignition application," *Journal of Applied Physics*, Vol. 114, 2013, pp. 083302-1-14.

# Corona igniter

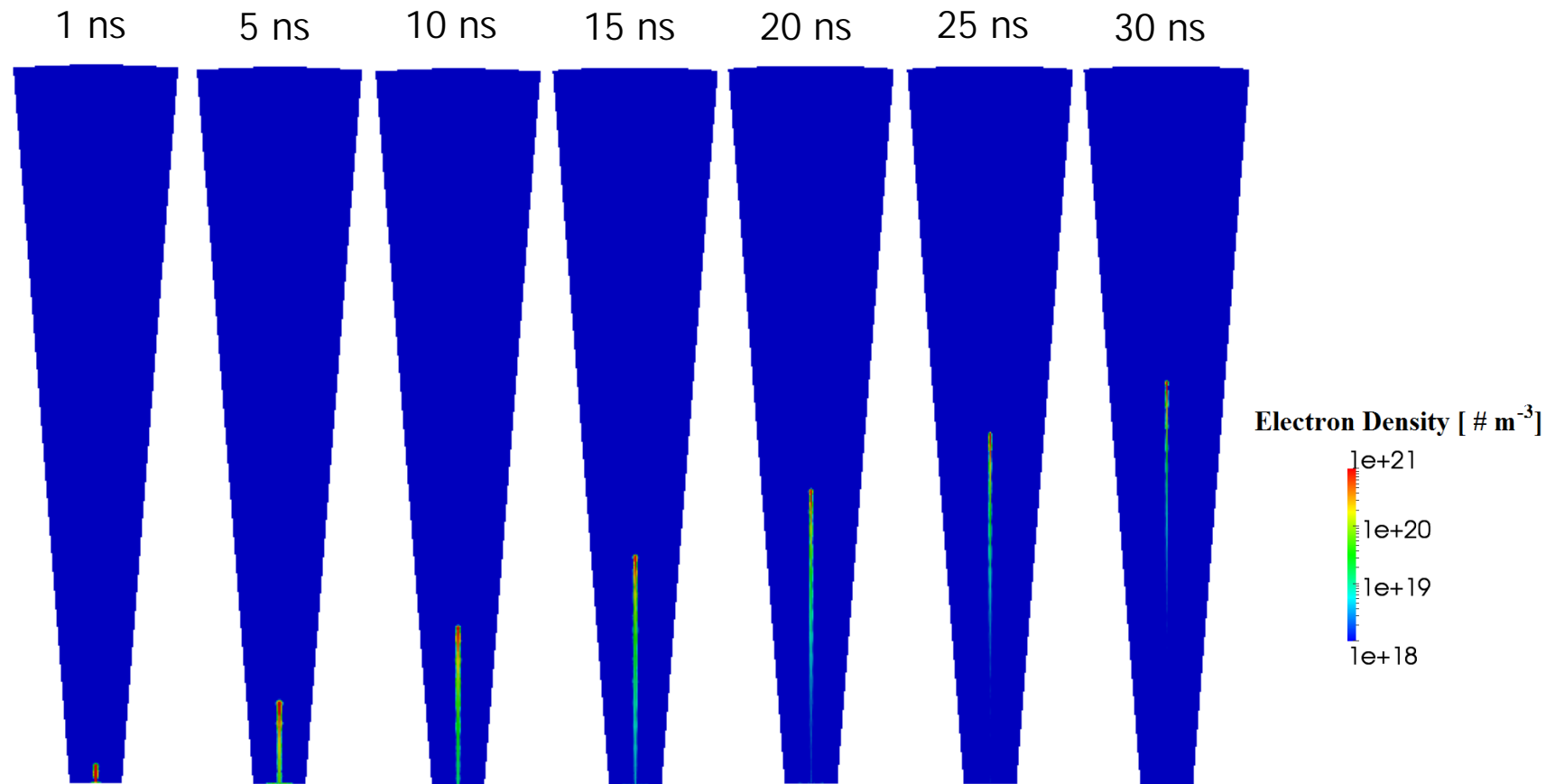


- Simulation conditions:
  - 10 atmospheres
  - 700 K fixed gas temperature
  - 115 kV applied voltage
  - lean A/F ratio (40:1 air/methane)



# Transient evolution of electron density

Conditions:  $P=10$  atm,  $T_{\text{gas}}=700$  K, 115 kV, 40:1 A/F ratio (lean)

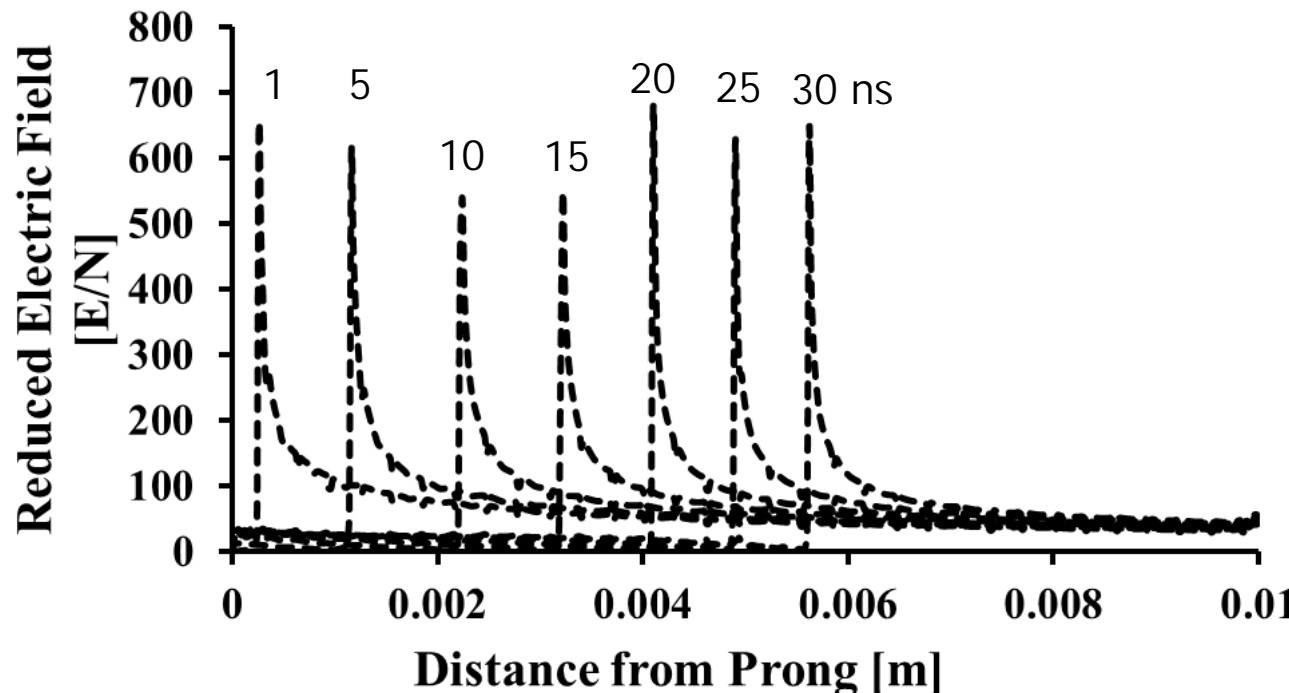


- Peak electron densities in streamer head ( $\sim 10^{21} \text{ m}^{-3}$ )
- Electron attachment in body

# Reduced electric field profiles along axis of coaxial electrode NSP

40

Conditions:  $P=10 \text{ atm}$ ,  $T_{\text{gas}}=700 \text{ K}$ , 115 kV, 40:1 A/F ratio (lean)

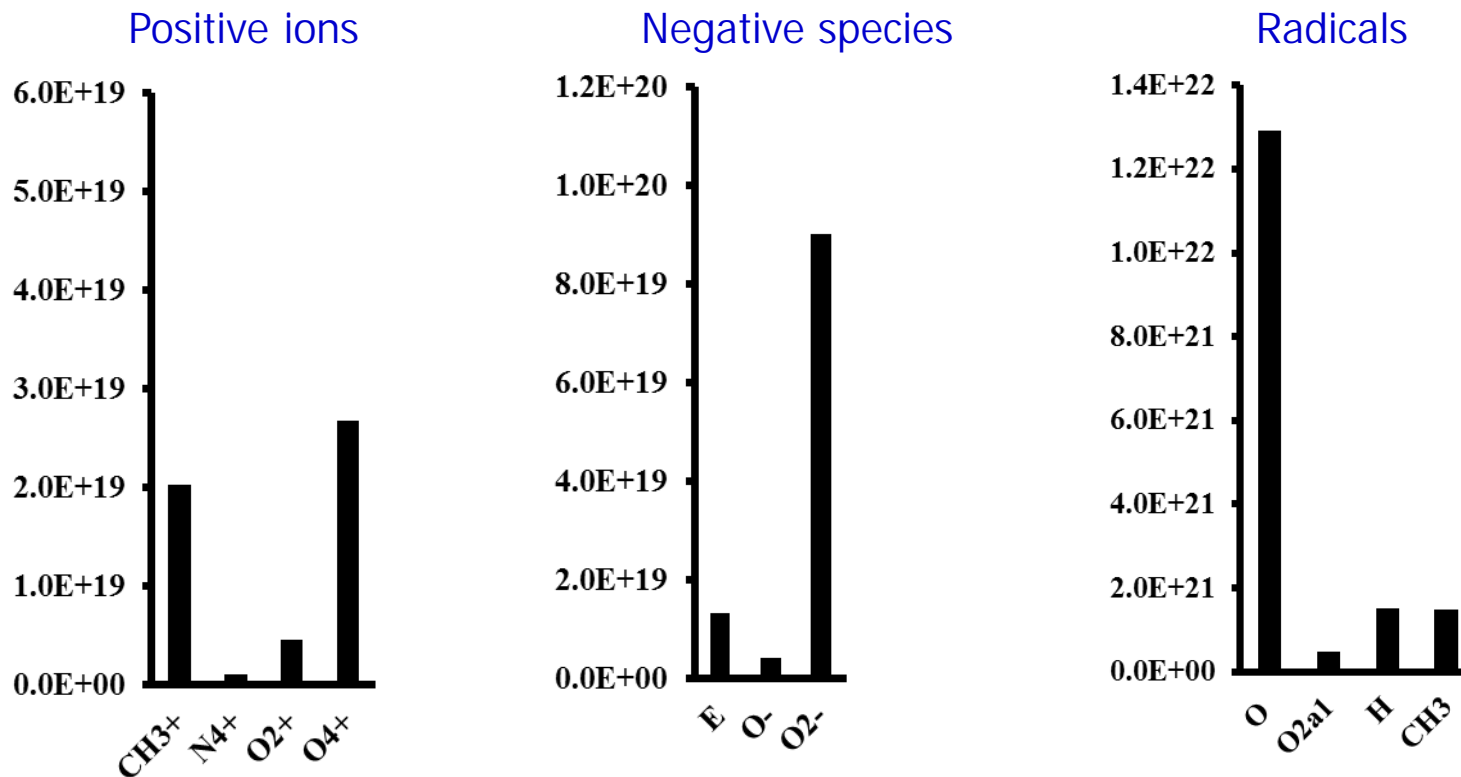


- Recall breakdown  $E/n$  about 120 Td (for air)
- Head of streamer has significant over-voltages ( $\sim 500 \text{ Td}$ )  $\rightarrow$  high  $T_e$
- Body of streamer has no sustaining E-field ( $E/n \sim 10 \text{ Td}$ )  $\rightarrow$  low  $T_e$
- No secondary streamer formation

# Species yields for single electrode geometry (volume-averaged at 30 ns)

41

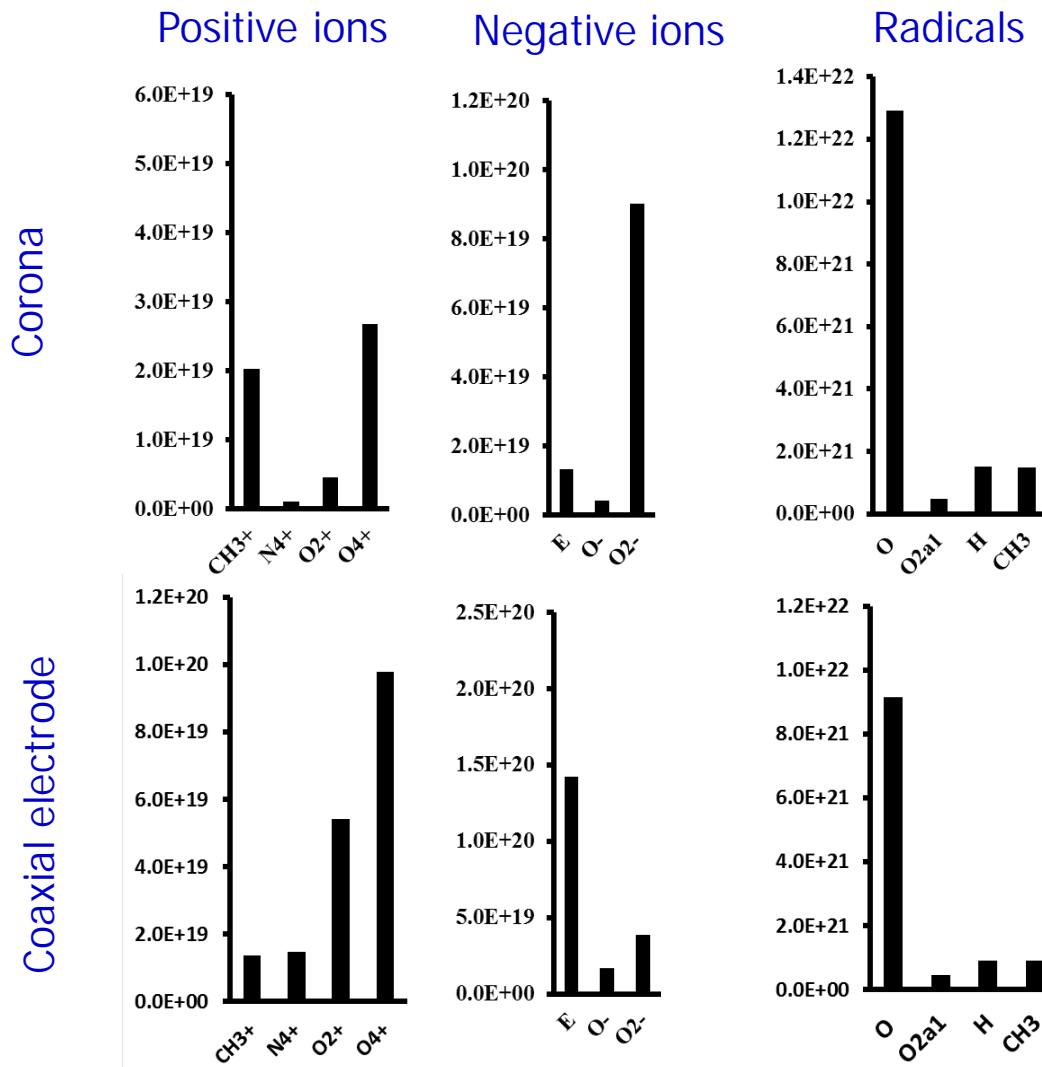
Conditions:  $P=10$  atm,  $T_{\text{gas}}=700$  K, 115 kV, 40:1 A/F ratio (lean)



- Charged species ( $\sim 10^{20} \text{ m}^{-3}$ )
- Dominant radical O ( $\sim 10^{22} \text{ m}^{-3}$ )

# Comparison of species yields for Corona and Coaxial electrode geometries

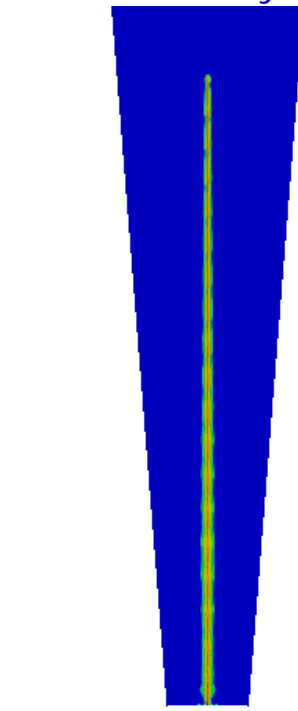
42



# Time evolution of radical densities and for coaxial electrode NSP

Baseline Conditions:  $P=10$  atm,  $T_{\text{gas}}=700$  K, 40 kV, 40:1 A/F ratio (lean)

O radical density at 30 ns



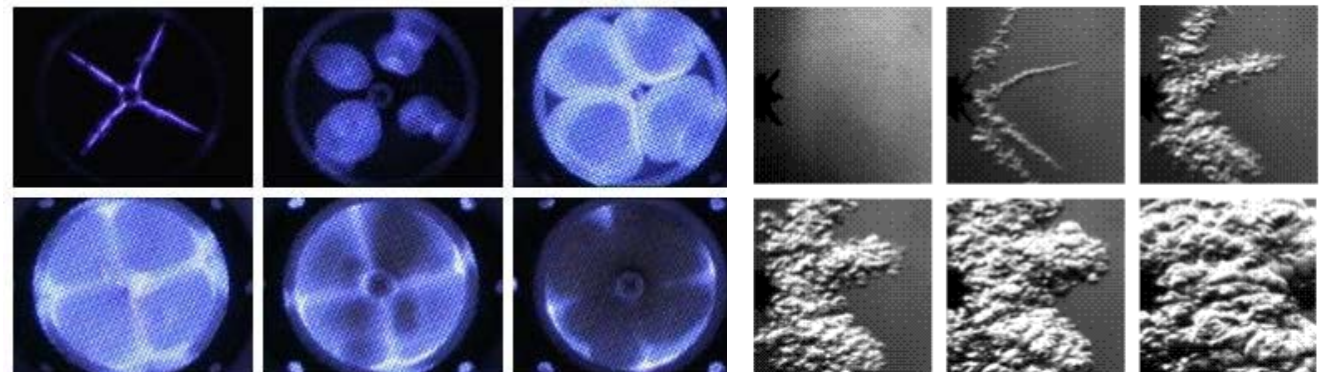
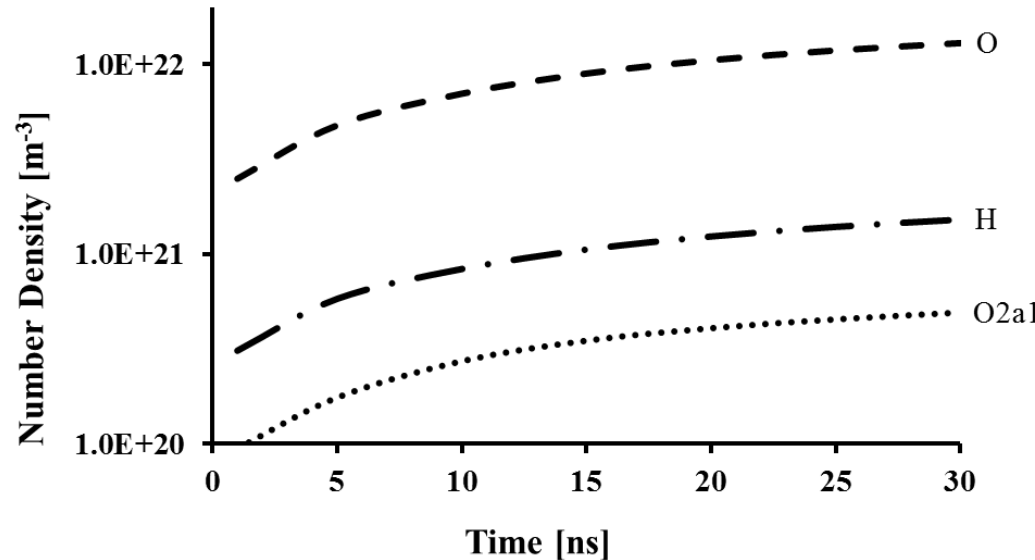
O Density [ $\text{m}^{-3}$ ]

$1\text{e}^{23}$

$1\text{e}^{22}$

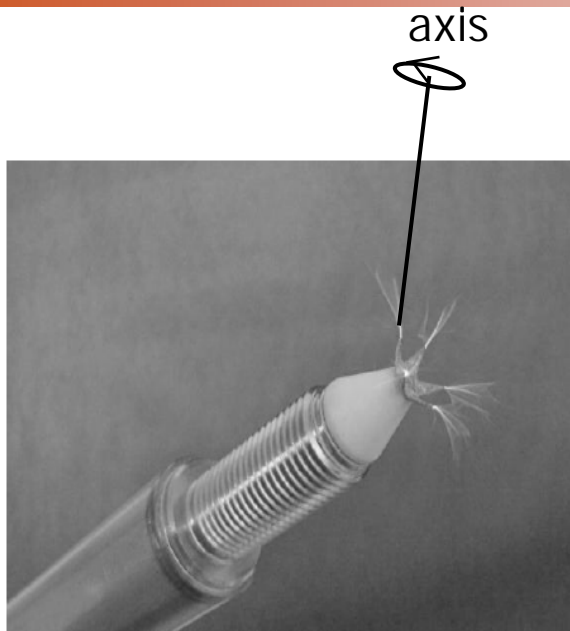
$1\text{e}^{21}$

$1\text{e}^{20}$

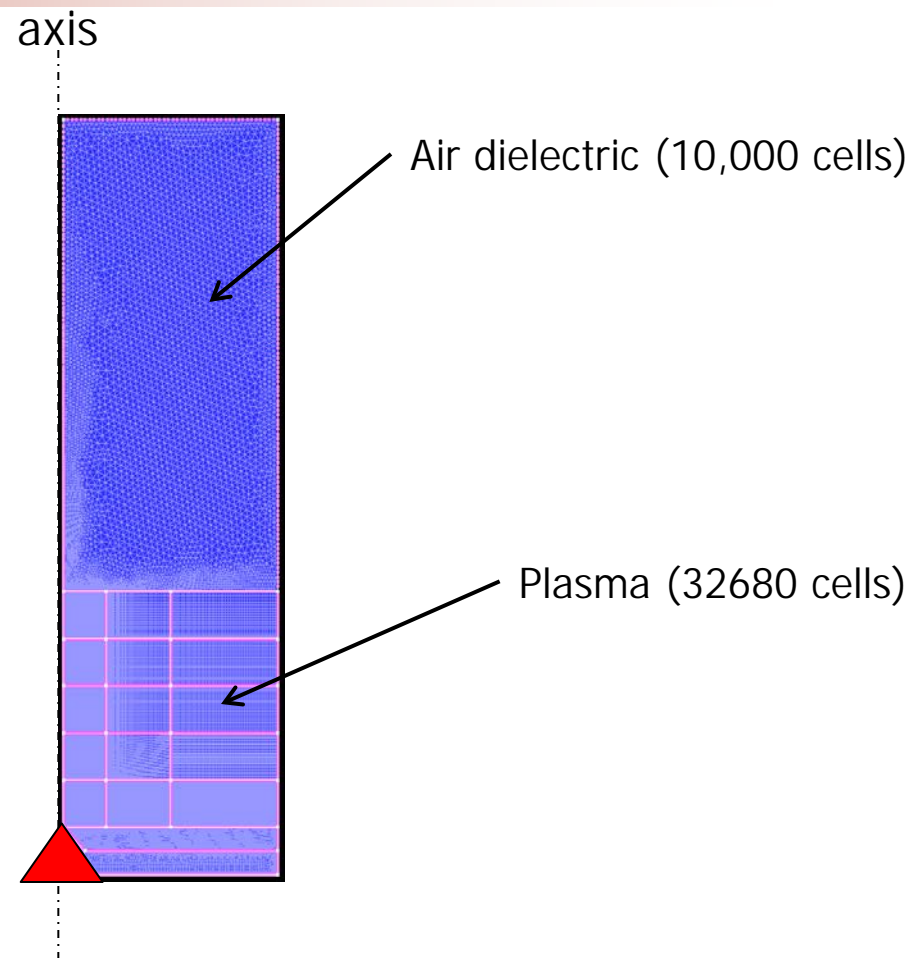


# Corona RF excitation

# Problem statement for Corona RF excited plasma igniter

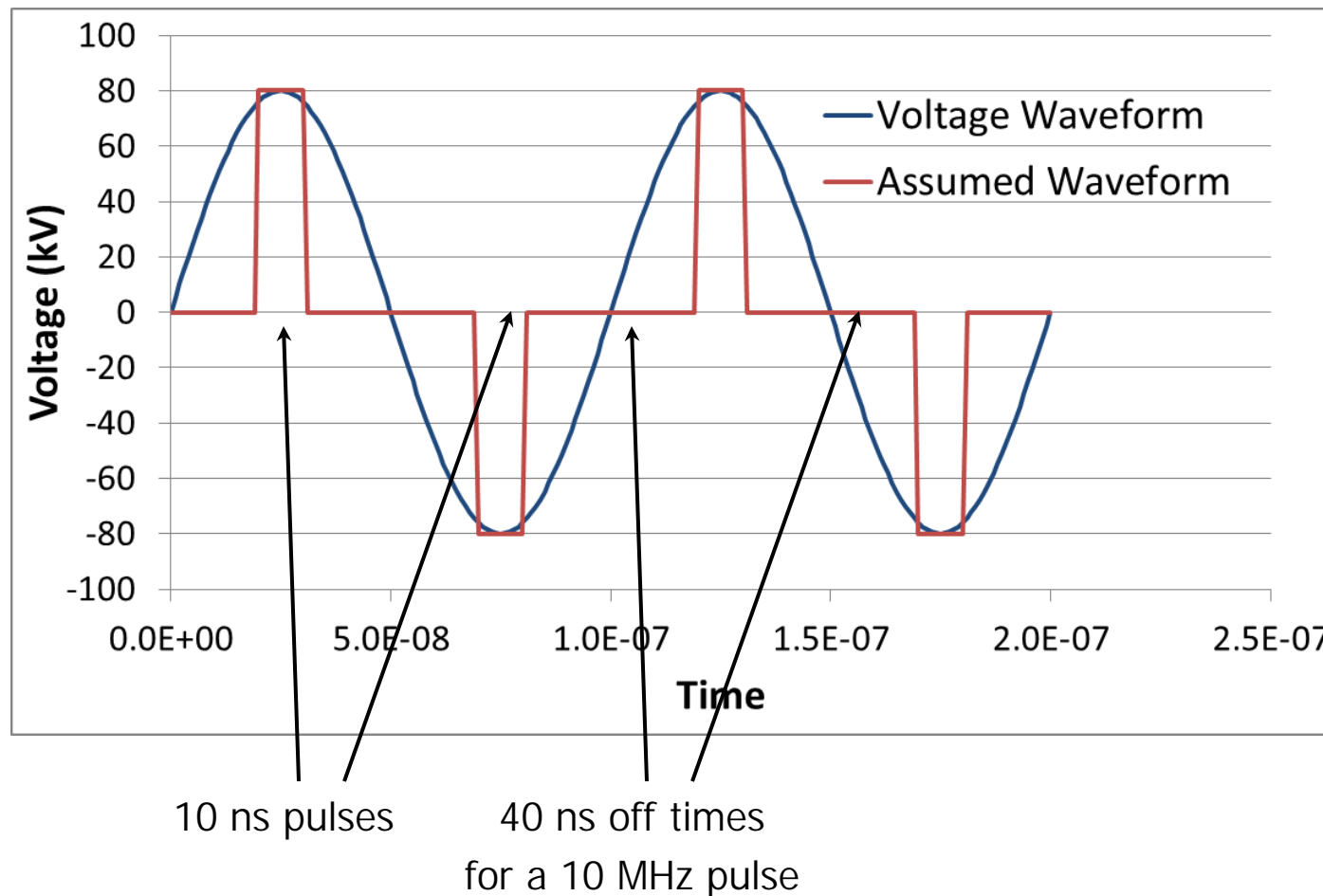


RF excitation :  
Freq. ~10 MHz  
Voltage ~100kV



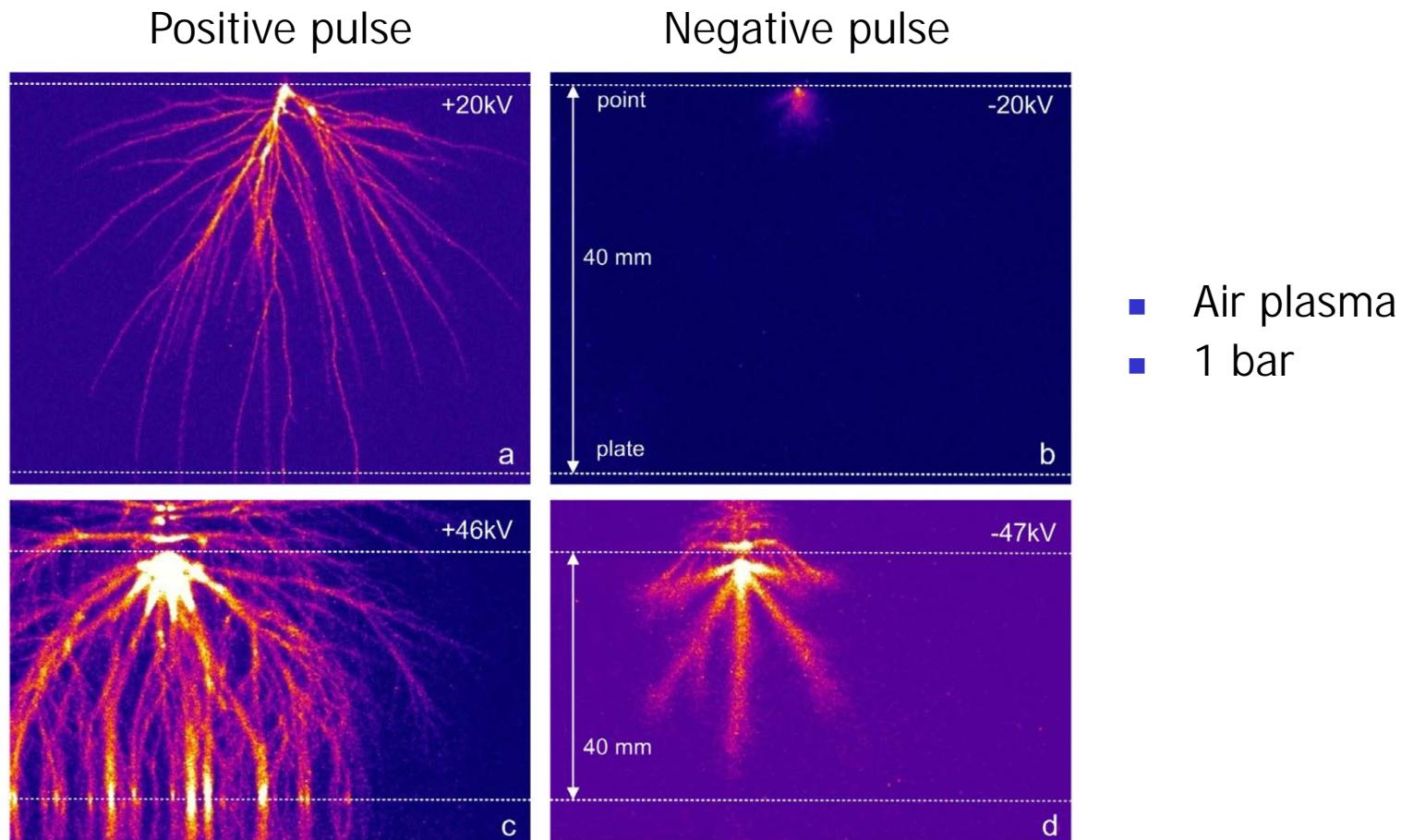
Conditions:  $P=10$  atm,  $T_{\text{gas}}=700$  K, 40:1 A/F ratio (lean),  
 $+90\text{kV} \rightarrow -80\text{kV} \rightarrow +80\text{kV}$  pulse train (10 ns each)

# Simulation strategy for multi-pulse excitation



Actual and Assumed Waveforms for a 10 MHz pulse  
(check attached spreadsheet)

# Discharge structure dependence on excitation polarity

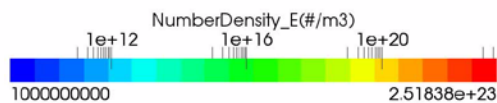


- Thin streamers for positive excitation with low over-voltages
- Voluminous glow-like discharge for negative excitation with low over-voltages
- Streamers for high over-voltages (positive and negative excitation)

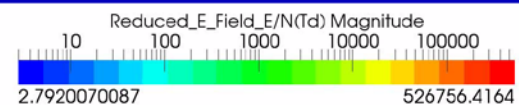
# Electron density evolution for excitation pulse train

Conditions:  $P=10 \text{ atm}$ ,  $T_{\text{gas}}=700 \text{ K}$ , 40:1 A/F ratio (lean),  
 $+90\text{kV} \rightarrow -80\text{kV} \rightarrow +80\text{kV}$  pulse train (10 ns each)

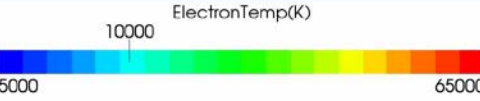
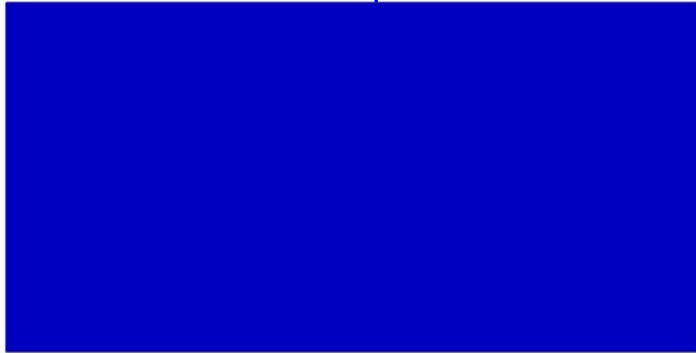
Electron density



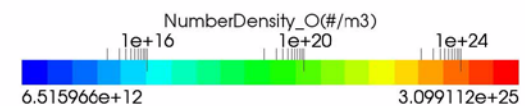
Reduced electric field (E/N)



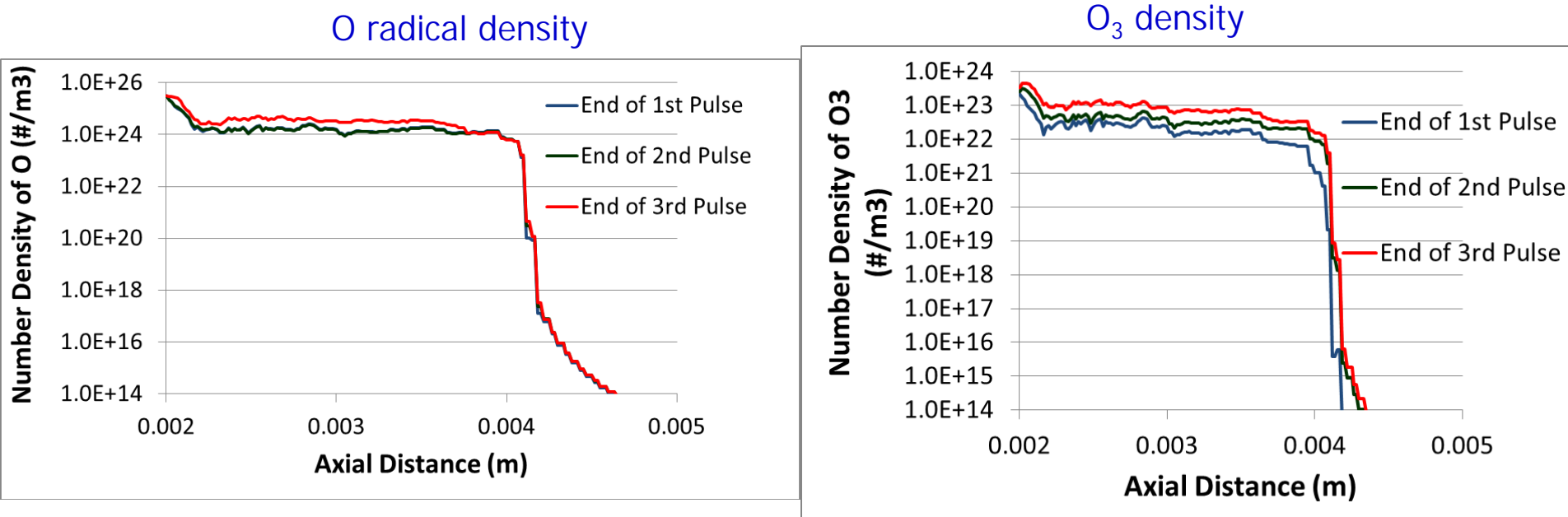
Electron temperature



O radical density



# Radical density evolution at end of each pulse

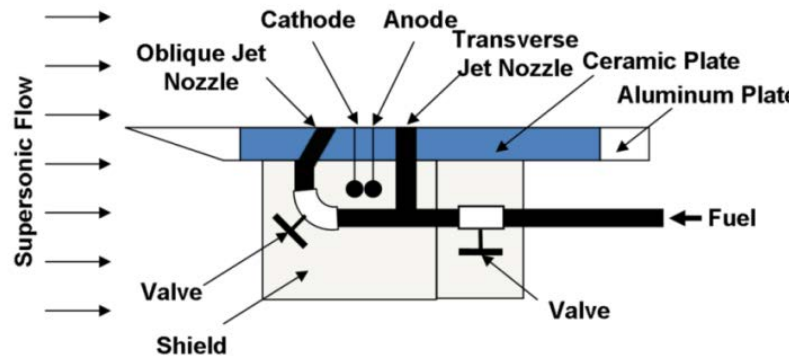


# Nanosecond pulsed ignition of supersonic combustion

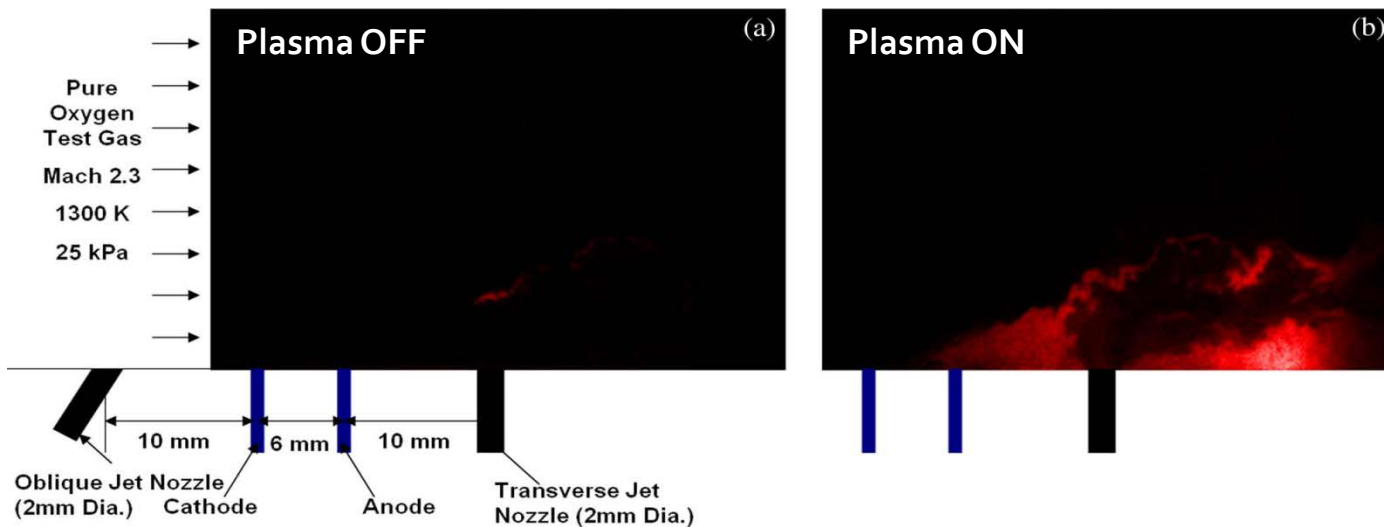
## Reference:

D. Breden and L. L. Raja, "Simulations of nanosecond pulsed plasmas in supersonic flows for combustion applications," *AIAA Journal*, Vol. 50, No. 3, Mar. 2012, pp. 647-658.

# Nanosecond pulsed ignition of supersonic combustion



- 7 kV unipolar pulses
- 20 ns pulse width
- 50 kHz pulse freq.



# Chemical reaction mechanism

H<sub>2</sub>-O<sub>2</sub> sub-mechanism :

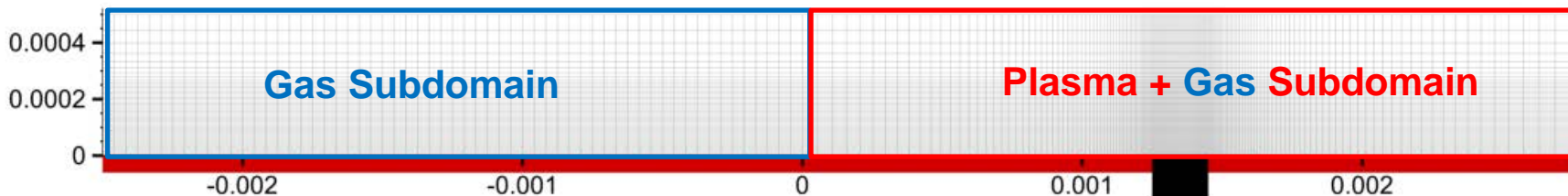
16 Species

e, O<sup>+</sup>, O<sub>2</sub><sup>+</sup>, O<sub>4</sub><sup>+</sup>, O<sup>-</sup>, O<sub>2</sub><sup>-</sup>, H<sup>+</sup>, H<sub>2</sub><sup>+</sup>, O, H, OH, O<sub>2</sub>, H<sub>2</sub>, O(<sup>1</sup>D), O<sub>2</sub>(a<sup>1</sup>Δ<sub>g</sub>), O<sub>2</sub>(b<sub>1</sub>Σ<sub>g</sub><sup>+</sup>)

Assumptions:

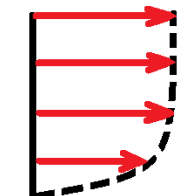
- Rotational energy immediately heats bulk gas
- Vibrational energy convected out of simulation domain

# Geometry, mesh, and operating conditions

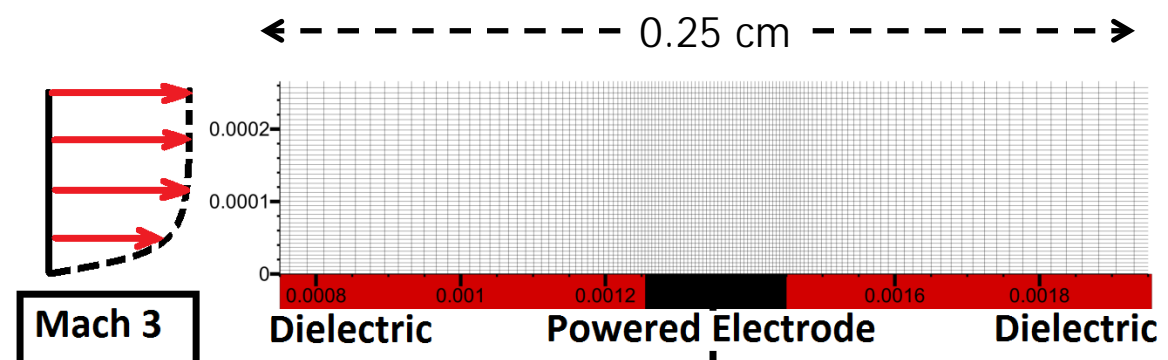


## Plasma Mesh

- 8000 cells



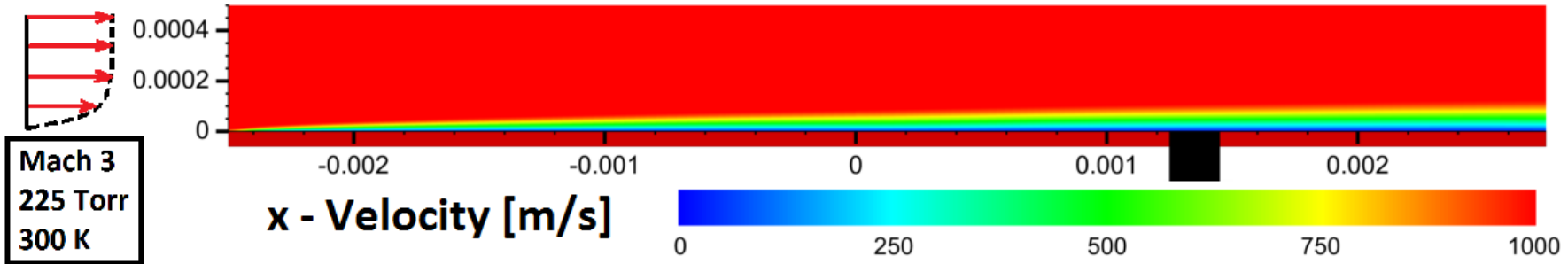
## 0.2 mm electrode



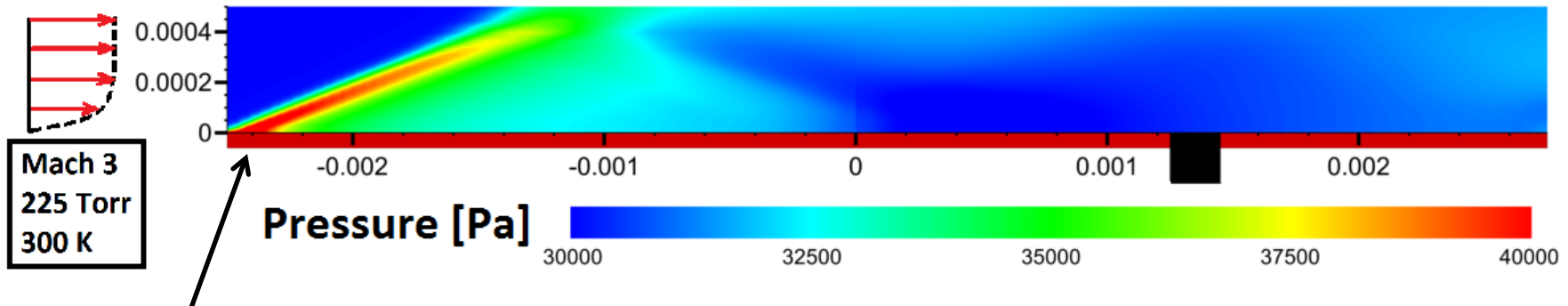
## Trapezoidal Pulse

- 10 ns pulse
- 2.5 ns rise/fall time
- 6 kV peak

# Unperturbed steady flow



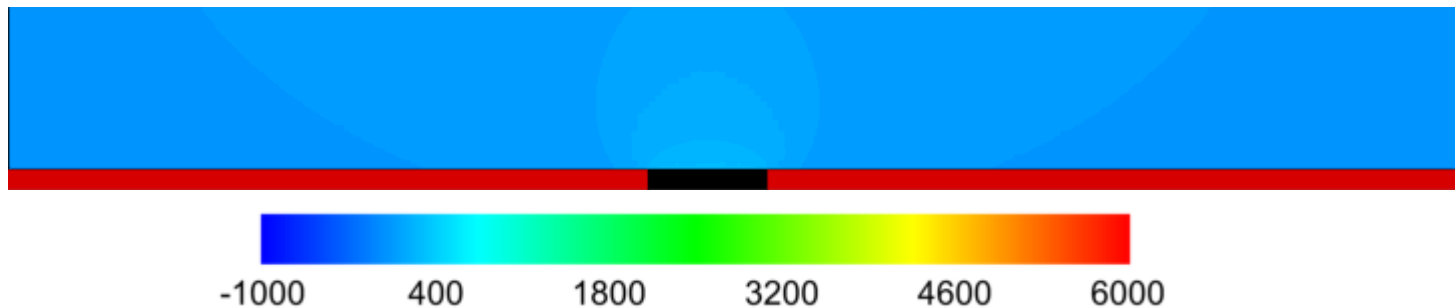
Laminar boundary layer with lower background number density



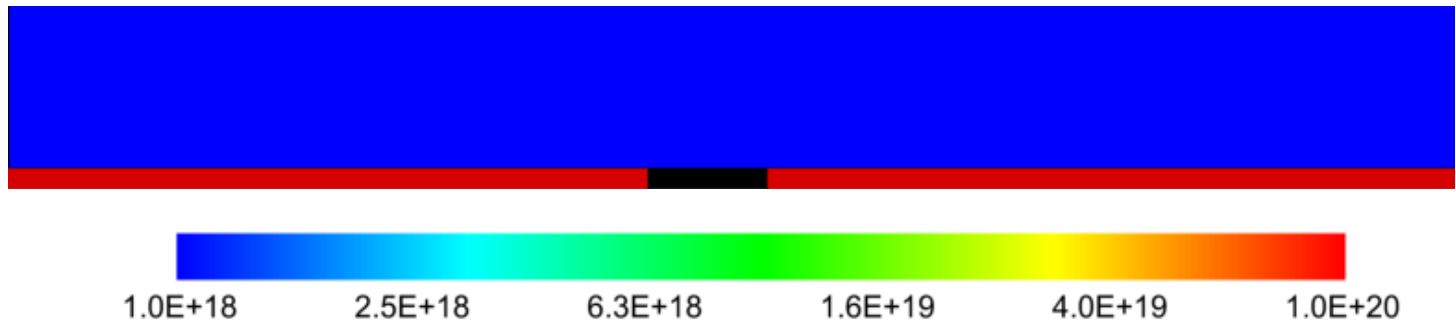
Flat-plate leading edge shock

# Electrostatic potential and electron density transients

Potential  
[V]

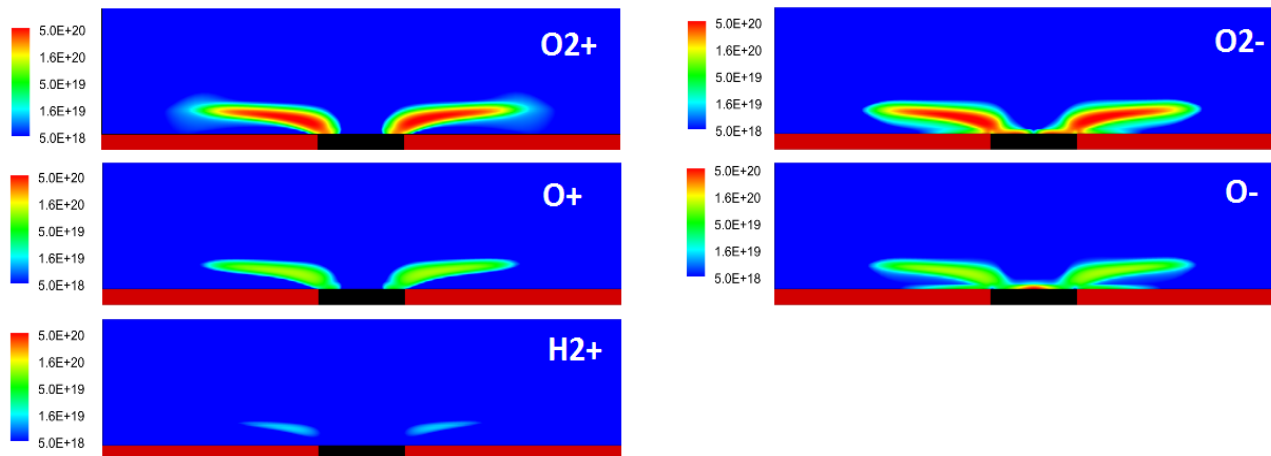


Electrons  
[#/m<sup>3</sup>]



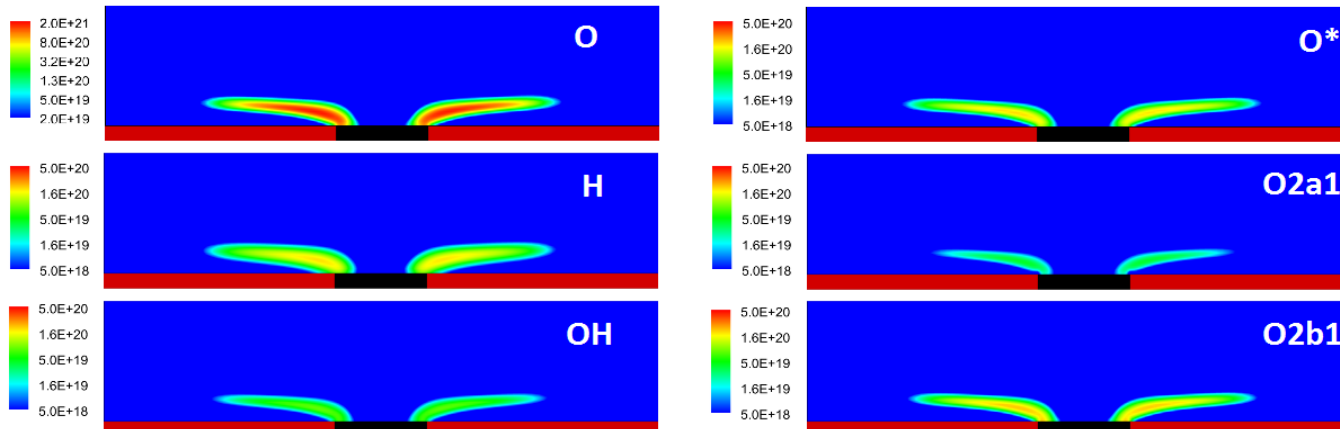
# Charged and radical species yields at end of pulse

## IONS



$O_2^+$  and  $O_2^-$  dominant positive and negative charge carriers

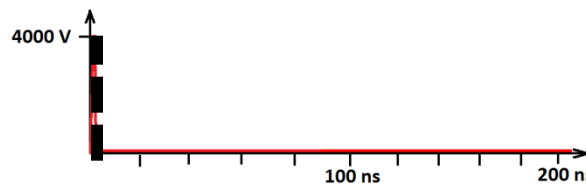
## RADICALS



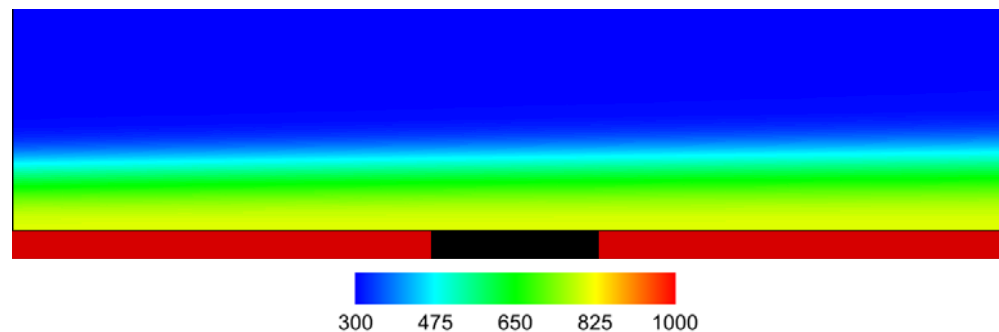
O dominant radical

# Gas dynamic response to nanosecond pulsed discharge

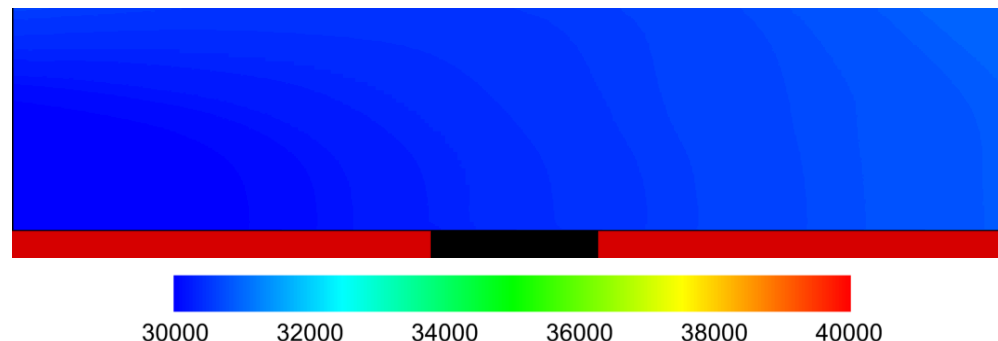
59



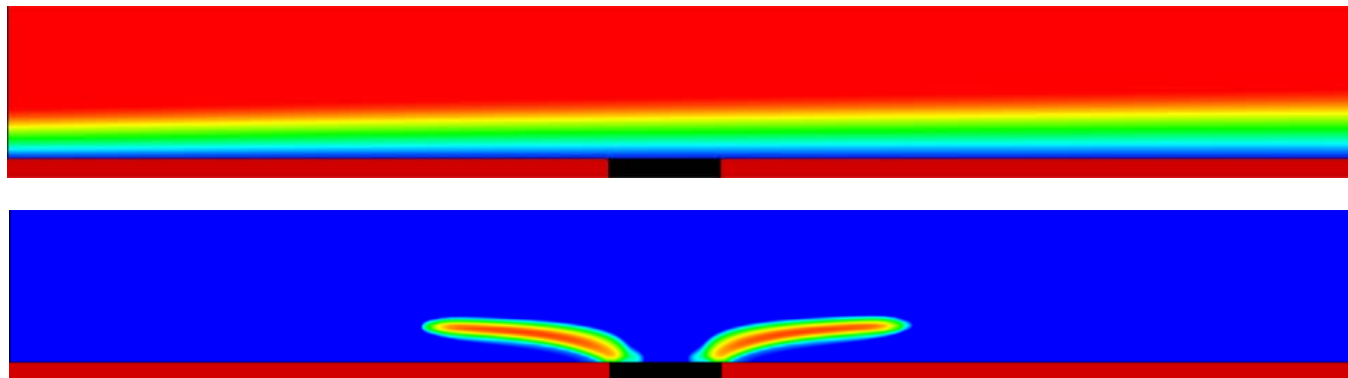
**temperature [K]**



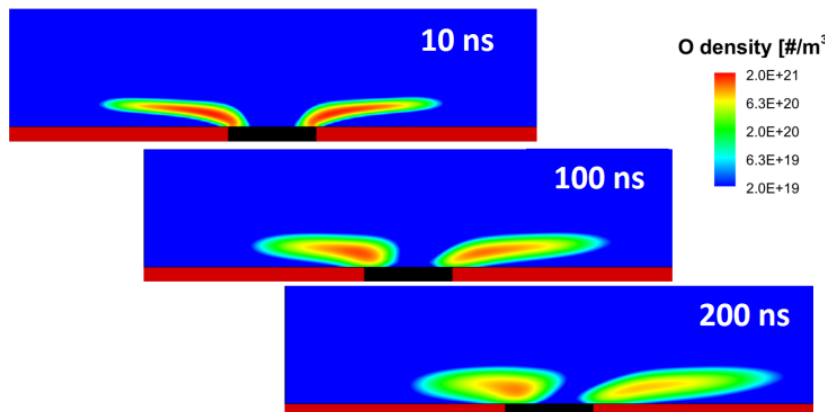
**pressure [Pa]**



# Effect of flow field on discharge dynamics



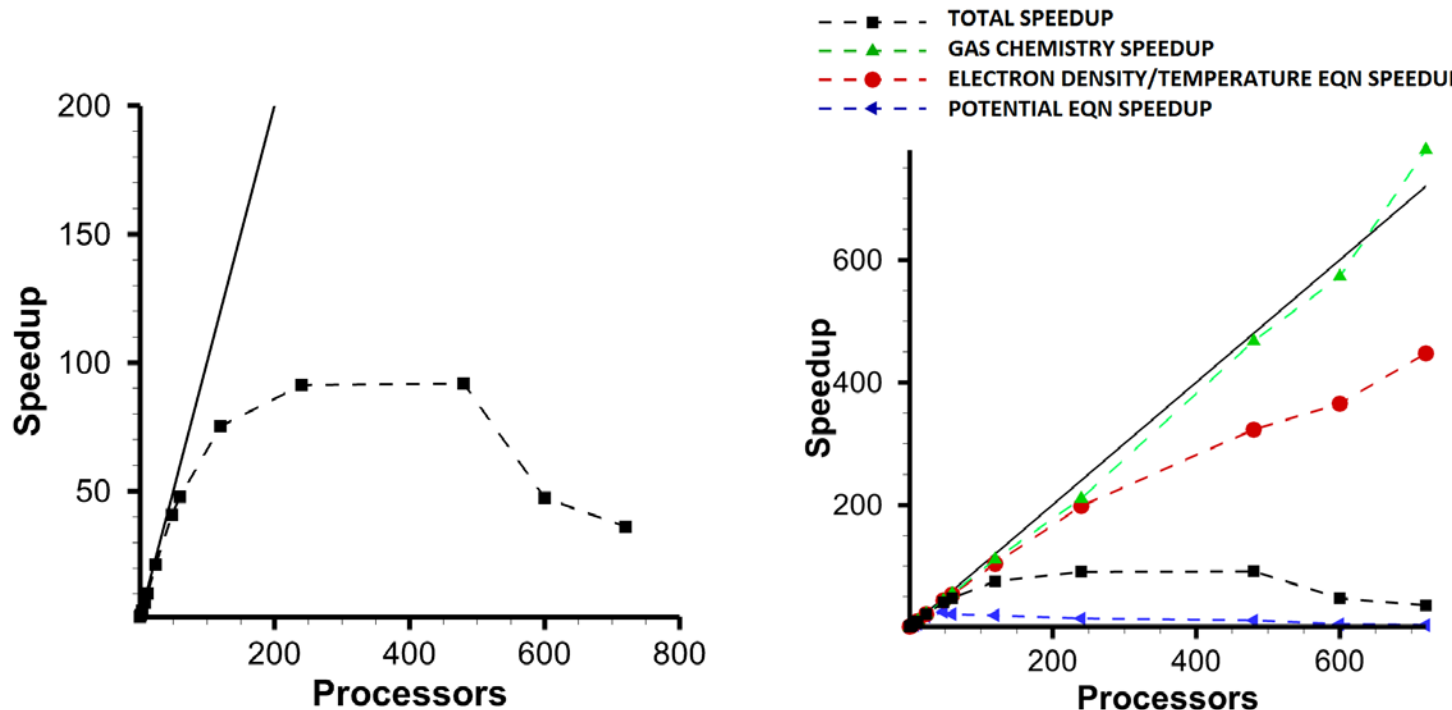
- Lower background number density in boundary layer → higher E/N
- Confinement of streamer to within the boundary layer



- Flow carries radicals downstream over micro/millisecond timescales

# A note on parallel computing for these class of problems

80,000 APPJ mesh for 500 iterations on Lonestar machine at Texas Advanced Computing Center (TACC)



- Problems with large two-dimensional meshes and large chemistries scales well to a few 100 processors, cutting simulation times from ~weeks to ~ 1 day. However further improvement in speed up improvement is limited by algorithmic bottlenecks (specifically the Poisson's eqn).
- New “parallel friendly” discretization approaches to the Poisson’s eqn. are required

# Summary

- High fidelity simulations of cold plasma (streamer) discharges at high pressure relevant to real application are demonstrated
  - Self-consistent plasma physics, multi-species, multi-temperature, gas chemistry, surface chemistry, gas dynamics
  - Computationally expensive and needs large-scale parallel computing to make simulations feasible
- Simulations provide insights into discharge physics and chemistry and coupling with gas-dynamics
- Extension to large scale problems with high-performance computing requires a rework of established computational plasma modeling approaches

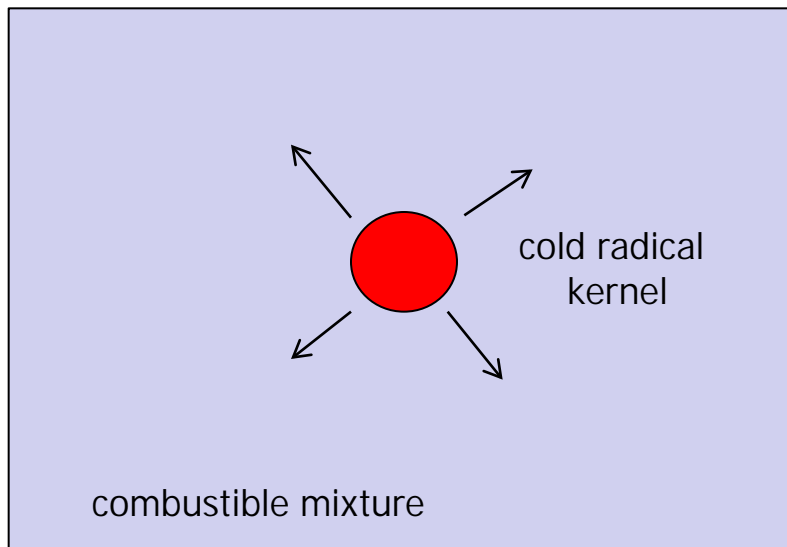


---

**End of Presentation**

# Plasma kernel formation with active radicals is not a sufficient condition for ignition

- Cold plasma generated radicals are accompanied with no additional gas heating
- Do radicals accelerate combustion (chain initiation and branching) reactions for ignition
- Finally are conditions suitable for flame spread

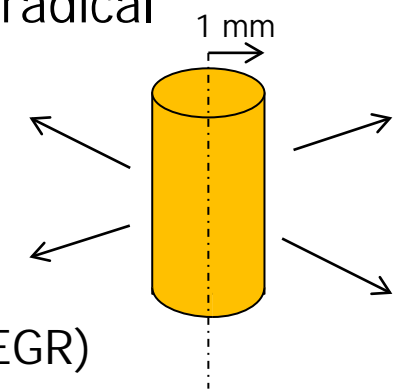


Question : Does the cold radical kernel grow in time or quench ?

Same as classic ignition kernel problem, except here kernel is a cold radical region, rather than hot gas region

# Preliminary computational modeling of combustion initiation and flame spread

- Solve reactive gas dynamics problem assuming an initial radical kernel
  - 1D Axisymmetric transient problem
  - 1 mm kernel size (~ multiple overlapping streamer widths)
  - No additional gas heating from plasma
  - 10 atm, 1500 K, lean mixture with EGR (A/F 20:1 + 50 % EGR)
  - 1 % of O radicals (consistent with yield from streamer)
- Chemistry Mechanism: DRM22 with 22 species and 105 reactions
  - Species: H<sub>2</sub>, O, O<sub>2</sub>, OH, H<sub>2</sub>O, HO<sub>2</sub>, H<sub>2</sub>O<sub>2</sub>, CH<sub>2</sub>, CH<sub>3</sub>, CH<sub>4</sub>, CO, CO<sub>2</sub>, HCO, CH<sub>2</sub>O, CH<sub>3</sub>O, C<sub>2</sub>H<sub>2</sub>, C<sub>2</sub>H<sub>3</sub>, C<sub>2</sub>H<sub>4</sub>, C<sub>2</sub>H<sub>5</sub>, C<sub>2</sub>H<sub>6</sub>, N<sub>2</sub>
- Reactive Flow model:
  - VizGlow (without plasma calculations) coupled to Compressible Navier-Stokes solver (VizFlow)



# Other approaches may be considered for automotive combustion ignition applications

67

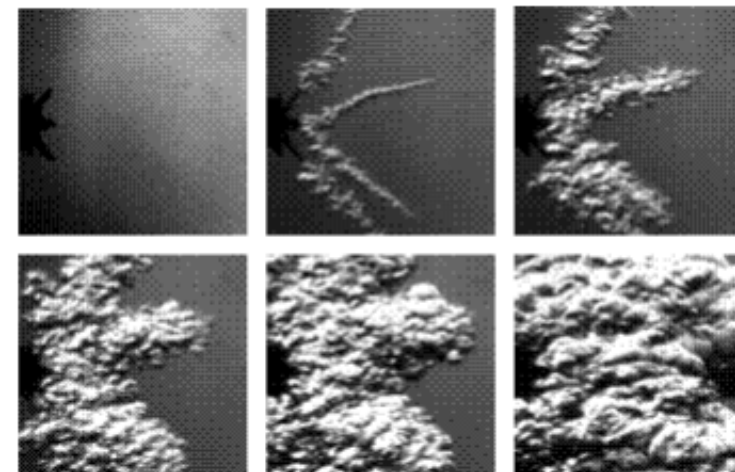
- Principle requirements :
  - Extended plasma kernel size
  - High radical yield
  - Low loss (volumetric; far away from surfaces)



Spark

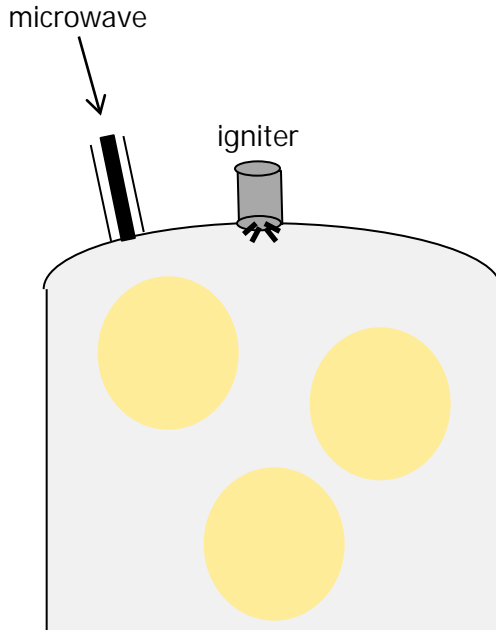


HSP



RFEIS or ECCOS

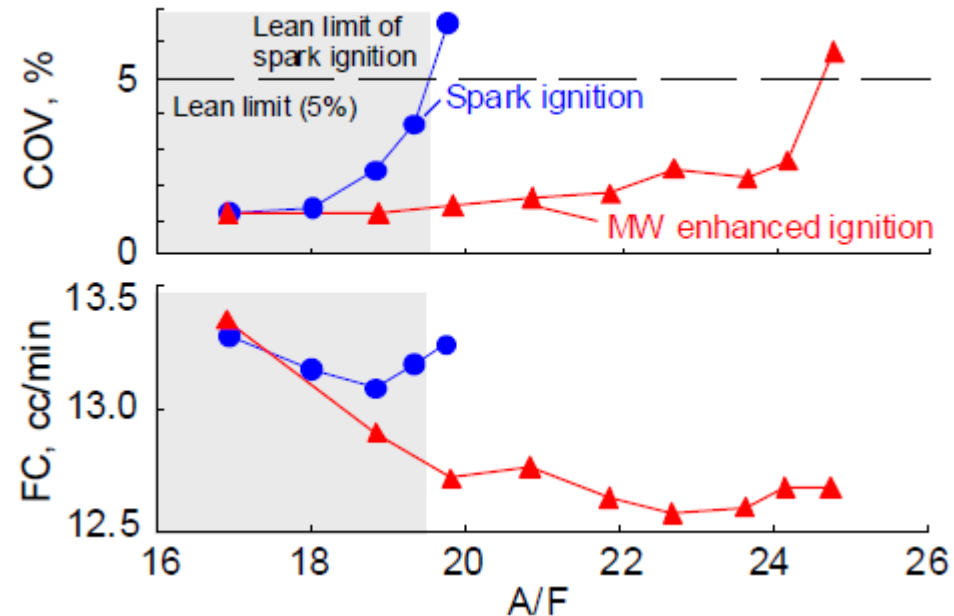
# Sub-critical microwave excitation with external plasma initiation is a possibility



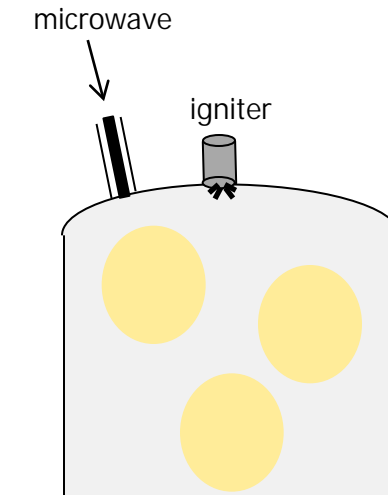
- Coax-fed microwave can provide a volume filling excitation field
- External plasma initiation can be used to keep microwave E-field subcritical

# Microwave excitation concept is not new for automotive ignition applications

69



- Igniter erosion concerns with Ikeda concept can potentially be overcome with coax-fed microwave



# High-fidelity modeling capability available to simulate microwave plasmas with VizGlow

70

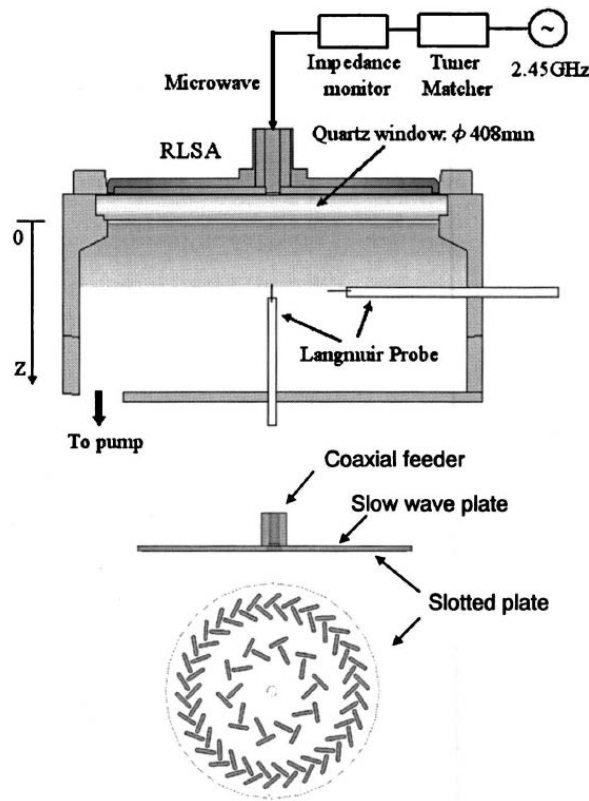
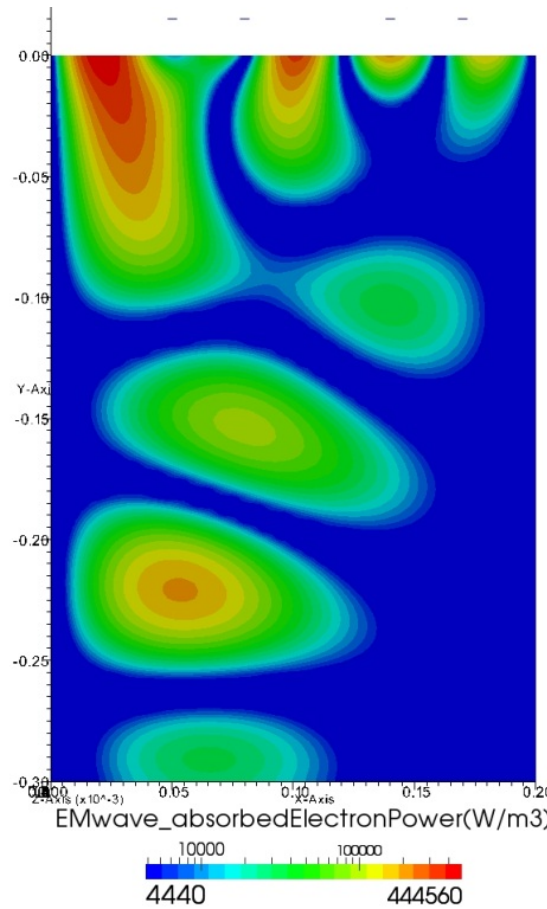


FIG. 1. Schematics of the RLSA for the microwave plasma system.



## Characteristics of large-diameter plasma using a radial-line slot antenna

C. Tian,<sup>a)</sup> T. Nozawa, K. Ishibasi, H. Kameyama, and T. Morimoto  
Tokyo Electron Ltd., TBS Broadcast Center, 3-6 Akasaka 5, Minato-ku, Tokyo 107-8481, Japan

# Summary

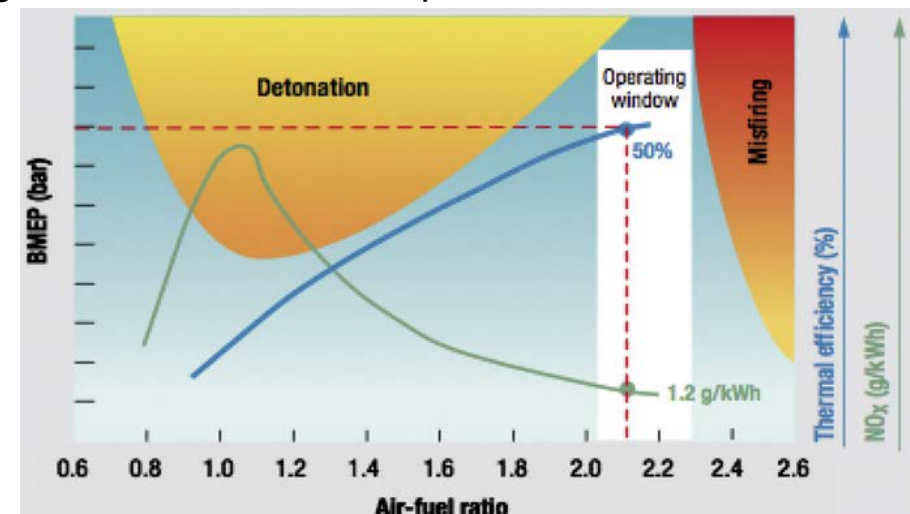
- Presented an overview of non-equilibrium plasma physics relevant to automotive ignition applications
  - Nano-second pulsed plasma are efficient way to generate non-equilibrium plasmas at high pressures
  - HSP, DBD, RFEIS devices leverage this concept in different ways
- High-fidelity simulation studies of HSP presented
  - Streamers produce copious amounts of radicals (particularly O radicals)
  - Radicals are concentrated at inner electrode possibly explaining the dynamics of flame spread from these ignition sources
- Showed initial studies of long time scale processes in ignition
  - Plasma radical kernel → local combustion initiation → gas dynamic relaxation → flame spread
- Extended volumetric radical kernel possible with subcritical microwave + NSP ignition





# Trends in automotive combustion engines are driving need for new ignition sources

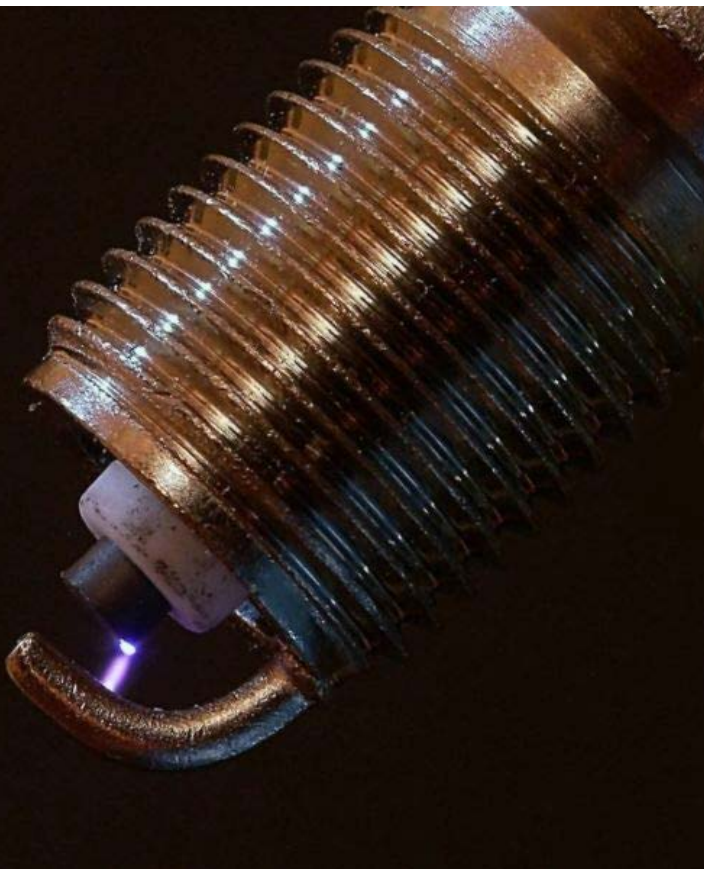
- Improved engine efficiencies and stringent emission norms are driving new technologies in automotive combustion devices
- Improved efficiencies achievable through 1) increased compression ratios in IC engines and 2) lean combustion
- Lean combustion →
  - Increase in efficiency (power/fuel rate)
  - Decrease in flame temperature  
→ low NOx
- Enabling technologies
  - Direct injection (no air intake throttling losses) → just in time combustion
  - Lean with Exhaust Gas Recirculation (EGR) → low flame temp → lower NOx
- Technological challenges
  - Lean combustion (with EGR) → ignitability issue is key problem



Starikovskiy and Aleksandrov, Prog. Energy Comb. Sci., 2013

# Conventional spark plug based IC engine ignition

75



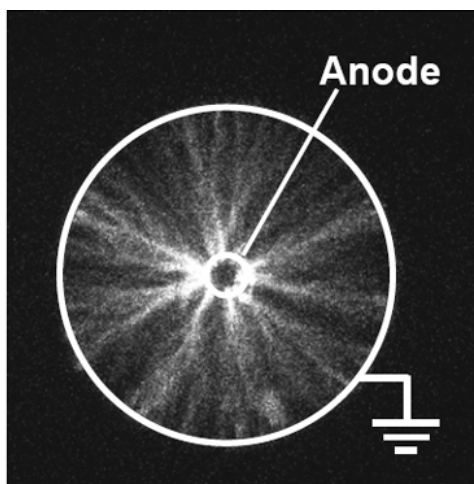
- Combustion ignition via highly constricted/localized spark
- Spark is a thermal plasma with very high sensible temperatures (~ 1000's K)
  - lifetime/reliability
- Chemical initiators for combustion not the same as in a cold plasma
- Limited control on plasma yield

# Nanosecond pulsed and Dielectric Barrier plasma-based ignition

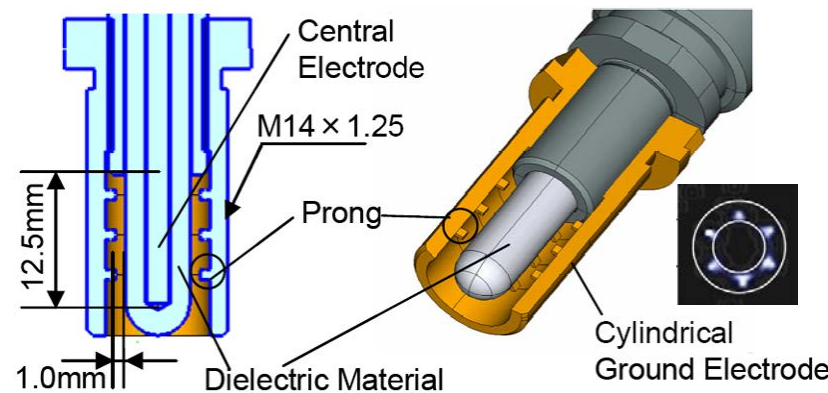
Conventional spark plug



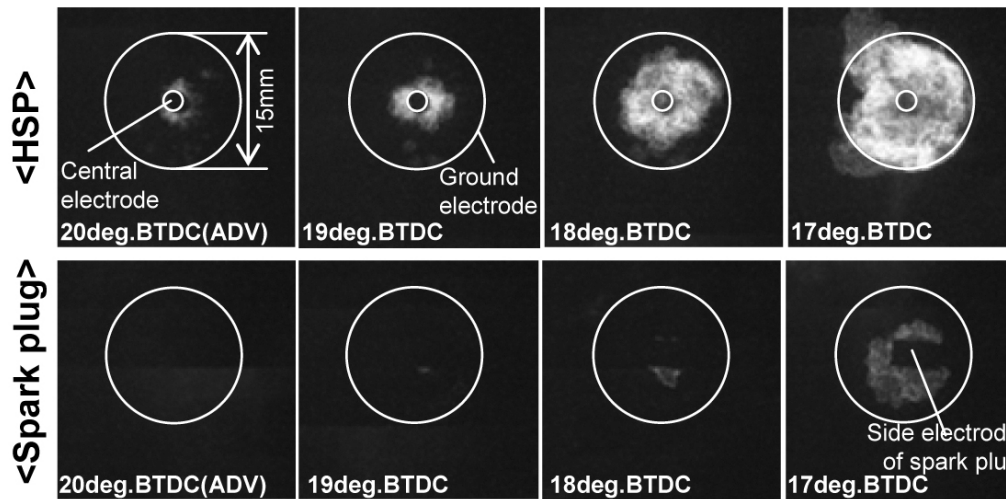
Nanosecond Pulsed



Dielectric barrier

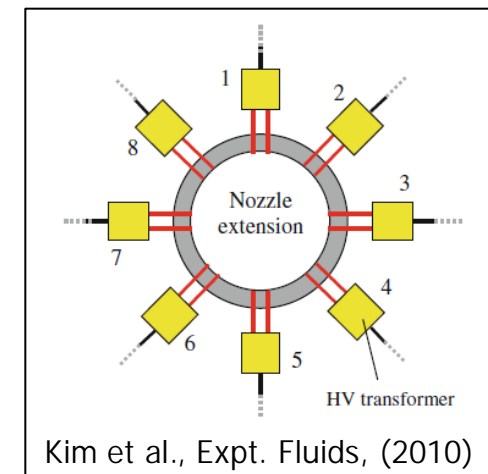
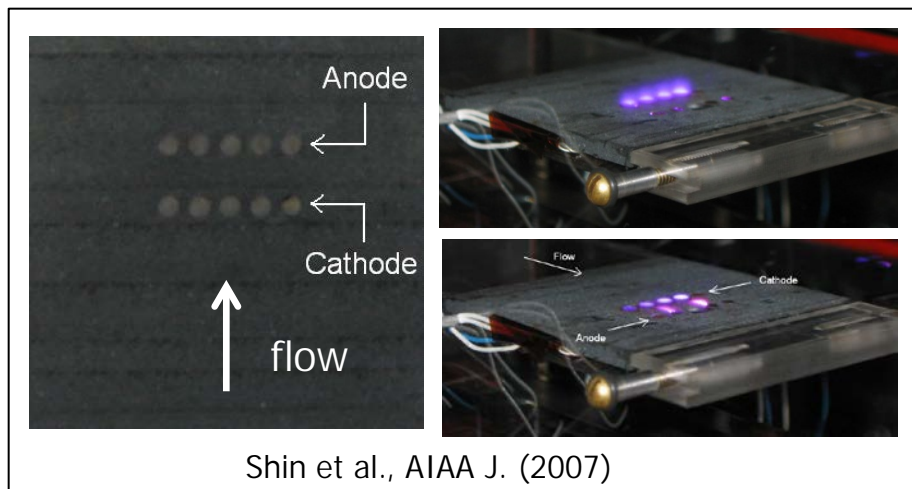
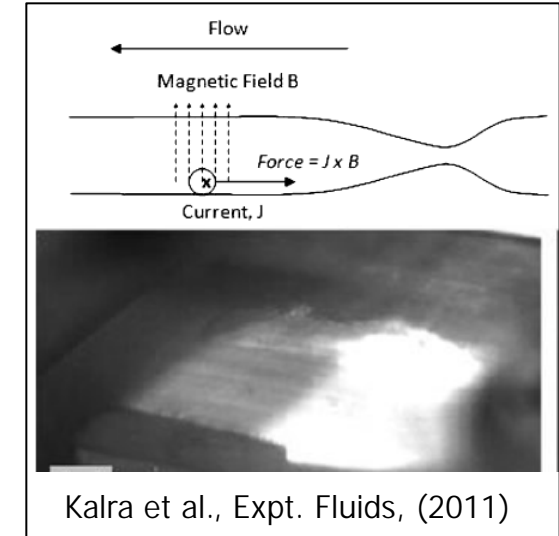
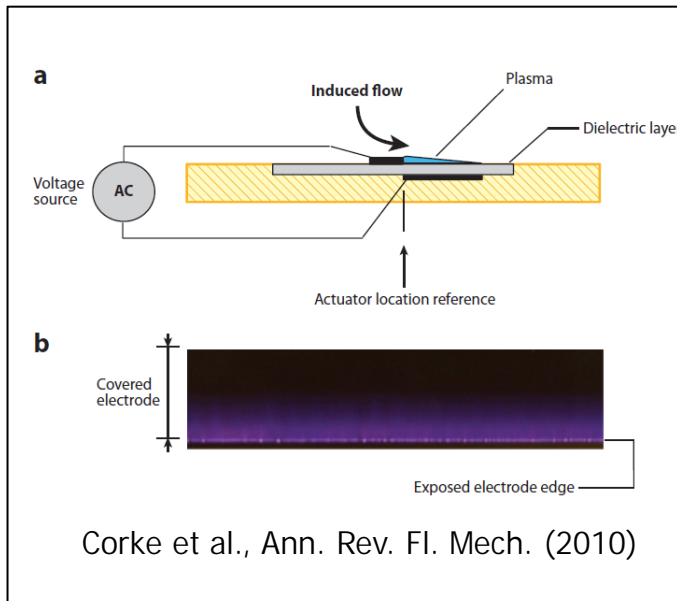
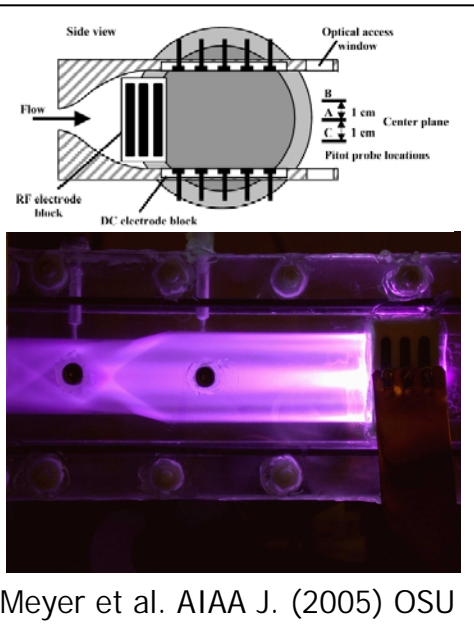


1200 rpm, A/F=15.1 ( $\Phi=1.0$ ), ADV: 20 deg.BTDC, iso-octane



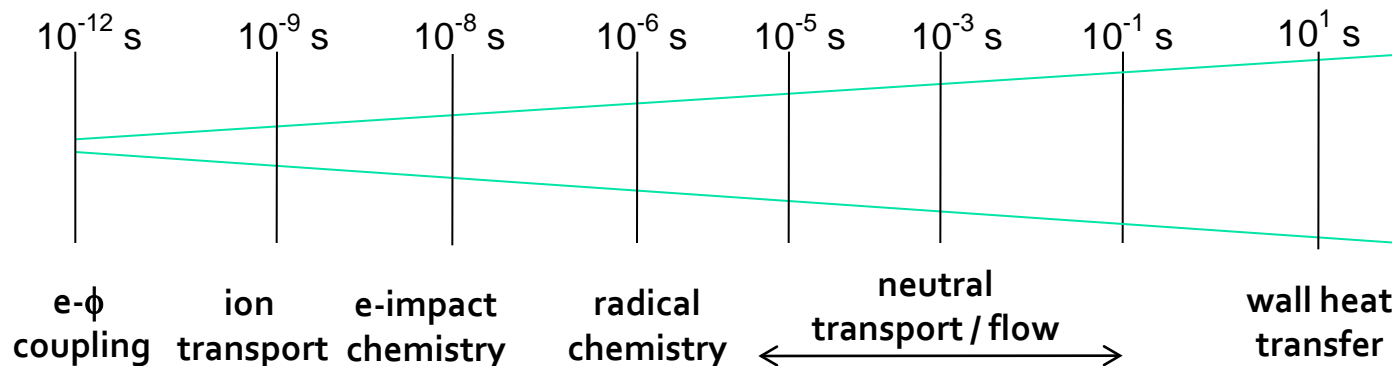
Shiraishi and Urushira,  
SAE\_2011-01-0660

# Variety of plasma actuator concepts exist for volumetric and surface flow control

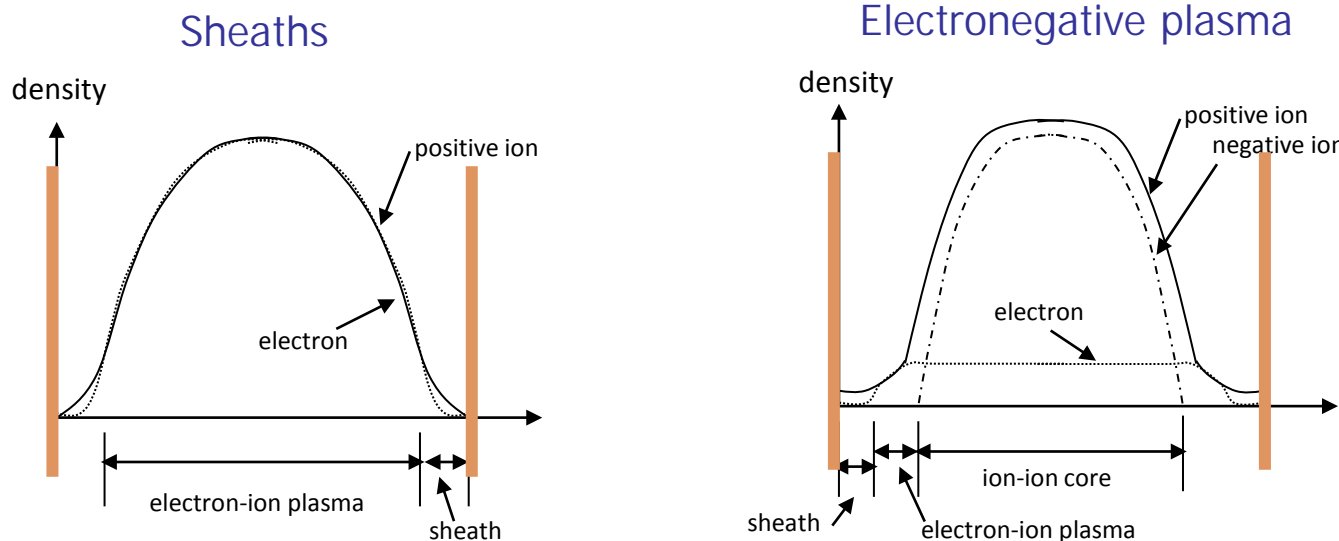


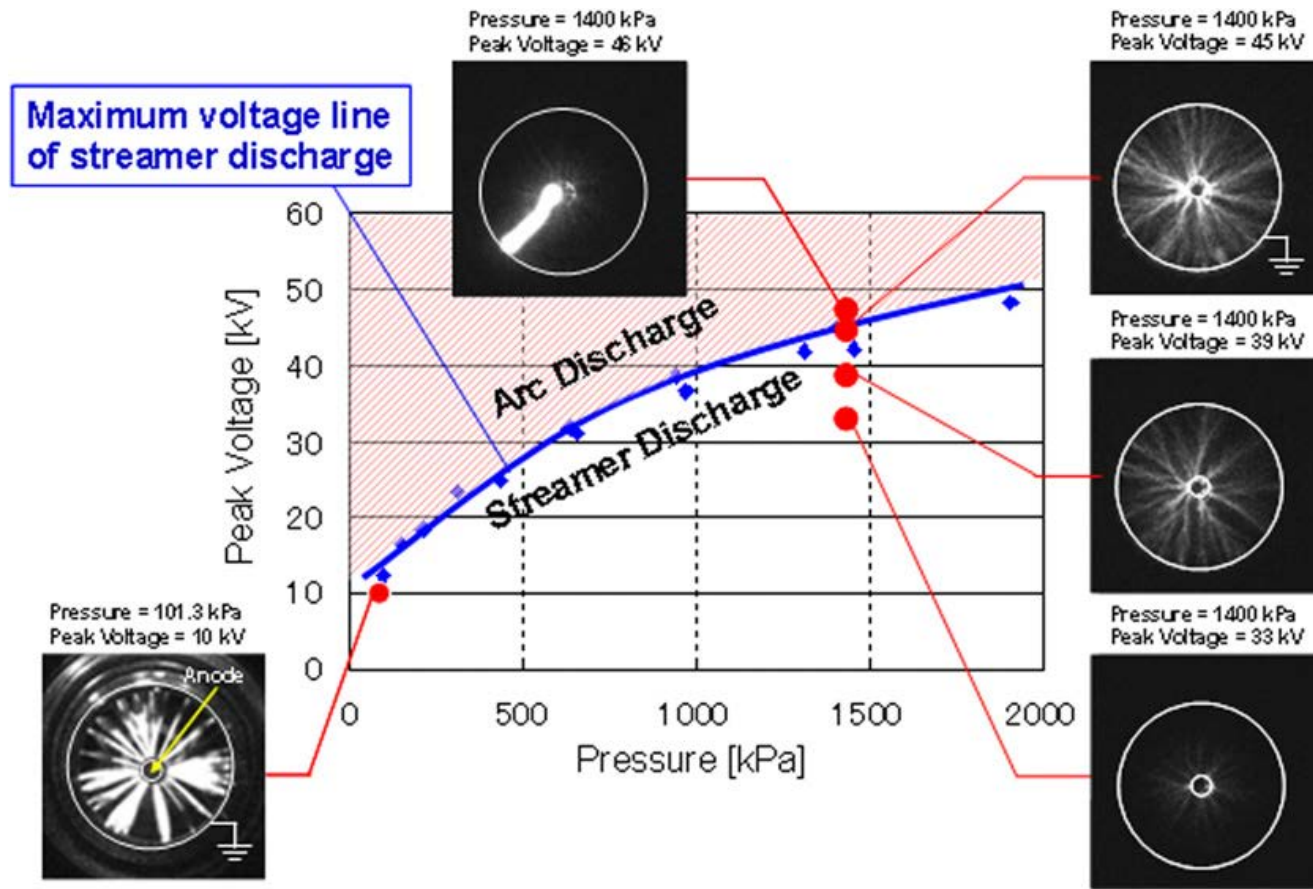
# Computational issues in the modeling of air plasma interactions with flows

- Extremely high degree of time disparity in component physics



- Spatial stiffness due to discharge structure





From: Shiraishi et al., J. Phys. D., 42, 2009, 135208.

# Photoionization (3-term Helmholtz equation model)

Integral Model (Zheleznyak et al 1982):

$$I(\vec{r}) = \frac{P_q}{P + P_q} \xi S_i(\vec{r})$$

$$S_{ph}(\vec{r}) = \iiint \frac{I(\vec{r}') g(R)}{4\pi R^2} dV$$

$$\frac{g(R)}{P_{O_2}} = \frac{\exp^{-\chi_{min} P_{O_2} R} - \exp^{-\chi_{max} P_{O_2} R}}{P_{O_2} R \ln(\chi_{max}/\chi_{min})}$$

Luque et al<sup>\*</sup> proposed approximating  $g(R)/P_{O_2}$  using two exponentials functions and expanded by Bourdon et al<sup>+</sup> to three terms

$$S_{ph}(\vec{r}) = S_{ph}^1 + S_{ph}^2 + S_{ph}^3$$

$$S_{ph}^j = \iiint \frac{I(\vec{r})}{4\pi R} A_j P_{O_2}^2 \exp^{-\lambda_j P_{O_2} R}$$

The integrals are solutions to three Helmholtz equations:

$$\nabla^2 S_{ph}^j - (\lambda_j P_{O_2})^2 S_{ph}^j = -A_j P_{O_2}^2 I(\vec{r})$$
$$(j = 1, 2, 3)$$

	$A_j \text{ (cm}^{-1} \text{ Torr}^{-1}\text{)}$	$\lambda_j \text{ (cm}^{-1} \text{ Torr}^{-1}\text{)}$
$S_{ph}^1$	0.0067	0.0447
$S_{ph}^2$	0.0346	0.1121
$S_{ph}^3$	0.3059	0.5994

\* Luque A, Ebert U, Montijn C and Hundsorfer W 2007 Appl. Phys. Lett. 90 08150

+ Bourdon A, Pasko NP, Liu NY, Celestin S, Segue P and Maroude E 2007 Plasma Sources Sci. Technol. 16 656

# Plasma chemistry mechanism used in studies

- Plasma Chemistry mechanism relevant to plasma time scale (~10's ns)

- Methane-air mixtures

- 26 Species :  
 $E, O, N_2, O_2, H, N_2^+, O_2^+, N_4^+, O_4^+,$   
 $O_2+N_2, O_2^-, O^-, O_2(a1), O_2(b1), O_2^*, N_2(A)$   
 $, N_2(B), N_2C, N_2(a1), CH_4, CH_3, CH_2, CH_4^+,$   
 $CH_3^+, CH_2^-, H^-$

- 85 Reactions :  
1) electron impact, 2) ion-ion, 3) electron neutral, 4) neutral-neutral

- Methane-air with EGR mixtures

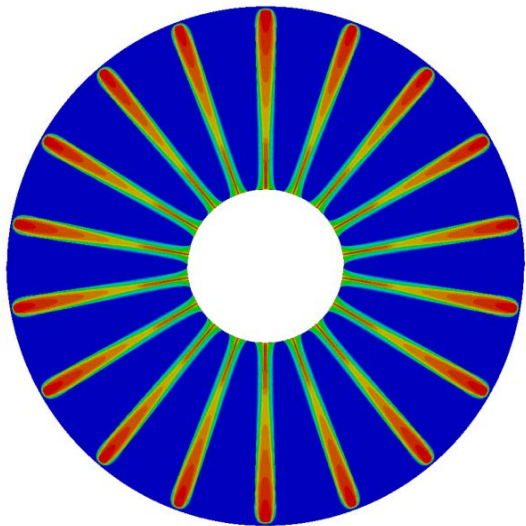
- 39 Species :  
 $E, O, N_2, O_2, H, N_2^+, O_2^+, N_4^+, O_4^+,$   
 $O_2+N_2, O_2^-, O^-, O_2(a1), O_2(b1), O_2^*,$   
 $N_2(A), N_2(B), N_2C, N_2(a1), CH_4, CH_3, CH_2,$   
 $CH_4^+, CH_3^+, CH_2^-, H^-$   
 $H_2O, H_2O^+, H_2, H^+, H_2^-, OH, OH^+, OH^-, O^+,$   
 $CO_2, CO_2^+, CO^-, O_3$

- 110 Reactions :  
1) electron impact, 2) ion-ion, 3) electron neutral, 4) neutral-neutral  
Additional : CO<sub>2</sub>, H<sub>2</sub>O and O<sub>3</sub> reactions

# Comparison of baseline and With EGR cases for HSP discharge streamer

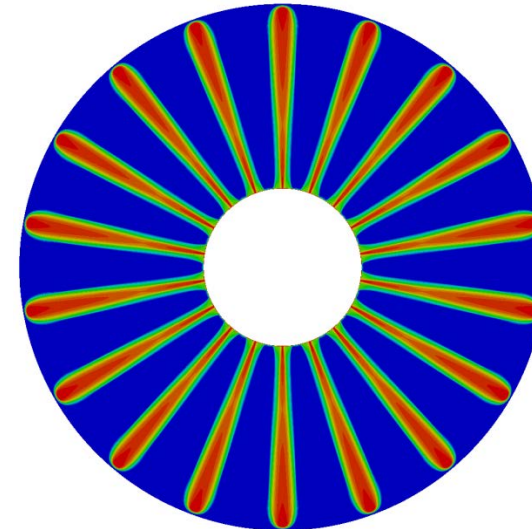
82

Baseline (lean A/F = 40:1)



9.7 ns

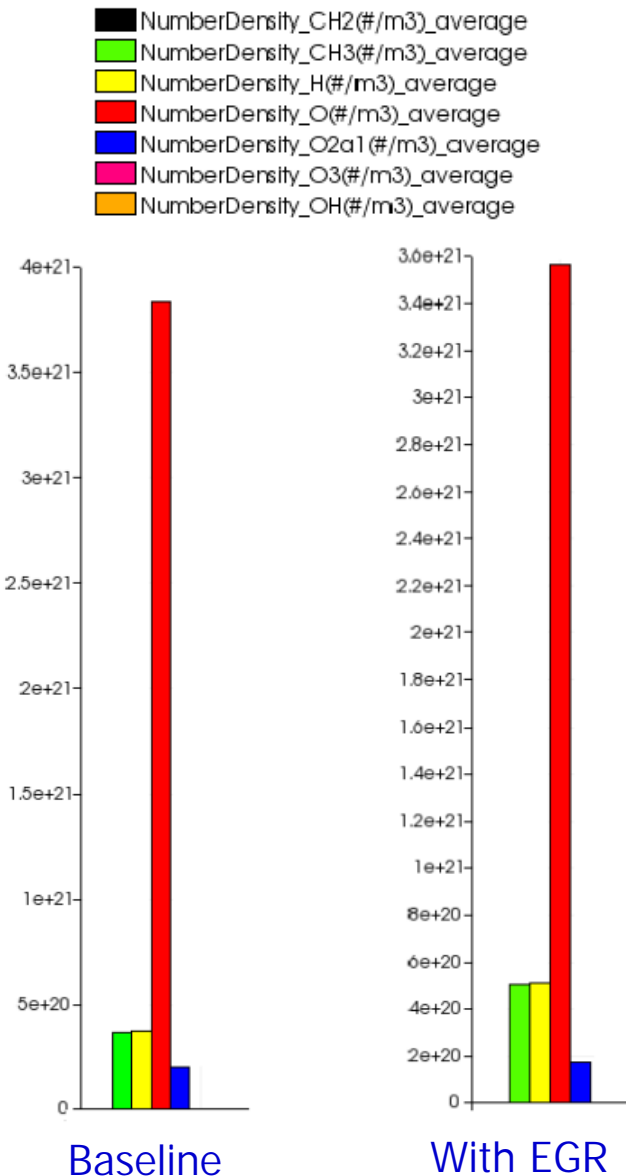
With EGR (A/F = 20:1 + 50% exhaust)



5.7 ns

- Propagation speeds higher with EGR
- Electron density slightly higher with EGR

# Radical densities for baseline and With EGR cases for HSP discharge streamer



- No significant changes in radical densities for case with EGR

Case 1: Pulse train of -90kV → +90 kV → -90 kV (gas temperature 700K)

Pulse Durations:

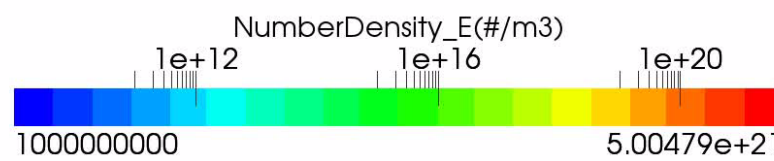
1<sup>st</sup> pulse: 7 ns

2<sup>nd</sup> pulse: 7 ns

3<sup>rd</sup> pulse: 7 ns

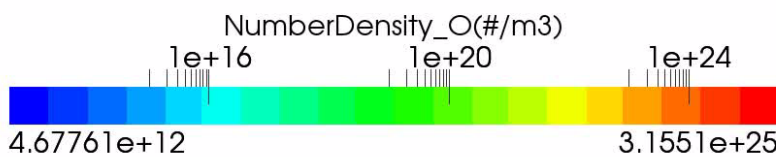
# Evolution of Number Density of Electrons

85



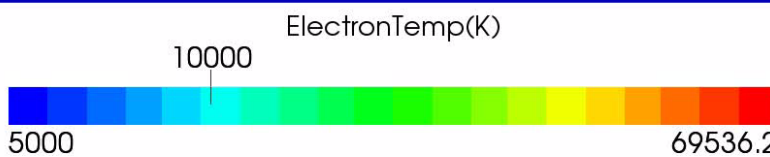
85

# Evolution of Number Density of O<sup>86</sup> radicals



# Evolution of Electron Temperature (K)

87



87

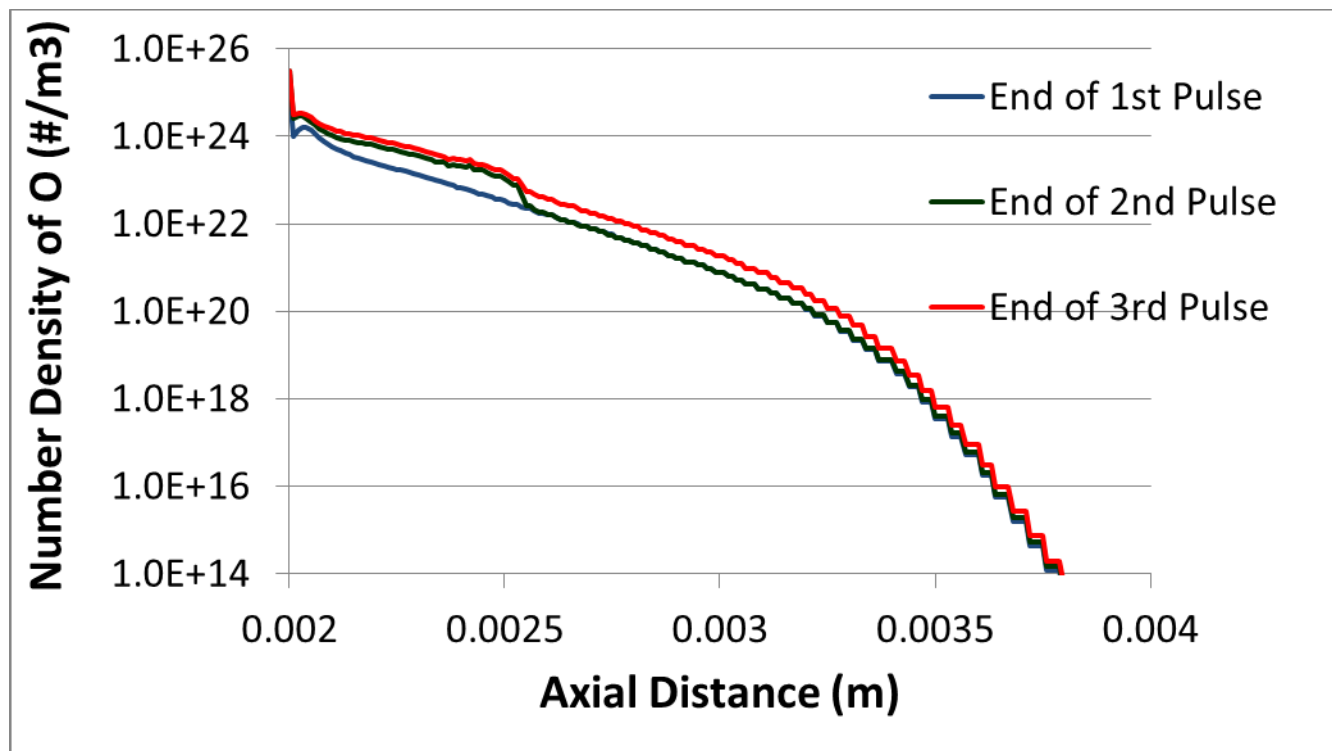
# Evolution of Reduced Electric Field ( $E/N$ )

88

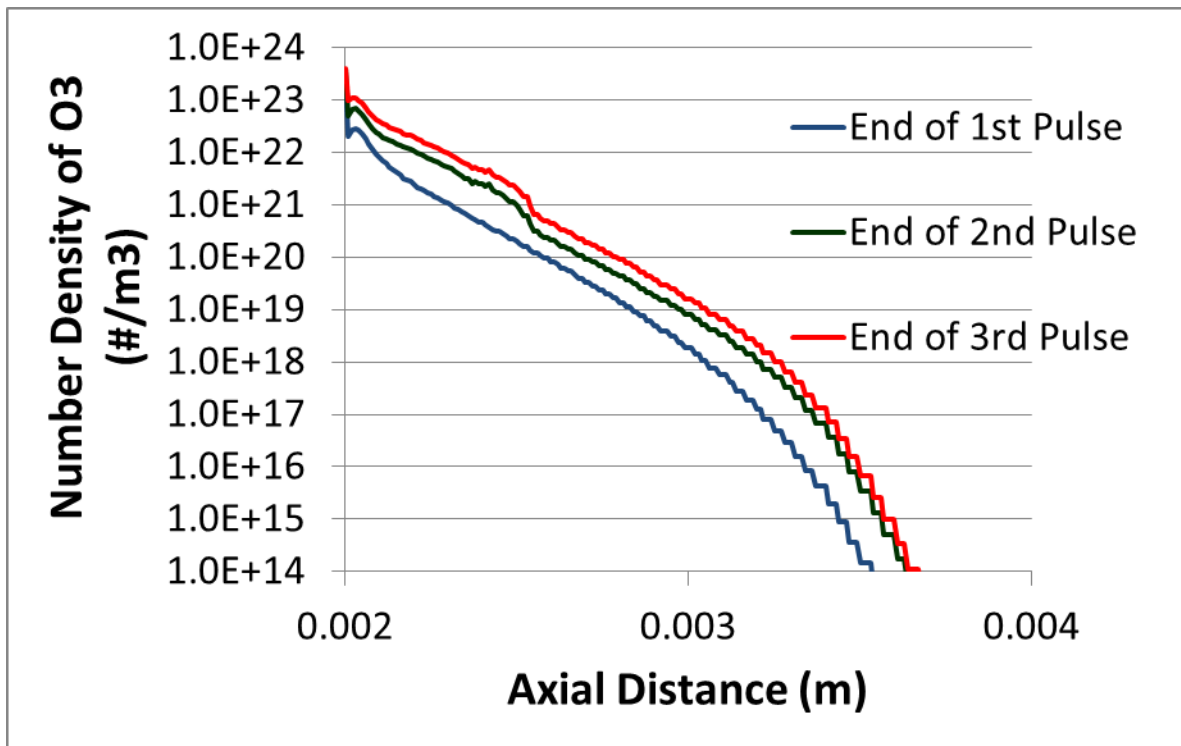


88

# O Radical Number Density at End of Different Pulses



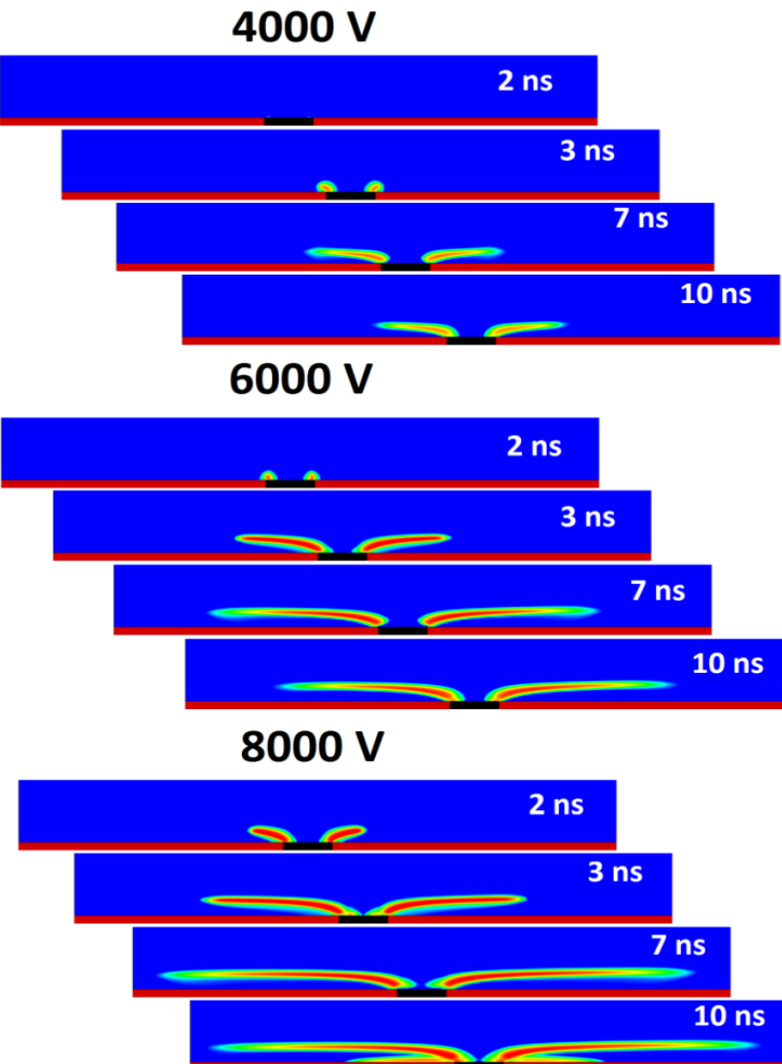
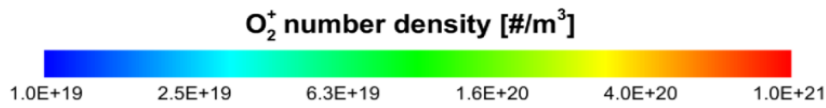
# O<sub>3</sub> Radical Number Density at End of Different Pulses





# **Voltage Amplitude Comparison**

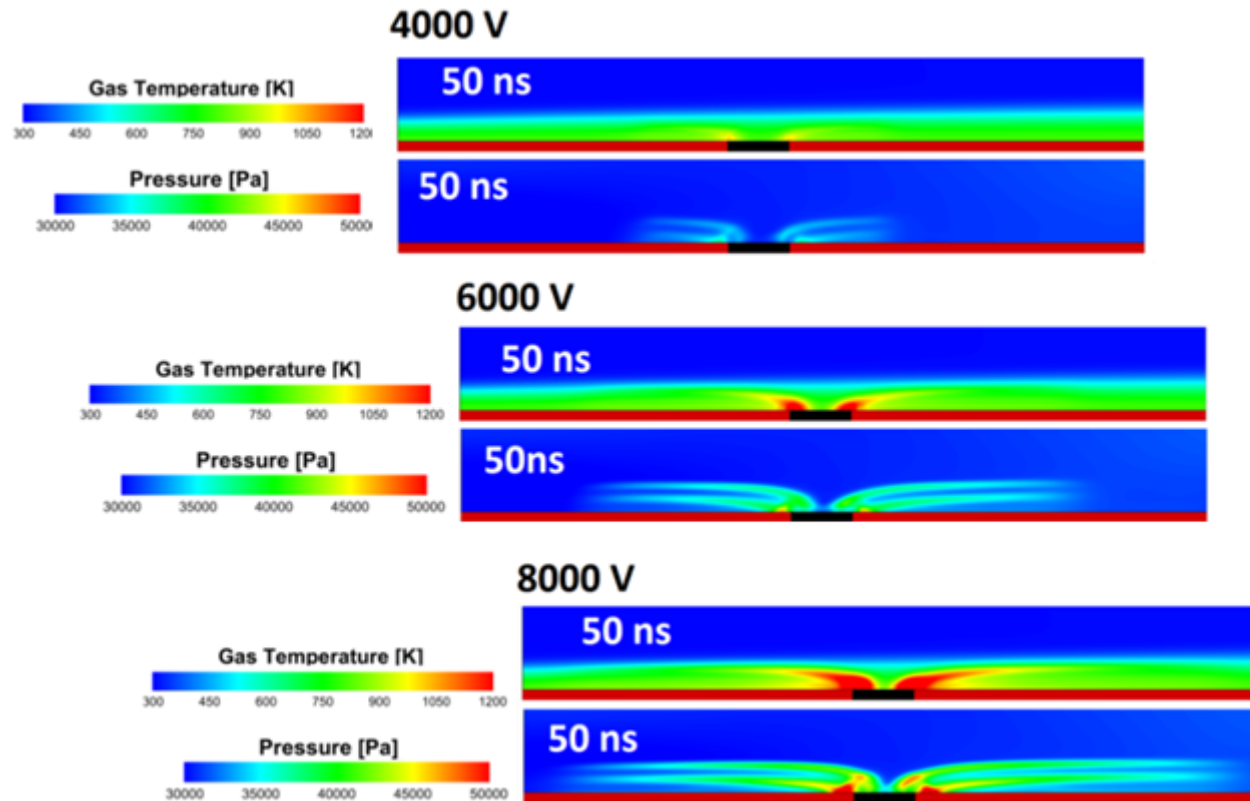
# Voltage: Streamer Propagation



Higher voltages result  
in stronger Electric  
Field

Streamers propagate  
further as voltage  
increases

# Voltage : Thermal Effects



Stronger Electric fields result in greater ion Joule heating

# Conclusions

- O radicals dominant species in plasma (~0.5% peak mole fraction)
- Ion Joule heating dominates gas temperature increase and results in blast waves
- Increasing Voltage increases peak densities, gas heating and volume of plasma formed
- Chemistry (electropositive vs electronegative plasma) affects –
  - Streamer propagation distance/speed
  - Region of plasma formation (inside/outside boundary layer)
  - Intensity of gas heating for different polarities
- Anodic pulses appear more efficient for supersonic combustion
  - Radicals produced over greater volume
  - Less power lost to heat (for O<sub>2</sub>-H<sub>2</sub>)